# MOLECULAR DYNAMICS SIMULATIONS OF PHASE BEHAVIOUR AND STRUCTURAL STUDIES OF GUANIDINIUM TRIFLATE IONIC LIQUID AND ITS MIXTURE WITH WATER AND *N*-METHYLDIETHANOLAMINE FOR CARBON DIOXIDE REMOVAL

NAIMAH BINTI HARON

FACULTY OF SCIENCE

UNIVERSITI MALAYA

KUALA LUMPUR

2020

# MOLECULAR DYNAMICS SIMULATIONS OF PHASE BEHAVIOUR AND STRUCTURAL STUDIES OF GUANIDINIUM TRIFLATE IONIC LIQUID AND ITS MIXTURE WITH WATER AND *N*-METHYLDIETHANOLAMINE FOR CARBON DIOXIDE REMOVAL

**NAIMAH BINTI HARON**

**THESIS SUBMITTED IN FULFILMENT OF THE REQUIREMENTS FOR THE DEGREE OF DOCTOR OF PHILOSOPHY**

**DEPARTMENT OF CHEMISTRY**
**FACULTY OF SCIENCE**
**UNIVERSITI MALAYA**
**KUALA LUMPUR**

**2020**

**UNIVERSITY OF MALAYA**

**ORIGINAL LITERARY WORK DECLARATION**

Name of Candidate: **NAIMAH BINTI HARON**

Registration/Matric No: **SHC120076**

Name of Degree: **DOCTOR OF PHILOSOPHY**

Title of Thesis ("this Work"):

**MOLECULAR DYNAMICS SIMULATIONS OF PHASE BEHAVIOUR AND STRUCTURAL STUDIES OF GUANIDINIUM TRIFLATE IONIC LIQUID AND ITS MIXTURE WITH WATER AND *N*-METHYLDIETHANOLAMINE FOR CARBON DIOXIDE REMOVAL**

Field of Study:

**THEORETICAL AND COMPUTATIONAL CHEMISTRY**

I do solemnly and sincerely declare that:

(1) I am the sole author/writer of this Work;
(2) This Work is original;
(3) Any use of any work in which copyright exists was done by way of fair dealing and for permitted purposes and any excerpt or extract from, or reference to or reproduction of any copyright work has been disclosed expressly and sufficiently and the title of the Work and its authorship have been acknowledged in this Work;
(4) I do not have any actual knowledge nor do I ought reasonably to know that the making of this work constitutes an infringement of any copyright work;
(5) I hereby assign all and every rights in the copyright to this Work to the University of Malaya ("UM"), who henceforth shall be owner of the copyright in this Work and that any reproduction or use in any form or by any means whatsoever is prohibited without the written consent of UM having been first had and obtained;
(6) I am fully aware that if in the course of making this Work I have infringed any copyright whether intentionally or otherwise, I may be subject to legal action or any other action as may be determined by UM.

Candidate's Signature Date:

Subscribed and solemnly declared before,

Witness's Signature Date:

Name:
Designation:

**MOLECULAR DYNAMICS SIMULATIONS OF PHASE BEHAVIOUR AND STRUCTURAL STUDIES OF GUANIDINIUM TRIFLATE IONIC LIQUID AND ITS MIXTURE WITH WATER AND *N*-METHYLDIETHANOLAMINE FOR CARBON DIOXIDE REMOVAL**

## ABSTRACT

Molecular dynamics (MDs) simulations with an all-atom force field have been carried out to understand the phase equilibrium behaviour of aqueous guanidinium triflate [gua][OTf] ionic liquid (IL) (binary system) at 440.15 K, as well as the phase equilibrium behaviour of *N*-methyl diethanolamine (MDEA) with aqueous [gua][OTf] IL (ternary system) at 298.15 K. This work further elaborated the understanding of absorption mechanism of carbon dioxide ($CO_2$) into ternary system at 298.15 K. For binary system, the simulations measured changes in different physical properties such as density, structural, bonding properties (radial distribution function (RDF)), water clustering and hydrogen bonding) and dynamic property (diffusion coefficient (*D*)). It was observed that water molecules started to connect with one another and formed a large hydrogen bond network throughout the system with an increasing water molar fraction. While for the ternary system, it is shown that the molecular level is slightly affected by the presence of MDEA and [gua][OTf] molar fractions. For MDEA-water interactions in [gua][OTf] media, MDEA prefers to be surrounded by water molecules rather than by MDEA molecules even at high MDEA molar fraction. Meanwhile, for [gua][OTf]-water interaction in MDEA media, as [gua][OTf] molar fraction increases, more water molecules replace counterions in the coordination shell of both [gua] and [OTf] ions, thus weakening their interaction. On the other hand, for MDEA-[gua][OTf] interactions in water media, it is found that, as the molar fraction of [gua][OTf] increases, a sulfonate group from [OTf] ion appears to have a stronger association by making hydrogen bonding with MDEA molecules. For the absorption mechanism of $CO_2$ into a ternary system, the continuous increase of $CO_2$ concentration does not affect the structure of IL, but $CO_2$

molecules are always captured by the cavity of [gua] ion. Based on the physical properties of the ternary system, these ternary solvents can potentially be further studied to remove $CO_2$ using aqueous MDEA and IL at high pressure in the natural gas industry.

**Keywords:** Molecular dynamics simulation, guanidinium triflate ionic liquid, water microscopic physical properties, *N*-methyl diethanolamine; carbon dioxide capture.

**SIMULASI DINAMIK MOLEKUL BAGI TINGKAH LAKU FASA DAN KAJIAN STRUKTUR BAGI CECAIR IONIK GUANIDINIUM TRIFLAT DAN CAMPURANNYA DENGAN AIR DAN *N*-METILDIETANOLAMINA UNTUK PENYINGKIRAN KARBON DIOKSIDA**

## ABSTRAK

Simulasi dinamik molekul (MD) dengan medan kekuatan atom telah dijalankan untuk memahami fasa keseimbangan bagi cecair ionik (IL) guanidinium triflate [gua] [OTF] (sistem binari) pada 440.15 K, fasa keseimbangan bagi *N*- metildietanolamina (MDEA) dengan akueus [gua] [OTf] IL (sistem ternari) pada 298.15 K dan juga memahami mekanisma penyerapan karbon dioksida ($CO_2$) di dalam sistem ternari pada 298.15 K. Bagi sistem binari, simulasi mengkaji sifat perubahan seperti ketumpatan, struktur, sifat ikatan (fungsi edaran jejari, kluster air dan ikatan hidrogen) dan sifat dinamik (pekali peresapan sendiri). Didapati bahawa, molekul air mula bergabung antara satu sama lain dan membentuk rangkaian ikatan hidrogen yang besar di seluruh sistem apabila pecahan molar air yang semakin meningkat. Manakala untuk sistem ternari, kajian menunjukkan bahawa tahap molekul campuran ternari sedikit terjejas dengan kehadiran pecahan molar MDEA dan [gua] [OTf]. Untuk interaksi MDEA-air di dalam media [gua] [OTf], MDEA lebih suka dikelilingi oleh molekul air dan bukannya oleh molekul MDEA walaupun pada pecahan molar MDEA yang tinggi. Sementara itu, untuk interaksi [gua] [OTf]-air di dalam media MDEA, semakin meningkat pecahan molar [gua] [OTf], semakin banyak molekul air menggantikan ion penimbal di dalam rangka luar koordinasi kedua-dua ion, sehinggakan melemahkan interaksi antara mereka. Sebaliknya, untuk interaksi MDEA-[gua] [OTF] di dalam media air, didapati bahawa semakin meningkat pecahan molar [gua] [OTf], kumpulan sulfonat dari anion mempunyai hubungan yang lebih kuat dengan pembentukan ikatan hidrogen dengan molekul MDEA. Bagi mekanisma penyerapan $CO_2$ ke dalam sistem ternari, peningkatan berterusan kepekatan $CO_2$ tidak menjejaskan struktur cecair ionik, tetapi molekul $CO_2$ sentiasa terjerat dalam rongga kation

guanidinium. Berdasarkan sifat-sifat fizikal sistem ternari, pelarut ternari ini berpotensi dikaji lebih lanjut untuk penyingkiran $CO_2$ menggunakan MDEA dan larutan akueus IL pada tekanan yang tinggi di dalam industri gas semulajadi.

**Kata kunci:** Simulasi dinamik molekul, guanidinium triflat cecair ionik, air
sifat fizikal mikroskopik, *N*- metildietanolamina; penjerapan karbon dioksida.

## ACKNOWLEDGEMENTS

Alhamdullilah, praise to ALLAH s.w.t for His blessings, guidance and strength to finish this project and thesis. I would like also to express my heartfelt gratitude and indebtedness to my project supervisor, Dr. Nor Asrina Sairi, who gave me the opportunity to conduct this research, for her continuous guidance, patience, constructive criticism, invaluable advice and unreserved assistance throughout out this project. I am also indebted to my co-supervisors, Associate Professor Dr. Vannajan Sanghiran Lee for her invaluable guidance, encouragement and criticism, which kept me in a right track and also a very thanks to Dr. António M. Baptista (Instituto de Tecnologia Química e Biológica, Universidade Nova de Lisboa, Portugal) for his script and method for the calculations. Without these people, this thesis would not have been possible.

A special thanks to my parents (Haron Mohd Don and Hasiah Abu Bakar), my husband (Ezaideen Ahmad Lokman), my three princesses (Erynna Ezara, Emilia Sabrina and Eeva Medina), my siblings as well as other friends for all the support, contribution, hope and prayers for me to endure the obstacles that I have been through. I also would like to thank to University Malaya Center for Ionic Liquids (UMCiL) laboratory members in Faculty of Science, University of Malaya: Zati Ismah Ishak, Dazylah Darji, Nor Rahimah Said, Azlan, Kak Nora, Wan Melissa Wan Mazlan, Kumuthini Chandrasekaram and other labmates for their consistent support and assistance.

## TABLE OF CONTENTS

## LIST OF FIGURES

## LIST OF TABLES

## LIST OF ABBREVIATIONS AND SYMBOLS

| | | |
|---|---|---|
| $x$ | : | mole fraction |
| $x_w$ | : | water molar fractions |
| ε | : | epsilon |
| $\eta$ | : | viscosity |
| $\rho$ | : | density |
| σ | : | sigma |
| [BMIM][$BF_4$] | : | 1-butyl-3- methylimidazolium tetrafluoroborate |
| [BMIM][$NO_3$] | : | 1-butyl-3- methylimidazolium nitrate |
| [BMIM][$PF_6$] | : | 1-butyl-3- methylimidazolium hexafluorophosphate |
| [$C_2$mim][$NTf_2$] | : | 1-ethyl-3-methylimidazolium bis(trifluoromethylsulfonyl)imide |
| [gua][OTf] | : | guanidinium triflate |
| [$N_{4111}$] | : | butyltrimethylammonium |
| [$Tf_2N$] | : | bis(trifluoromethanesulfonyl)imide anion |
| AMBER | : | Assisted Model Building with Energy Refinement |
| B3LYP | : | Becke's three-parameter hybrid functional Lee Yang and Parr |
| $CH_4$ | : | methane |
| CHARMM | : | Chemistry at Harvard Macromolecular Mechanics |
| $CO_2$ | : | carbon dioxide |
| COM | : | Center Of Mass |
| $D$ | : | self-diffusion coefficient |
| DEA | : | diethanolamine |
| $g(r)_{aa}$ | : | radial distribution function for anion-anion |
| $g(r)_{ca}$ | : | radial distribution function for cation-anion |
| $g(r)_{cc}$ | : | radial distribution function for cation-cation |
| GAMESS | : | General Atomic and Molecular Electronic Structure System |

| | | |
|---|---|---|
| GROMACS | : | Groningen Machine for Computer Simulations |
| $H_2S$ | : | hydrogen sulphide |
| IL | : | ionic liquid |
| MDEA | : | *N*-methyldiethanolamine |
| $MD_S$ | : | Molecular Dynamics |
| MEA | : | monoethanolamine |
| MM | : | Molecular Mechanics |
| OPLS | : | Optimized Potential for Liquid Simulation |
| PEO | | poly(ethyleneglycol) dimethyl ether |
| $PF_6^-$ | : | hexafluorophosphate anion |
| PZ | : | piperazine |
| QM | : | Quantum Mechanics |
| *R(t)* | : | time correlation function |
| RDF, *g(r)* | : | Radial Distribution function |
| SDF | : | Spatial Distribution functions |
| $V_m$ | : | excess molar volume |
| VMD | : | Visual Molecular Dynamics |

## LIST OF APPENDICES

# CHAPTER 1: INTRODUCTION

## 1.1 Background study

$CO_2$ is one of the major greenhouse gas contributing to global warming (Moya et al., 2017). A set of technical, economic and environmental reasons supports the idea of $CO_2$ capture. This technology concerns the separation of $CO_2$ from gaseous stream either in combustion units as flue gas or in the natural gas treatment plants. One of the most common technologies used for capturing the $CO_2$ is an absorption-desorption process within which different kinds of physical and/or chemical solvents are used to separate $CO_2$ from gaseous streams (Rashidi & Yusup, 2016; Theo et al., 2016). This process takes place in two different process units usually called absorption and stripper columns. It has been common practice in $CO_2$ capturing to be done in transport and reaction-controlled absorption process, by employing aqueous solutions of alkanolamine mainly MEA, DEA and MDEA.

In industrial applications, an aqueous solution of MDEA is usually mixed with activators of fast reactivity, including MEA, piperazine (PZ) and DEA. Back in the 2000s, researchers started to explore IL as a solvent for $CO_2$ capture (Dai et al., 2016; Zeng et al., 2017; Zhang et al., 2016). Their researches focus on the solubilities and diffusivities of $CO_2$ in ILs as well as the viscosity of IL. ILs consists of an organic cation and either an inorganic or organic anion. ILs appeared as a new attractive solvent because of its almost zero volatility, which amongst other remarkable properties; make them suitable solvents for energy-efficient gas separations including further solvent regeneration (Dai et al., 2016; Kumar et al., 2014; Seo et al., 2014). Unfortunately, most ILs have drawbacks in $CO_2$ separation such as having relatively high viscosities in pure state (Aghaie et al., 2018). When it contacts with $CO_2$, the viscosity will increase dramatically and forming a gel-like substance.

This kind of viscosity will affect the transport properties such as diffusion. To increase $CO_2$'s solubility in ILs, amine-functionalized ILs are preferable (Qian et al., 2017; Uehara et al., 2018; Zeng et al., 2017). Functionalized ILs show both physical and chemical absorptions behaviour. Therefore, researchers have turned their interest towards functionalized ILs as solvents for $CO_2$ capture and acid gas removal rather than aqueous amine solvents ( Huang et al., 2018; Nematollahi & Carvalho, 2018; Uehara et al., 2018). Hence, the ternary system (MDEA – ILs – $H_2O$) for $CO_2$ capture was developed to lower the viscosity of ILs. Researches also discovered that the properties of [gua][OTf] IL make it an effective solvent, especially in the acid gas absorption process such as sulfur dioxide and $CO_2$ (Sairi et al., 2015). [gua][OTf] is one of the simple protic IL developed by Rusell et al. (1994). It was produced by combining guanidine hydrochloride with triflic acid using the Brønsted acid-base method. For [gua][OTf] IL, the Brønsted base acts as a proton receptor from the Brønsted acid and serves as a proton carrier in liquid.

Due to its importance and significant application in major industries, we had chosen [gua][OTf] IL to be the main subject for our studies. To make good use of this [gua][OTf] which has an amine group, we need to determine the relationship between structural and physical properties of binary and ternary aqueous systems. In conjunction with this work, MDs simulation used to achieve a better understanding of the phase behaviour of binary and ternary systems. MD simulations based on classical potentials have played an important role in helping researchers understand how the properties of these materials are linked to chemical structure and composition. Simulations have also predicted many properties and unexpected phenomena that have subsequently been confirmed experimentally. This research aims to investigate the phase behaviour, interactions and structural studies of binary and ternary systems. Besides, it will examine the effect of water on the physical properties (density, viscosity and $CO_2$ solubilities) and also understand the absorption mechanism of $CO_2$ into ternary system.

Moreover, analysis of the influence of the chemical structure of the [gua][OTf], MDEA and water molar fraction on the evolution of microstructures mixtures and transport properties such as self-diffusion coefficients in the mixtures as well as absorption mechanism of $CO_2$ into the ternary system are discussed in detail.

## 1.2 Problem statement

$CO_2$ has been considered as a major greenhouse gas contributing to global warming from time to time. In this situation, ILs are solvents that consist entirely of ions are usually considered as promising novel solvents for $CO_2$ capture applications (Theo et al., 2016; Zeng et al., 2017) due to their unique features such as negligible vapour pressure and high selectivity towards $CO_2$ over other gases such as $O_2$ and $N_2$ (Lei et al., 2014). Unfortunately, some pure ILs have a high melting point and more viscous if compared to other solvents. When ILs combine with either inorganic or organic compounds, such as edalkanolamine, their physical properties such as density and viscosity can be reduced (Gonzalez-Miquel et al., 2014; Malek & Ijardar, 2016). Therefore, a better understanding of the phase behaviour and structural studies of binary and ternary systems can be done using MD simulation before it can be applied for $CO_2$ capture application.

## 1.3 Scope of the research

MD simulation approach was chosen to investigate the phase behaviour, interactions and structural studies of binary and ternary systems as well as to understand the absorption mechanisms in a molecular scale for the ternary aqueous. These simulations are divided into three major different simulation sets; (1) MD simulation for binary systems (aqueous [gua][OTf]); (2) MD simulation for ternary systems ([gua][OTf]-water-MDEA); (3) mechanism studies for $CO_2$ removal using one of the ternary system (system b from ternary system) using MD simulation.

This required to step into the molecular modelling and QM world. Initially, a comprehensive literature review had to be done to specify the composition of the binary and ternary systems (Sairi et al., 2015) to determine the true concentration of each species inside the solution. In other words, this was necessary to approximate speciation of the mixture according to experimental determinations. The next step involved modelling of different molecules ($[gua]^+$, $[OTf]^-$, MDEA, water, $CH_4$ and $CO_2$) which have major attention inside the solution. This step required to select a suitable force field which fits the requirements of a liquid mixture. OPLS all-atom force field was chosen for this research. Thus, modelling of the molecules is based on quantum mechanical calculations to calculate the geometry optimization, dihedral angle investigation and partial atomic charge calculation. Once modelling part of the work was finished for molecules, MD simulation was performed for all major different simulation sets.

## 1.4 Research objectives

The main objective of this research is to theoretically understand the phase behaviour and structural studies of guanidinium triflate IL and its mixture with water and *N*-methyl diethanolamine for carbon dioxide removal. Therefore, the research was done with the following specific objectives:

1. To understand the phase behaviour and structural studies of pure and aqueous [gua][OTf] IL using RDF, SDF and self-diffusion coefficient.
2. To study how water affects the ion-pairing intrinsic to ILs using SDF and to investigate whether water percolates into IL using VMD and SDF.
3. To investigate the phase behaviour and structural studies of aqueous [gua][OTf] IL in MDEA media, aqueous MDEA in [gua][OTf] media as well as MDEA–[gua][OTf] in aqueous media using RDF, SDF and self-diffusion coefficient.

4. To understand the absorption of $CO_2$ into the ternary system (MDEA – [gua][OTf] - $H_2O$) using RDF.

## 1.5 Thesis outline

To accomplish all the objectives, several detailed studies were conducted and presented in the following chapters:

*Chapter 1: Introduction*

In this chapter, the research background, problem statements, objectives, the scope of work and layout of the thesis are described.

*Chapter 2: Literature review*

This chapter presents a study on structural and phase behaviour of IL and its mixtures with water and amine. Application of IL and its mixture with water and *N*-methyl diethanolamine for $CO_2$ removal were also reviewed.

*Chapter 3: Material and Methods*

This chapter explains methodology, limitations and assumptions information on the molecules used in this research. Principles of QM and detail description concerning the topic of MD simulation, concepts and computational techniques are also discussed.

*Chapter 4: Results and discussions*

Results and discussion are divided into subchapters in Chapter 4 as follows:

*4.1 Microstructures, interactions and dynamics properties studies of aqueous guanidinium triflate ionic liquid using molecular dynamics simulations.*

- This chapter reports on the phase equilibrium behaviour of ILs [gua][OTf] solution (binary solvent) at 7 different molar fractions of water ranged from 0.1 to 0.7 at 440.15 K using MD simulations with an all-atom force field.

*4.2 Microstructures, interactions and dynamics properties studies of MDEA + [gua][OTf] ionic liquid + water tertiary system at the standard temperature.*

- This chapter reports on the phase equilibrium behaviour of ternary aqueous mixtures containing [gua][OTf] IL and water mixed with MDEA in different function composition at the standard temperature of 298.15 K using MD simulations with an all-atom force field.

*4.3 Absorption $CO_2$ in MDEA + [gua][OTf] Aqueous Solution*

- This chapter reports on the use of MD simulations with an all-atom force field to understand the absorption of $CO_2$ from a binary mixture of $CO_2$ and $CH_4$ into ternary solution. The MD simulations were performed at a constant temperature of 298.2 K for five systems to provide insight into molecular distribution in the ternary solution and to enhance understanding of absorption mechanisms on the molecular scale.

*Chapter 5: Conclusions and recommendations*

Summaries of the findings in each objective are provided under this chapter. Furthermore, recommendations for future work are also provided.

# CHAPTER 2: LITERATURE REVIEW

## 2.1 Ionic Liquid

ILs is rapidly developing for the past two decades. From 1996 to 2018, the number of SCI papers published on ILs has increased simultaneously with the annual growth rates of other popular scientific areas including its application in chemistry, material science, chemical engineering and environmental science. Based on the unique properties, ILs have been further divided into many types, *e.g.,* room temperature ILs (Chatel & MacFarlane, 2014; Lei et al., 2017; Lei et al., 2014; Mai & Koo, 2016), task-specific ILs (Ruckart et al., 2015), and polyionic liquids (Qian et al., 2017; Rojas et al., 2014). Some typical structures of ILs are shown in Figure 2.1.

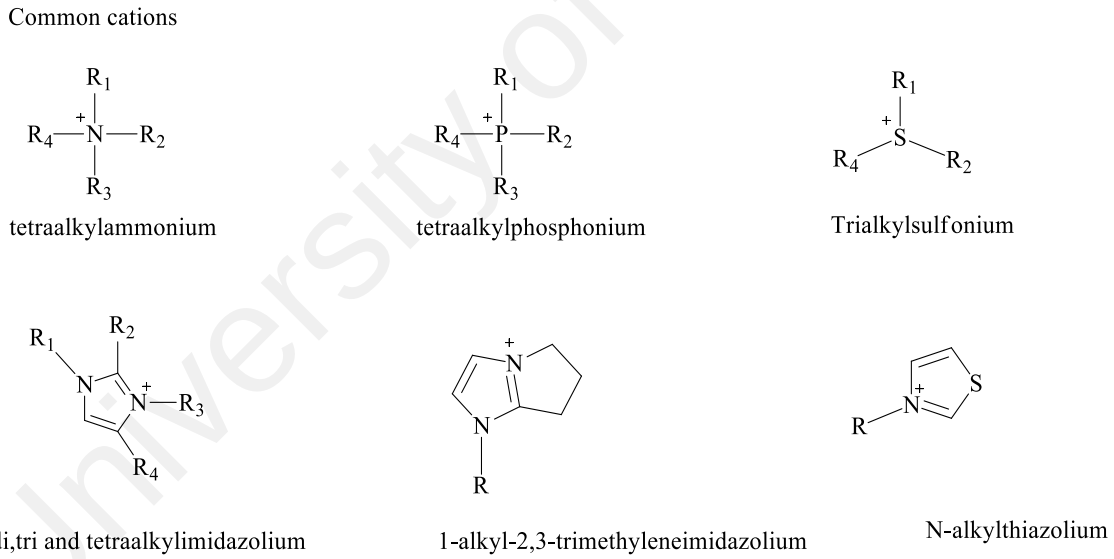


**Figure 2. 1:** Common cations and anions of ILs

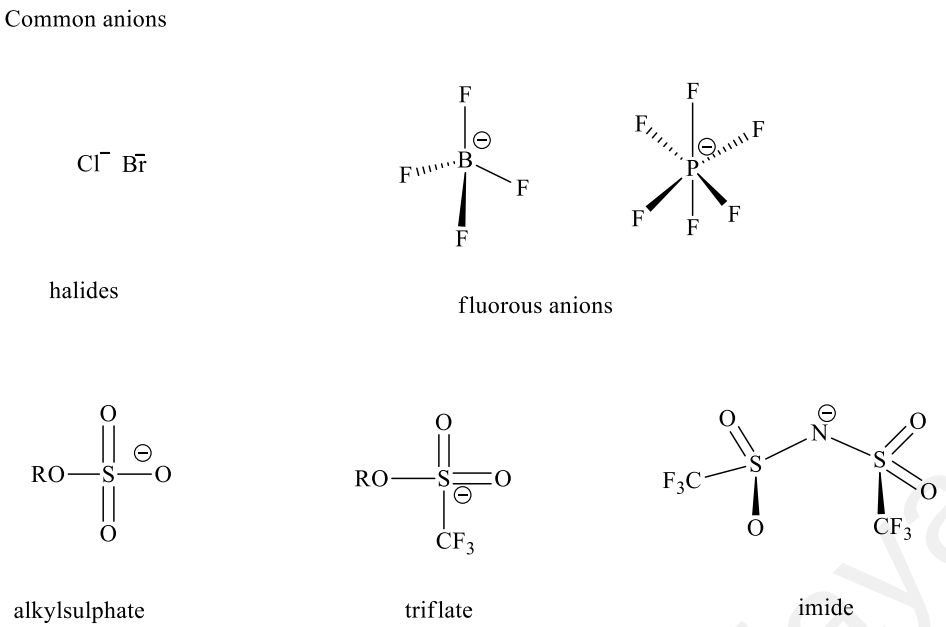


**Figure 2. 1,** continued.

The history of ILs started in 1914 when Paul Walden synthesized ethylammonium nitrate [$EtNH_3$][$NO_3$] with a melting point of 12 $^oC$ (Walden, 1914). The compound was developed by the military for usage in liquid propellants and now it is widely used in the structuring of surfactants and the study of protein folding (Walden, 1914). In 1948, the first IL with chloroaluminate anion which contains halide anion was patented by Hurley (Hurley, 1948). In the early 1970s and 1980s, the ILs that consist of alkyl-substituted imidazolium or pyridinium as cations and halides or trihalogenoaluminate as anions were regularly synthesized because these ILs are stable to water and air. Most ILs have some unusual physical properties *i.e.* reusability, eco-friendly nature, high thermal stability, lack of inflammability, low volatility, chemical stability and excellent solubility with many organic compounds (Lei et al., 2017; Zeng et al., 2017). As a result, ILs can act as solvents and also as greener alternatives to conventional organic solvents aimed at facilitating sustainable chemistry. ILs also is known as alternative green solvents because they have negligible vapour pressure and non-flammability.

Besides, they also immiscible with water and organic solvents which can produce two phases. ILs have currently been applied as promising solvents in organic synthesis (Canales & Brennecke, 2016; Larriba et al., 2016; Larriba et al., 2017; Nascimento et al., 2015; Ratti, 2014), catalysis (Mohamed et al., 2017; Płotka-Wasylka et al., 2017; Vekariya, 2017) and media for gas and liquid separations (Dai et al., 2016; Larriba et al., 2016; Theo et al., 2016; Zhang et al., 2015). The advantages of ILs is that they can be recycled and reused (Amado Alviz & Alvarez, 2017; Jing Lu et al., 2015; Rigual et al., 2017). Most ILs acts as designer solvents because their chemical and physical properties such as melting point, viscosity and density could be changed by altering the nature of the cation or anions pairs. Thus, ILs can be modified by changing the cation and the anion structures to justify the solvent requirements for $CO_2$ solubility in IL.

Based on the previous researches, the main factor controlling the $CO_2$ absorption capacity of ILs is the anion nature, which is fluorinated anions. These fluorinated anions, is the ones showing the highest $CO_2$ affinity $(BF_4]^-$, $[PF_6]^-$ or $[NTf_2]^-$) (Zhang et al., 2013). In 2011, Sairi et al. (2011) reported that aqueous [gua][OTf] has a lower density and viscosity in comparison with other aqueous ILs such as aqueous 1-hexyl-3-methylimidazolium bromide, aqueous butylpyridinium tetrafluoroborate and other pure ILs. [gua][OTf] IL developed by Russell et al. (1994) was poorly characterized by the structural point of view. The cation of IL consists of a guanidinium ion $[gua]^+$ to which a ternary amine moiety is covalently tethered.

## 2.2 Computational Chemistry

Computational chemistry, in general, refers to a mathematical description of chemistry that implemented with the usage of a computer. The term theoretical chemistry may be defined as a mathematical explanation of chemistry, whereas computational chemistry term is usually used when a mathematical method is sufficiently well developed that it can be automated for implementation on a computer (Cramer, 2013). Computational studies can be carried out to find a starting point for a laboratory synthesis or to assist in understanding experimental data, such as the position and source of spectroscopic peaks. Besides, computational helps to design more productive and efficient processes (Gorain et al., 2018; Katiyar & Jha, 2018; Miranda et al., 2018; Modarres et al., 2018), characterize new compounds and materials (Gillet et al., 2018) as well as to study the fundamental properties of atoms, molecules and chemical reactions (Huang et al., 2017; Reid et al., 2017; Sheridan et al., 2018).

Therefore, computer modelling can both support and predict experimental work. Complementary to experiments, computational modelling has provided reliable details into the nature of their interactions. Computational chemistry can also be used to study physical, chemical and biological phenomena (Gorain et al., 2018; Katiyar & Jha, 2018; Miranda et al., 2018; Modarres et al., 2018). There are two major important techniques in molecular modelling, namely QM and MM. Theoretical chemistry is often considered equal with quantum mechanics, whereas computational chemistry encompasses not only quantum mechanics but also molecular mechanics, minimization, simulations, conformational analysis and other computer-based methods for understanding and predicting the behaviour of molecular systems. Many of the problems that we would like to tackle in molecular modelling are unfortunately too large to be considered by quantum mechanical methods.

QM dealt with the electrons in a system, even some of the electrons are being ignored (as in the semi-empirical schemes). A large number of particles must still be considered and the calculations involved are time-consuming. Force field method (also known as molecular mechanics) ignores the electronic motions and calculates the energy of a system as a function of the nuclear positions only. Thus, MM was used to perform calculations on systems containing a significant number of atoms. In some cases, force fields can provide answers as accurate as of the highest level of quantum mechanical calculations, in a fraction of the computer time.

## 2.3 Molecular Dynamics Simulation

MD provides a huge amount of information about the conformational properties of molecular systems, and a way in which the conformation changes with time. Molecular modelling programs facilitated the analysis of such simulation by displaying the structural parameter of interest in a manner that enables the time dimension to be taken into account (Leach, 2001). MD consists of force solution of Newton's equations of motion. Simulation acts as a bridge between theory and experiment. A well-focused simulation may help one understand what is measured in the laboratory and test a postulated explanation at a fundamental level. In MD, successive configurations of the system are generated by integrating Newton's laws of motion. The result is a trajectory that specifies how the positions and velocities of the particles in the system varies with time. The trajectory is obtained by solving the differential equations embodied in Newton's second law (F=ma):

$$\frac{d^2x_i}{dt^2} = \frac{F_{x_i}}{m_i} \qquad (2.1)$$

Equation 2.1 describes the motion of a particle of mass $m_i$ along one coordinate ($x_i$) with $F_{xi}$ being the force on the particle in that direction (Leach, 2001).

Simulations have also predicted many properties and unexpected phenomena that have subsequently been confirmed experimentally. Computer simulation techniques can either support or complement an experimental work. Theoretical studies such as MD simulations have been proven useful and indispensable in establishing the relationship between structures and properties of binary and ternary solvents. Molecular-based computer simulations can either support or complement an experimental work. Several computational studies of the properties of pure ILs, ILs/water and amines/water mixtures have been reported in many years dealing with thermodynamic and structural properties and single-particle dynamics.

## 2.4 Molecular Mechanics Force Field

In science, any calculation of a model must be constructed based on a real model. The empirical approach gives a more accurate estimation of weak long-range attractions called dispersion terms. It is an empirical potential energy function that models the main interactions found on a molecular system including bond, angles, dihedral, Coulomb, van der Waals. Determination on the behaviour of the molecules by calculating the energies based on a potential energy function or force field (Leach, 2001) is shown in Equation 2.2 and Figure 2. However, if the force field is designed primarily to treat large systems, such as protein or deoxyribonucleic acid, the functional forms are kept as simple as possible. This means that only harmonic functions are used for $E_{bond}$ and $E_{angle}$ (or these terms are omitted, forcing all bond lengths and angles to be constant), no cross-terms are included, and the Lennard-Jones potential is used for $E_{vdw}$ (Jensen, 2016).

$$v(r^N) = \sum_{bonds} \frac{k_a}{2} (l_i - l_0)^2 + \sum_{angles} \frac{k_b}{2} (\theta_i - \theta_{i,0})^2 + \sum_{dihedral} \frac{Vn}{2} (1 + \cos(n\omega - \gamma)) + \sum_{i=1}^{Na} \sum_{j=i+1}^{Nb} \left( 4\varepsilon_{ij} \left[ \left( \frac{\sigma_{ij}}{r_{ij}} \right)^{12} - \left( \frac{\sigma_{ij}}{r_{ij}} \right)^{6} \right] + \frac{q_i q_j}{4\pi\varepsilon_0 r_{ij}} \right) \quad (2.2)$$

where $v(r^N)$ denotes the potential energy which is a function of the positions ($r$) of $N$ particles (usually atoms). The stretching energy equation is based on Hooke's law. The $k_a$ value is the stretching constant of a bond which controls the stiffness of the bond string, while $l_0$ is the reference value of the bond. The bending energy equation also based on Hooke's law. The $k_b$ value is the stretching constant of the angle which controls the stiffness of the angle spring, while $\theta_{i,0}$ is the reference value of the angle. The $V_n$ value is often referred to as the 'barrier' height. $n$ is the multiplicity; its value gives the number of minimum points in the function as the bond is rotated through 360°. $\gamma$ (phase factor) determines where the torsion angle passes through its minimum value. $\omega$ is torsion angle. $N_a$ and $N_b$ are the numbers of point charges in the two molecules. $q$ (charge) control the depth and position (interatomic distance) of the potential energy well for a given pair of non-bonded interacting atoms. $\sigma_{ij}$ determines the degree of 'stickiness' and 'hardness' of the atoms in van der Waals attraction. $\varepsilon_0$ is the dielectric constant in a vacuum. $r_{ij}$ is the distance between two atoms.

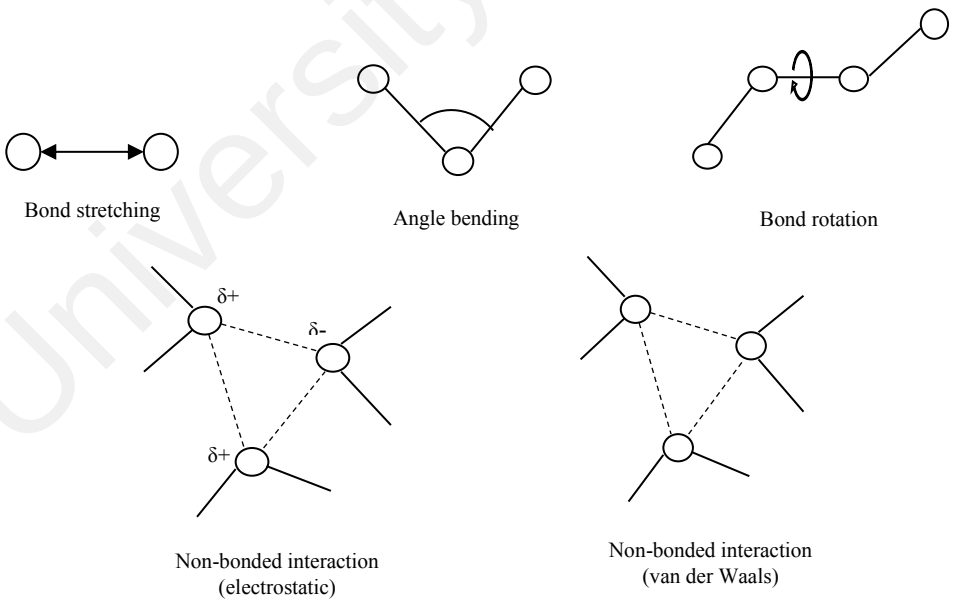


**Figure 2. 2:** Schematic representation of the four key contributions to a molecular mechanics force field: bond stretching, angle bending, dihedral terms and non-bonded interactions

Force fields designed for treating macromolecules can be simplified by not considering hydrogen explicitly known as united atom approach (an option present in for example the AMBER, CHARMM and GROMOS force fields). The main advantage of force field methods is the speed with which calculations can be performed, enabling a large system to be simulated. Even with a desktop personal computer, molecules with several thousand atoms can be optimized. This puts the applications in the region of modelling biomolecular macromolecules, such as proteins and deoxyribonucleic acid, and molecular modelling is now used by most pharmaceutical companies. The ability to treat a large number of particles also makes force filed models the only realistic method for performing simulations where solvents effects or crystal packing can be studied (Jensen, 2016).

## 2.5 Molecular Dynamic of Aqueous IL (Binary System)

ILs are designed by changing the nature of their cation or anion, or through the mixing and matching of different ion pairs. ILs are also known as "designer solvents" since their physical properties can be altered by changing the nature of their cation or anion, or through the mixing and matching of different ion pairs. When ILs combine with either inorganic or organic compounds, especially water, they become extremely important in various applications (Hegde et al., 2016; Saha & Mukherjee, 2018; Yaghini et al., 2015). The presence of water modified the characteristics of ILs including alteration of fundamental properties such as density, viscosity, and heat capacity (Haron et al., 2017; Hegde et al., 2016; Kaneko et al., 2018; Reid et al., 2017; Sharma & Ghorai, 2016; Yaghini et al., 2015). Interaction between different types of ILs and water are important and cannot be avoided (Kaneko et al., 2018; Sharma & Ghorai, 2016) because ILs absorb a large amount of water from the atmosphere (Hegde et al., 2016; Reid et al., 2017).

The roles of cation and anion in ILs remain undeveloped, for instance, the studies on hydrogen bonding degrees within bulk mixtures which have not been explored (Hegde et al., 2016; Reid et al., 2017; Sharma & Ghorai, 2016; Yaghini et al., 2015). However, the emergence of computational based dynamics simulations in recent years provided critical information on the properties of ILs with water (Haron et al., 2017; Kaneko et al., 2018; Reid et al., 2017; Sharma & Ghorai, 2016; Yaghini et al., 2015) at its atomistic level. Several research groups have also shared their findings and research topics related to the binary mixture of ILs-water structure and dynamics studies with the presence of water. Sharma and Ghorai (2016) investigated the properties (structure, thermodynamics, ion transport and dynamics) of pure and aqueous hydrophobic [BMIM][$PF_6$] IL using MD simulation. They found that water does not affect dissociated ions in pure [BMIM][$PF_6$] IL even at low concentration of water since $PF_6$ anion is hydrophobic in nature (see Figure 2.3). However, based on Figure 2.4, water has more affinity towards the fluorine atom of anion rather than imidazolium cation by hydrogen bonding interaction.

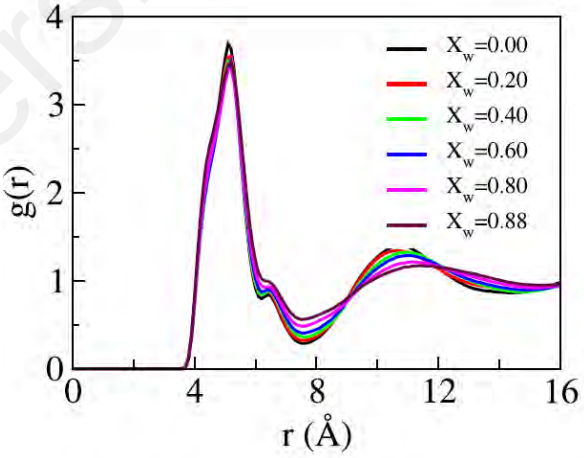


**Figure 2. 3:** RDFs between imidazolium ring and anion as a function of $x_w$ (Sharma & Ghorai, 2016)

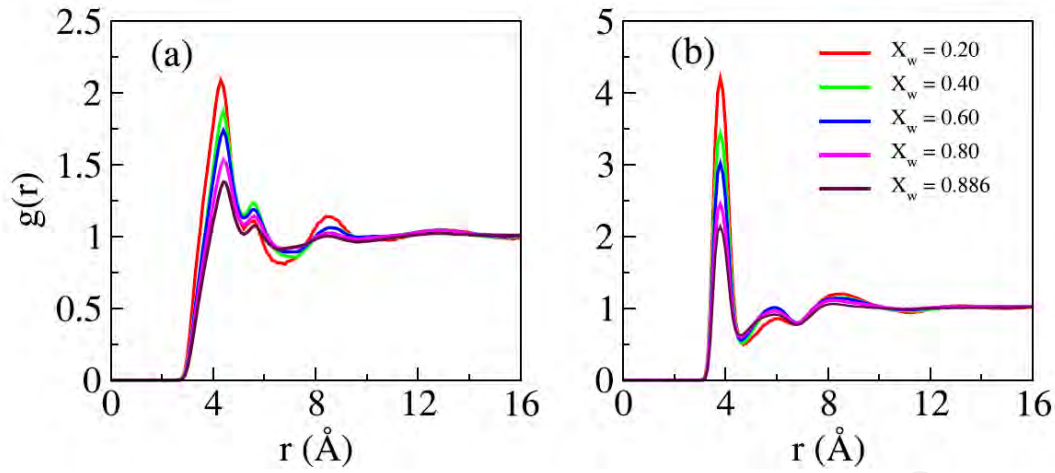


**Figure 2. 4:** RDFs as a function of $x_w$: (a) Head–water COM and (b) anion-water COM (Sharma & Ghorai, 2016)

MD simulations of ILs and its mixture with water such as imidazolium-based acetate IL with differing chain lengths with water (Hegde et al., 2016), imidazolium-based tetrafluoroborate with differing chain lengths with water (Kaneko et al., 2018) and MDEA paired with aqueous [gua][OTf] (Haron et al., 2015) have shown that when water is added at very small concentrations it situates at interstitial sites between the anion and cation, mainly coordinating to the anion and disrupting the cation-anion association. For these researches, authors have used QC calculation and MD simulations in their work. QC calculation was used to study the specific interaction between the ions and water.

In addition, *i.e.* MD simulations, were used to accurately determine the spatial correlations at nanometer scale. In order to gain a better understanding about interaction between ILs and water, Haron et al., (2017) studied the phase equilibrium behaviour of aqueous [gua][OTf] at 7 different molar fractions of water ranged from 0.1 to 0.7. They observed that, water molecules intercalated in the coordination shell of both ions, thus weakening their electrostatic interaction. Besides, they also proved that water molecules started to connect and formed a large hydrogen bond network throughout the system with the increasing water molar fraction. Reid et al. (2017) also studied the interaction between protic IL with water and aprotic IL with water.

They noticed that the sensitivity of these ILs to water affects their physical and chemical properties, even at relatively low concentrations. Therefore, they used the rigorous Kirkwood−Buff theory of solutions to interpret the data. They concluded that aprotic IL shows stronger interactions with water at low water concentrations rather than protic IL having stronger water−ion interactions at higher water contents, despite water−ion interactions weakening with increasing water content in both systems. Huang et al. (2017) reported the unique behaviour of protic IL-water mixtures at a molecular level. Based on Figure 2.5, the first peaks of anion−water, cation−water, and water−water RDFs decreasing with increasing the concentration of water. The peak height of cation−anion RDF based on different water mole fraction is very sharp compared to other kinds of RDFs, suggesting the interactions between anions and cations are the strongest due to the presence of both electrostatic interactions and hydrogen bonds between them. Besides, cation−anion pairs are preferred to aggregate together at high water concentrations.

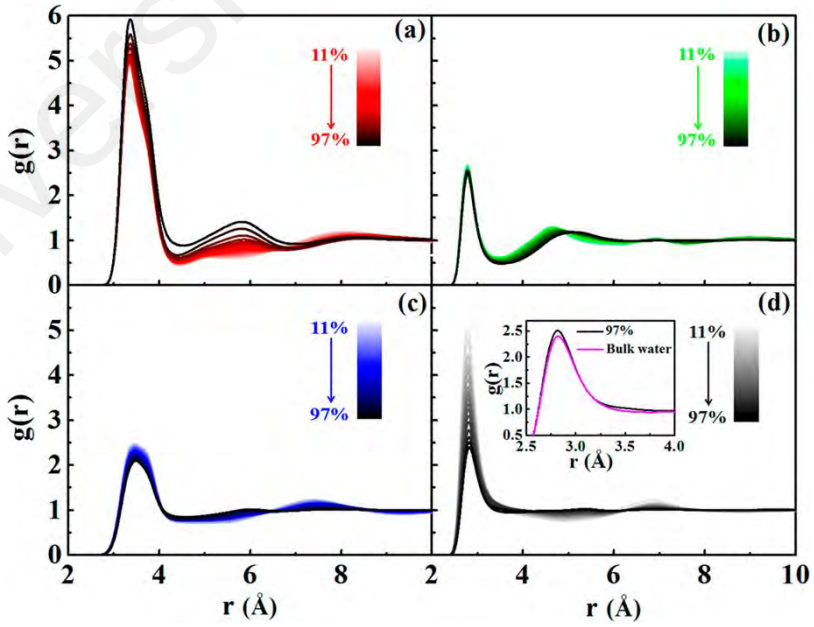


**Figure 2. 5:** RDF curves of (a) cation−anion, (b) cation−water, (c) anion−water, and (d) water−water in ethylammonium nitrate −water mixtures with different water mole fractions, $x_w$ (%) (Huang et al., 2017)

Figure 2.6 proved that hydrogen bond behaviour of ethylammonium nitrate protic IL with water can weaken with increasing water concentration by considerably all $NH_3^+$ - $NO_3^-$ , $NH_3^+$ - $H_2O$, $NO_3^-$ - $H_2O$ and $H_2O$-$H_2O$. The order of hydrogen bond strength is $NH_3^+$ - $NO_3^-$ > $NO_3^-$ - $H_2O$ > $NH_3^+$ - $H_2O$ > $H_2O$-$H_2O$.

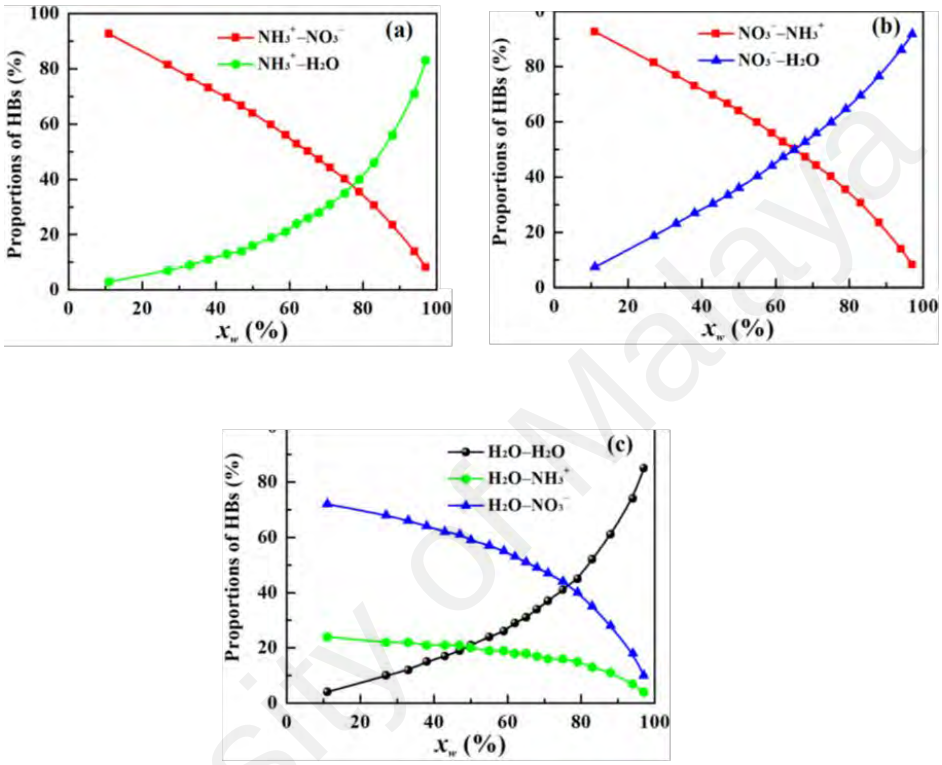


**Figure 2. 6:** Proportions of different HBs with (a) cations, (b) anions, and (c) water molecules in EAN−water mixtures as a function of water mole fraction, $x_W$ (%) (Huang et al., 2017)

## 2.6 Molecular Dynamic of ternary IL (ternary system)

ILs have currently been applied as promising solvents in organic synthesis (Canales & Brennecke, 2016; Larriba et al., 2016; Larriba et al., 2017; Nascimento et al., 2015; Ratti, 2014), catalysis (Mohamed et al., 2017; Płotka-Wasylka et al., 2017; Vekariya, 2017) and media for gas and liquid separations (Dai et al., 2016; Larriba et al., 2016; Theo et al., 2016; Zhang et al., 2015). However, their relatively high cost and viscosities in comparison with classic solvents, as well as the effect of impurities on their properties, have resulted in limited commercial use to date.

Therefore, researchers have turned out their interest to mix ILs with organic solvents in order to decrease the viscosity and cost, even if this leads to the vapor pressure of these mixtures increasing with the organic solvent concentration (Gonzalez-Miquel et al., 2014; Malek & Ijardar, 2016). For instance, high priced and viscous IL could be mixed with lower price and less viscous solution, *e.g* amine (Nookuea et al., 2017). Nookuea et al. (2017) studied the effect of temperature and concentration of [BMIM][$BF_4$] on the viscosity of MDEA–[BMIM][$BF_4$] aqueous solution. They found that the viscosity of MDEA–[BMIM][$BF_4$] aqueous solution was directly proportional with the concentration of [BMIM][$BF_4$] but inversely proportional with temperature (see Figure 2.7).

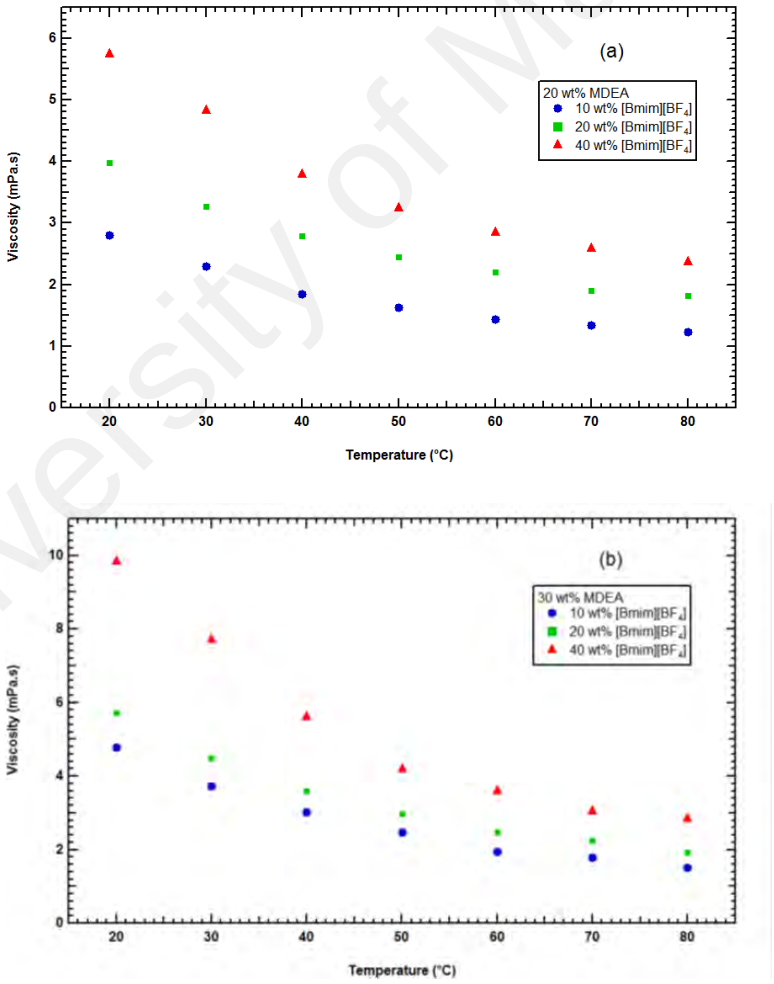


**Figure 2. 7:** Viscosity of MDEA–[Bmim][$BF_4$] aqueous mixtures as a function of temperature at (a) 20 wt% of MDEA, (b) 30 wt% of MDEA and (c) 40 wt% of MDEA (Nookuea et al., 2017)

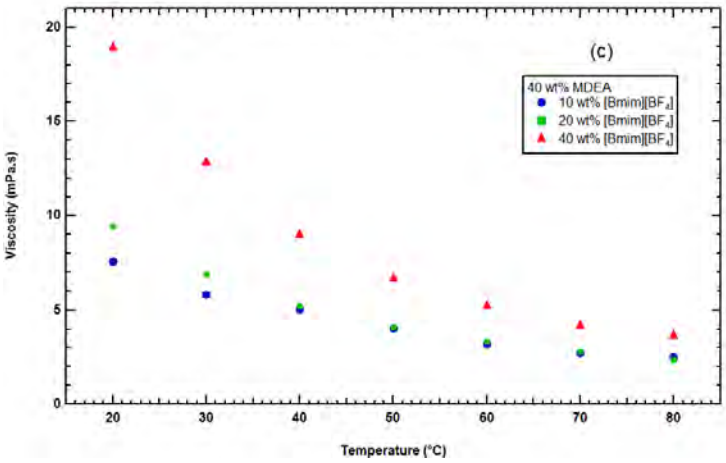


**Figure 2. 7,** continued.

Moreover, a large number of possible ternary mixtures could be prepared by mixing targeted ILs with different amines. When ILs mixed with amine, they are expected to encompass environment-friendly characteristics. While, when ILs and amines are combined, they give a better performance than amine-functionalized ILs. Based on plant experience and laboratory data, the relative corrosivity of amines is ranked as follows: MEA > DEA > MDEA (DuPart et al., 1993). Thus, MDEA is prominent among others, due to its unique properties *i.e* less corrosive behaviour, resistance to chemical and thermal degradation and low vapour pressure (Songolzadeh et al., 2014).

For ILs to be applied in industrial processes, a good understanding of phase behaviour and solvent-solute interactions are crucial. Molecular-based computer simulations could be used to predict properties of interest and identify a ternary system for experimental testing, thereby avoiding the impracticality of performing experiments on a large number of different liquids. Several computational studies of the properties of pure ILs, ILs/water and amines/water mixtures have been reported in many years, dealing with thermodynamic and structural properties and single-particle dynamics. For example, Orozco et al. (2014) used MDs simulation to study the mixture properties and structural analysis of aqueous solutions of amines and alkanolamines. They found that amines at all concentrations favour being surrounded by water molecules rather than by amine molecules (see Figure 2.8).

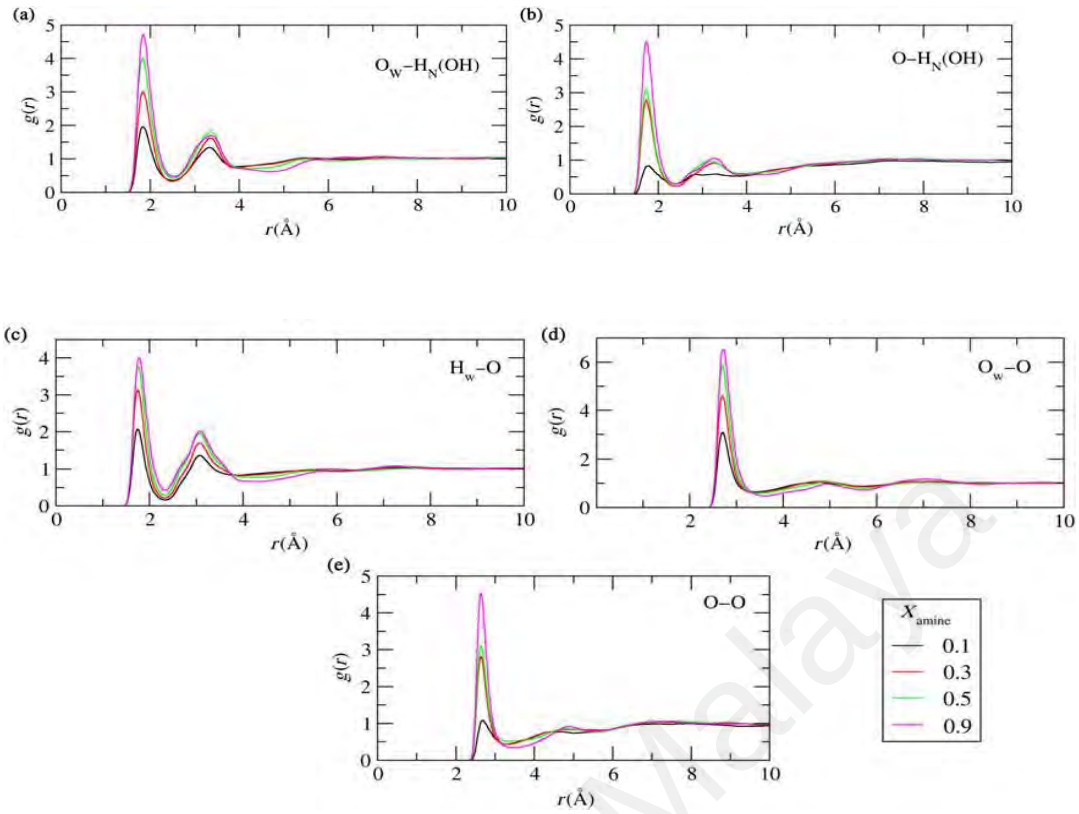


**Figure 2. 8:** Intermolecular radial distribution function water + MDEA at 313K and atmospheric pressure. $O_W$ and $H_W$ refer to oxygen and hydrogen of water, O and $H_N$(OH) refer to oxygen and hydrogen belonging to the hydroxyl group of the alkanolamine molecule (Orozco et al., 2014)

Fu et al., (2016) reported the solubility of water in the hydrophobic IL 1-ethyl-3-methylimidazolium bis(trifluoromethylsulfonyl)imide ([$C_2$mim][$NTf_2$]) increased significantly in the presence of $HNO_3$. They found that [$C_2$mim][$NTf_2$] was completely miscible with $HNO_3$, unfortunately, immiscible with water. Therefore, they used MD simulation to investigate the interaction between [$C_2$mim][$NTf_2$], $HNO_3$ and water. It was found that $NO_3^-$ ions interact with both $[C_2mim]^+$ and water via H-bonding and act as a bridge to induce a large amount of water to be dissolved in the hydrophobic IL phase. Haron et al., (2015) also used molecular dynamics simulations with an all-atom force field to understand the phase equilibrium behaviour of ternary mixtures containing [gua][OTf] and water mixed with MDEA in different function composition at standard temperature of 298.15 K.

The analysis of structural and dynamic properties showed that the molecular level of ternary mixtures was slightly affected by the presence of MDEA and [gua][OTf] molar fractions. Based on Figure 2.9, for MDEA–[gua][OTf ] interactions in water media, they noticed that as the molar fraction of [gua][OTf ] increases, a sulfonate group from anion appeared to have a stronger association by making hydrogen bonding with MDEA molecules. Besides, the mobility of MDEA and rotation of MDEA's alkyl chain easily rotate in mixing IL with water, unfortunately, is very difficult to rotate in pure IL.

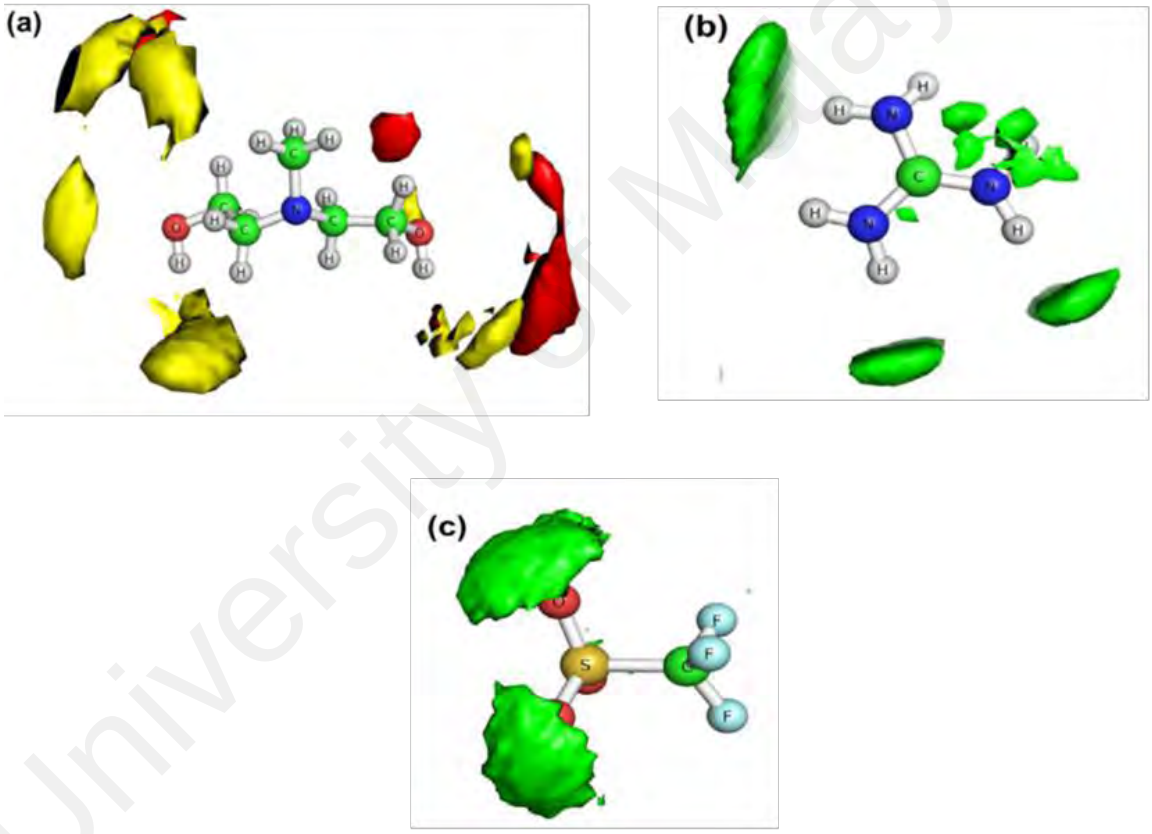


**Figure 2. 9:** SDF: (a) $[gua]^{+}$ ions (red cap) and $[OTf]^{-}$ ions (yellow cap) around MDEA molecule; (b) MDEA (green surfaces) around [gua]+ ion; (c) MDEA (green surfaces) around $[OTf]^{-}$ ion (Haron et al., 2015)

## 2.7 Carbon Dioxide Absorption in Ternary Systems Using Molecular Dynamics Simulation

Nowadays, one of the most crucial challenges for the industry is to find alternatives that improve the energy efficiency of processes and suitability. The processes where gas separations are present normally require a vast use of energy. Yet, a huge amount of pollutant gasses such as $CO_2$, $CH_4$, nitrous oxide, sulphur dioxide, carbon monoxide and all kind of volatile organic hydrocarbons, has been emitted since the beginning of industrialization. The sectors that carry out a considerable amount of gas separation processes are the oil and gas production, refining industry, chemical industry and energy producers. Therefore, gas separation processes became a key operation for diminishing the conventional greenhouse contaminant gases and improving energy balance in the industry. The efficiency of these two acid gases separation by gas absorption can be enhanced by finding low volatile solvents that require less energy for regeneration and exhibit high thermal stability.

For many years until now, amine absorption towers, have been applied in natural gas processing to remove $CO_2$ and hydrogen sulphide ($H_2S$) sour gases, are the best obtainable technology for performing post-combustion $CO_2$ capture from coal-fired power plants (Dutcher et al., 2015; Sheridan et al., 2018). The main reasons why amine is used as $CO_2$ removal because the reaction of $CO_2$ with amines occurs based on 1:2 $CO_2$/amine reaction stoichiometry. However, when amines mixed with 70% of water, it will cause significant parasitic energy loss in the regenerator (Kar et al., 2018; Shi et al., 2014; Zhang et al., 2017). Over the last two decades, most of the researchers have turned their interest to use amine solution mixed with IL as a solvent for $CO_2$ removal. Most of the ILs can be reused and recycled. These attractive properties could lead the way to clean gas separation technologies that eliminate emissions of the liquid absorbent into the atmosphere.

The advantages of blended aqueous amine solution and IL as a solvent for $CO_2$ capture are the extremely low volatility, low heat capacity and high thermal stability (Yang et al., 2014). Akhmetshina et al., (2017) studied the absorption of acid gases ($H_2S$ and $CO_2$) by 2-hydroxyethylammoium (MEA)-protic ILs at various temperatures and partial gases pressures. They observed that absorbents based on the 2-hydroxyethylammonium cation, performed high absorption properties toward the $H_2S$. Computer simulations have verified boundless potential in understanding the fundamental behaviour of ILs from molecular interactions such as the design of amines or ILs that chemically bind $CO_2$ as well as the design of optimal ILs for $CO_2$ separations. Back in the 2000s, there are some works of literature reported the properties of IL-$CO_2$ systems from a microscopic view of molecular interactions and molecular structures.

Most of these researchers have greatly developed the research of IL-$CO_2$ systems from the microscopic view. Xu et al. (2014) investigated 1-butyl-3- methylimidazolium nitrate ([BMIM][$NO_3$]) and [BMIM][$PF_6$] ILs at different concentration react with $CO_2$ systems from the aspect of molecular interactions and molecular structures. They found that the addition of $CO_2$ had influenced the properties of ILs. For example, the addition of $CO_2$ significantly decreases the viscosity of [BMIM][$NO_3$] and [BMIM][$PF_6$] (see Figure 2.10) and increase their diffusion coefficient (see Table 2.1). These two properties will be helpful for its applications in some fields which are restricted by the high viscosity.

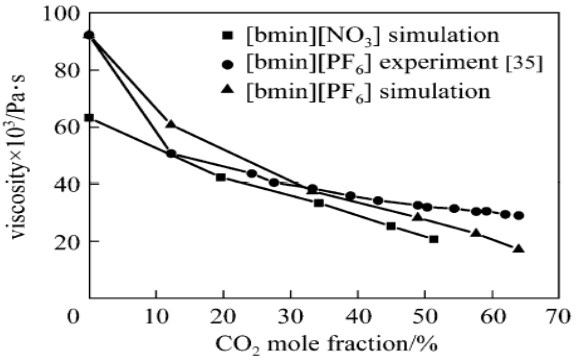


**Figure 2. 10:** Viscosity of [BMIM][$NO_3$] and [BMIM][$PF_6$] with the increase of the mole fraction of $CO_2$ (Xu et al., 2014)

**Table 2. 1:** Diffusion coefficient of ILs and $CO_2$ (Xu et al., 2014)

| ILs | $x_{CO_2}$ | $D_{CO_2}$ x $10^{10}/m^2s^{-1}$ | $D_{ILs}$ x $10^{10}/m^2s^{-1}$ |
|---|---|---|---|
| [bmim][$PF_6$] | 0 | — | 7.50 |
| | 0.123 | 1.47 | 7.70 |
| | 0.333 | 2.49 | 21.10 |
| | 0.490 | 4.17 | 26.50 |
| | 0.576 | 6.74 | 41.30 |
| | 0.639 | 12.88 | 59.30 |
| [bmim][$NO_3$] | 0 | — | 13.67 |
| | 0.200 | 1.59 | 14.17 |
| | 0.342 | 2.13 | 17.17 |
| | 0.451 | 3.90 | 23.50 |
| | 0.512 | 5.34 | 61.40 |

**Note**: $x_{CO_2}$ refers to the mole fraction of $CO_2$ in IL-$CO_2$ mixtures. $D_{CO_2}$ and $D_{ILs}$ refer to difussion coefficient of $CO_2$ and IL in IL-$CO_2$ mixtures, respectively.

Yang et al., (2014) used MEA mixed with [BMIM][$BF_4$] IL as a solvent for $CO_2$ capture to decrease the energy consumption and operating cost of $CO_2$ capture from low-pressure flue gas streams of power plants. Simulation data showed that the energy consumption of the mixed ionic liquid solution for absorbent regeneration was 37.2% lower than that of aqueous MEA solution. While, the MEA loss per ton of captured $CO_2$ for the mixed solution was 1.16 kg, which is much lower than that of 3.55 kg for the aqueous amine solution. Bernard et al., (2016) used MD simulations to understand corrosion and $CO_2$ absorption behaviour of the mixed IL-amine solutions. The absorption tests were performed at 318.15 K under 0.1−2.7 MPa.

As a result, the addition of [BMIM][$BF_4$] IL in aqueous alkanolamine solutions reduces the corrosion rate for MEA by up to 72%. Based on the simulations data, [BMIM][$BF_4$] appeared in the gas capture through H-bonding, even though the number of amine molecules was enough to capture all supplied $CO_2$ molecules. Cardoso et al., (2018) studied the properties of [$N_{4111}$][$NTf_2$], with PEO as $CO_2$ absorbers using MD simulation. Based on Figure 2.11 proved that $CO_2$ molecules are mainly located close to the oxygen and fluorine atoms of $NTf_2^-$. While, RDF graphs from Figure 2.12 showed that, the stronger interactions of $CO_2$ with $NTf_2^-$ happen between the oxygen and fluorine atoms of $NTf_2^-$. Therefore, $CO_2$ more soluble with $NTf_2^-$ rather than $N_{4111}^+$ and PEO.

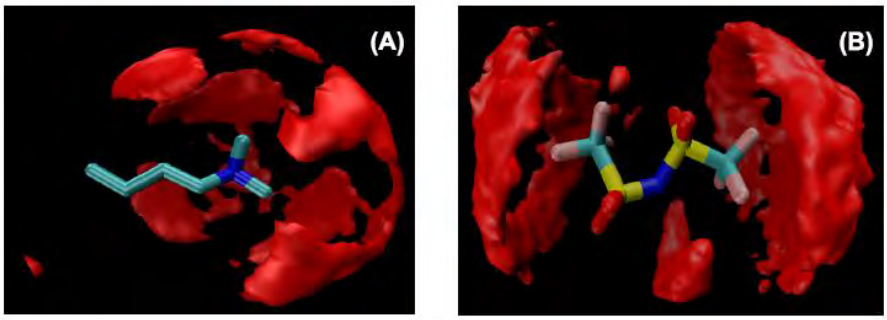


**Figure 2. 11:** Spatial distribution functions of $CO_2$ around (a) $N_{4111}^+$ (b) $NTf_2^-$ (Cardoso et al., 2018)

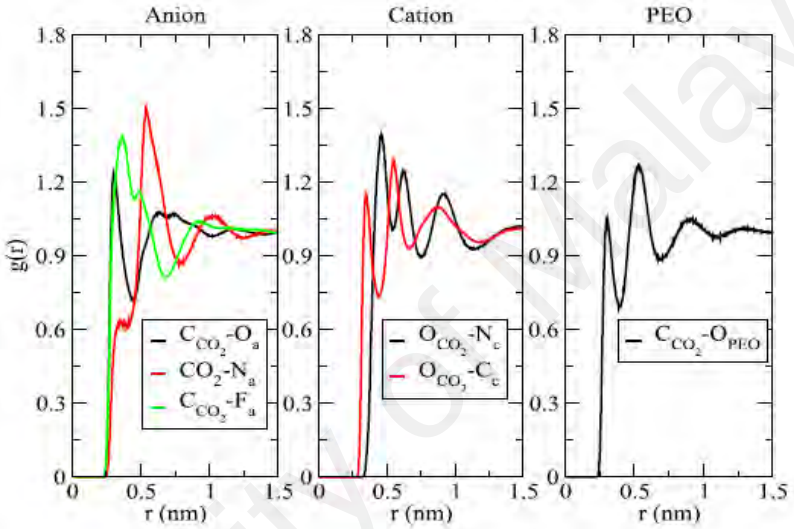


**Figure 2. 12:** Partial radial distribution functions of $CO_2$ in $[N_{4111}][NTf_2]$ and in $PEO_{1000}$ (Cardoso et al., 2018)

Harun & Masiren (2017) studied the absorption of $CO_2$ into aqueous solutions containing piperazine and MDEA from molecular level point of view to improve $CO_2$ removal process using amine-based solvents to be more energy efficient, reduce losses and corrosion. The strength of intermolecular interaction will represent the effectiveness of absorption process. MDEA cannot react directly with $CO_2$ due to the lack of hydrogen atom at amino group. Based on Figure 2.13- Figure 2.15, they found that there is strong intermolecular interaction between MDEA and $CO_2$ in blended MDEA/piperazine system. The presence of activator amine, piperazine, improved the intermolecular interaction of MDEA with $CO_2$.

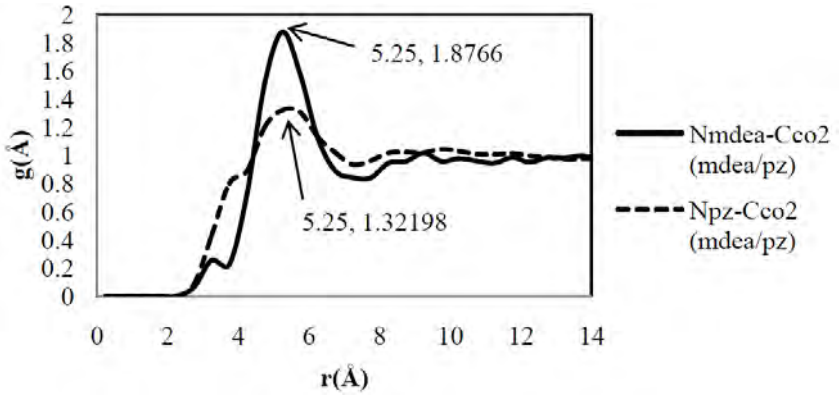


**Figure 2. 13:** Intermolecular interaction of (a) MDEA and water (b) PZ and water for tertiary system of blended MDEA/PZ (Harun & Masiren, 2017)

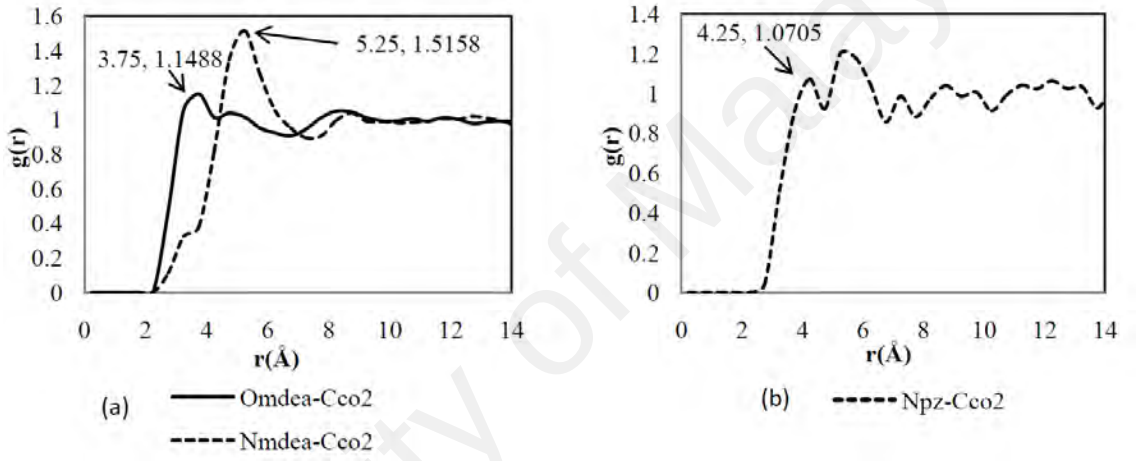


**Figure 2. 14:** Intermolecular interaction of amine and $CO_2$ in tertiary system using (a) MDEA and (b) PZ solution (Harun & Masiren, 2017)

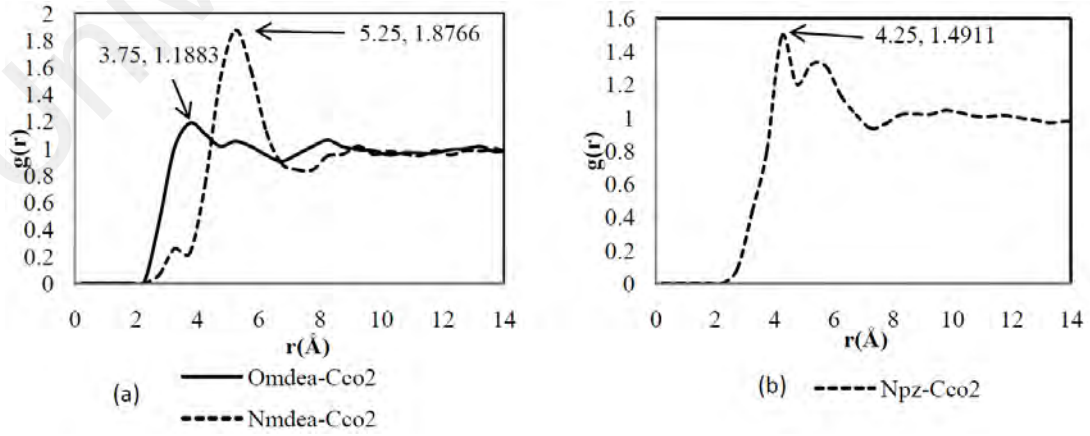


**Figure 2. 15:** Intermolecular interaction of (a) MDEA and $CO_2$ and (b) PZ and $CO_2$ for tertiary system of blended MDEA/PZ (Harun & Masiren, 2017)

# CHAPTER 3: MATERIALS AND METHODS

Most computational chemistry methods involve two major groups. The first group is QM which dealt with the electrons in a system. QM is still considered even for the electrons with a large number of particles. Also, geometry optimization and force field parameterization were involved in this calculation. The second group is MM which was used to perform calculations on systems containing a significant number of atoms. MD simulations were also involved in this calculation. As a final point, the calculation must be analyzed, not only to calculate properties but also to check that it has been performed properly. Therefore, three different methodologies were applied in this research, first for binary systems, secondly for ternary systems and the final one is a mechanism study for $CO_2$ removal in a ternary system (system *b* from the ternary systems) using MD simulation. The general methodologies are summarized in Figure 3.1.

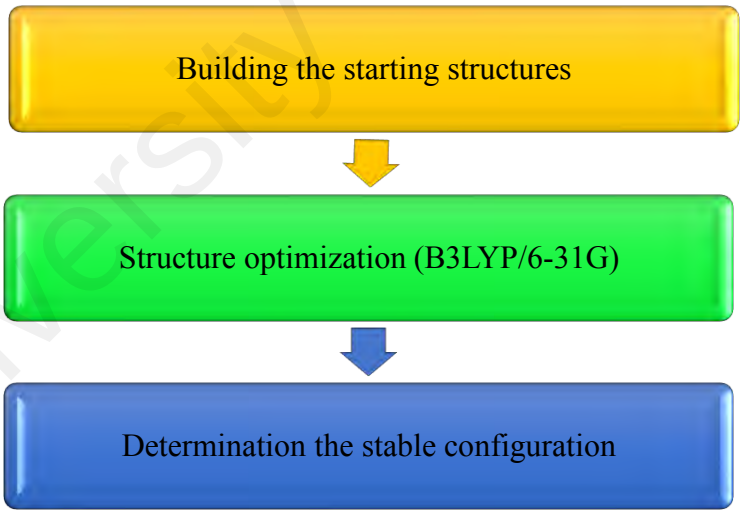


(a) Chronology indicating steps of geometry optimization using MacMolPlt and winGAMESS

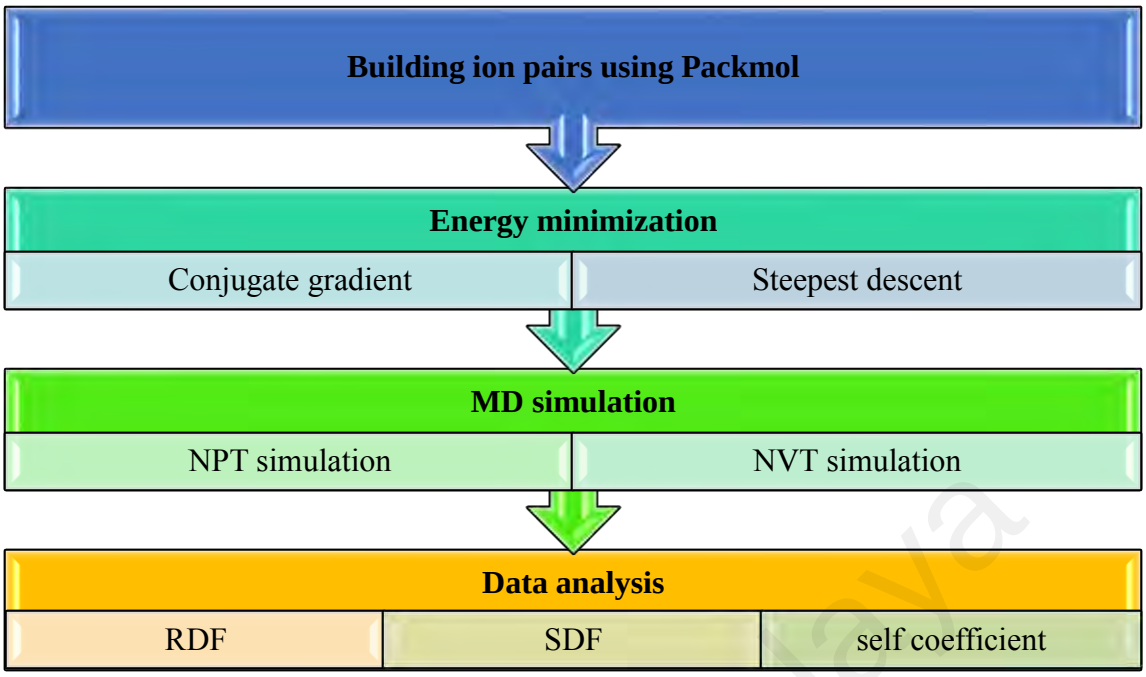


(b) Chronology indicating steps for molecular dynamics simulations

**Figure 3. 1:** General steps involved in the project

## 3.1 Hardware and software

### 3.1.1 Hardware

A Dell Precision Workstation equipped with Intel® Xeon® Processor, 12 GB of DDR2-RAM memory, and 1.5 TB of Hard Disk. The operating system in used was Ubuntu 14.04.2 LTS, with MPICH v1.2.7pl installed for parallel calculations up to 12 nodes.

### 3.1.2 Software

1. GROMACS version 4.5.5 – Manufacturer: Universiti of Groningen, Netherlands.
2. PyMOL – Warren Lyford DeLano, DeLano Scientific LLC, San Carlos, CA, USA.
3. Packmol – Manufacturer: Universidade Estadual de Campinas (UNICAMP), Brazil.

### 3.2 Geometry optimization

MacMolPlt version 7.3 (Bode & Gordon, 1998) was used to build up the starting geometry of each molecule for guanidinium cation, triflate anion and MDEA. The QM calculations for these molecules were performed using GAMESS software package (Schmidt et al., 2013) to obtain a stable conformation for all structures. The density functional theory method with B3LYP method (Becke, 1993) was adopted to study the energy between molecules. Initial geometry optimization was performed at 6-31G basis set (see Appendix A) due to the large size of the system. The method that gave the lowest energy were used as starting geometry for the highest basis set calculation. Afterwards, the obtained geometries were re-optimized by employing the 6-31++G** basis set which includes polarization functions (Appendix B) since the inclusions of polarizable and diffuse functions for the H atom are important for descriptions of hydrogen-bonded interactions (Mou et al., 2008; Wu & Zhang, 2009).

### 3.3 Force Field

In this work, the parameterization of the ions was made in the framework of the OPLS-AA force field (Jorgensen et al., 1996):

$$E(r^N) = \sum_{bonds} K_r\,(r - r_0)^2 + \sum_{angles} K_q\,(\theta - \theta_0)^2 + \sum_{torsions} \frac{K_\emptyset}{2}\,(1 + cos(n\emptyset - \gamma)) + \sum_{i=1}^{N}\sum_{j=i+1}^{N}\left(4e_{ij}\left[\left(\frac{\sigma_{ij}}{r_{ij}}\right)^{12} - \left(\frac{\sigma_{ij}}{r_{ij}}\right)^{6}\right] + \frac{q_i q_j}{r_{ij}}\right) \quad (3.1)$$

The first three terms in Equation 3.1, bonds, angles, and torsions represented the bonded interaction. The non-bonded interactions were described in the last two terms, including van der Waals (vdW, in the Lennard-Jones (LJ) 6-12 form) and Coulombic interactions of atom-centred point charges. Electrostatic and vdW interactions were calculated for the atoms in different molecules or in the same molecule separated by more than three bonds.

The non-bonded interactions separated by exactly three bonds (1-4 interactions) were reduced by a scale factor, which was optimized as 1/2 for vdW and 1/1.2 for electrostatic interaction (MacKerell et al., 1998). The LJ parameters for unlike atoms were obtained from the Lorentz-Berthelot combining rule (Liu et al., 2004). The three-dimensional structures of all molecules in this study are shown in Figure 3.2. The structures and assignment of the atom types for [gua] cation, [OTf] anion and MDEA atoms were adopted from OPLS-AA force field (Jorgensen et al., 1996) (please refer to Figure 3.2). However, the force field parameters for $[OTf]^-$ ions were obtained from Sambasivarao et al. (Sambasivarao & Acevedo, 2009) and Sunda and Venkatnathan (Sunda & Venkatnathan, 2011). But for those of $[gua]^+$ ions and MDEA, the values were taken directly from OPLS-AA force field (Jorgensen et al., 1996).

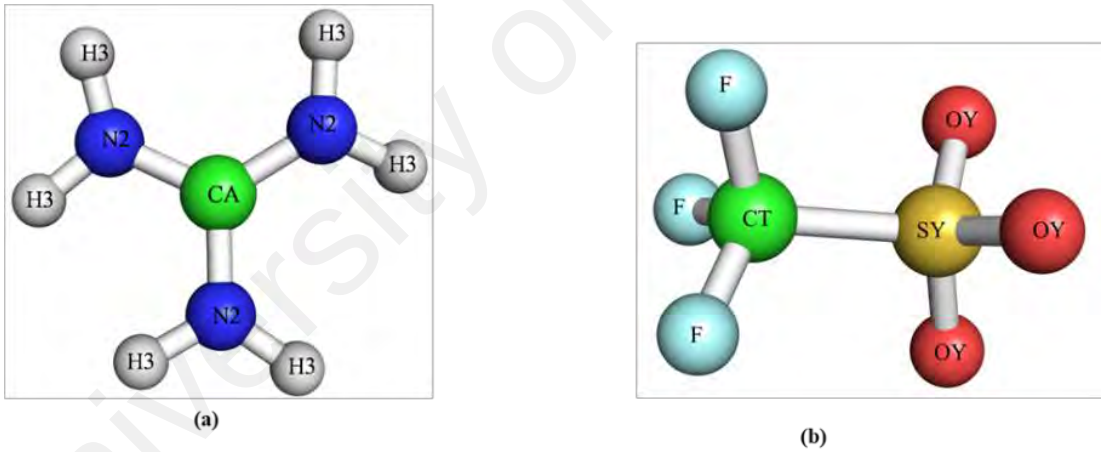


**Figure 3. 2:**Three-dimensional structures of (a) $[gua]^+$; (b) $[OTf]^-$; (c) MDEA. Image made with Pymol. Assignment of the atom types for the cation, anion and MDEA: (a) $[gua]^+$; (b) $[OTf]^-$; (c) MDEA. The nomenclature of the atoms is adopted from OPLS-AA as follows: N2 = N in guanidinium; H3 = H in guanidinium; CA = C in guanidinium; SY = S in sulfonamide; OY = O in sulfonamide; CT = C in perfluoroalkanes; F = F in perfluoroalkanes; CT = $CH_3$(N) tertiary aliphatic amines; $CT^{L1}$ = $CH_2$(N) tertiary aliphatic amines; $CT^{L2}$ = $CH_2$ all atom C: alkanes; HC* = H all-atom H:alkanes; HC = H(C) for carbons directly bonded to N in amines, diamines.

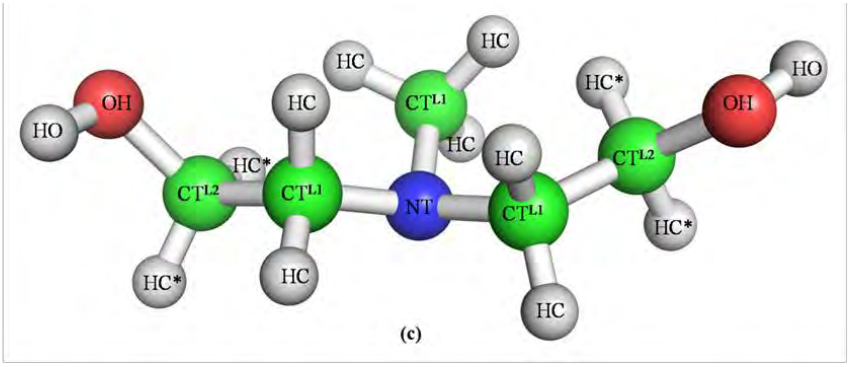


**Figure 3. 2,** continued.

Water molecules were described by the rigid SPC model (Pullman et al., 1981). Further refinement of [gua][OTf] model was made by varying the sigma (σ), epsilon (ε) and vdW parameters, based on the comparison of density's experimental (Russell et al., 1994) data of this IL at 297 K. Low σ and ε values were assigned to C and S atoms of $[OTf]^-$ ions because they were shielded by the surrounding covalently bounded F and O atoms of $[OTf]^+$ ions. The same set of modified parameters was used to determine the densities of [gua][OTf] IL at higher temperatures up to 440 K. The full set of force field parameters for $[gua]^+$ and $[OTf]^-$ ions as well as MDEA are available in Appendix (Please refer to Appendix C, D and E, respectively).

## 3.4 System setup

### 3.4.1 Binary systems

MD simulations for pure [gua][OTf] IL and its mixtures with water were performed using GROMACS (van der Spoel et al., 2010) version 4.5.5 software package. During initial system set up for MD simulations, a list of precautionary steps was strictly followed to avoid the possibilities of simulating existing system trapped in local minima due to preliminary imposed of artificial ion ordering. It involved random placement of the cations and anions in a cubic box also relatively long simulation performance (Micaelo et al., 2006).

[gua][OTf] exists in a solid-state at ambient temperature and melted at T = 429.65 - 430.65 K, the highest melting temperature ever recorded (Russell et al., 1994). For this work, MD simulations were performed on two different cases. Firstly, at a temperature of pure [gua][OTf] at 297 - 440 K. Secondly, on liquid state of IL-water mixtures which was carried out at 440 K, such measures were taken for the later to ensure that IL-water mixtures remain in its liquid phase. Both of these cases were simulated by building an initial molecular system using PACKMOL (Martínez & Martínez, 2003; Martinez et al., 2009) with their position and orientation randomly assigned in a cubic box. All molecules were distributed in random positions and orientations inside a cubic box consists of maximum coordinates *x, y, z* = (40, 40, 40) Å, with molar fractions values of water for the mixtures being varied, $x_{water}$ = 10%, 20%, 30%, 40%, 50%, 60% and 70% (Appendix F). Table 3.1 shows the combinations of [gua][OTf] molecules and water molecules for each simulation.

**Table 3. 1:** Terms and conditions used for MDs simulation at 440 K.

| **Molecule numbers** | **Water molar fraction, $x_w$ (%)** | | | | | | |
|---|---|---|---|---|---|---|---|
| | **10** | **20** | **30** | **40** | **50** | **60** | **70** |
| $[gua]^+ = [OTf]^-$ | 306 | 306 | 306 | 306 | 256 | 256 | 256 |
| Water | 34 | 77 | 131 | 204 | 256 | 384 | 597 |
| System size/Å | 40.0 | 40.0 | 40.0 | 40.0 | 40.0 | 40.0 | 40.0 |

### 3.4.2 Ternary systems

MDs simulations for five ternary systems (system *a-e*) in which the number of water molecules is fixed and the number of [gua][OTf] and MDEA molecules is increased to study the effect of concentration. The mole fractions of the ionic pairs are from 0.03-0.12 whereas those from MDEA are in the range of 0.09-0.20. The compositions and density values for system *a, b* and *d* were based on experimental value reported by Sairi et al. (2015). All the MDs calculations were performed using GROMACS (van der Spoel et al., 2010) version 4.5.5 software package.

The composition of all systems is an important issue for any studies involving simulation of alkanolamine, IL and water especially in our case, where we wanted to study the interactions between aqueous [gua][OTf] in MDEA media, aqueous MDEA in [gua][OTf] media and MDEA–[gua][OTf] in aqueous media as well as to evaluate their dependence on the structural characteristics and properties of the mixture involved. Table 3.2 represents the composition for all systems. When setting up a system for MD simulation, some precautionary steps need to be followed such as avoiding the possibility of simulating a system trapped in local minima due to an initially imposed artificial ion ordering.

**Table 3. 2:** Terms and conditions used for MD simulation at 298.15 K as well as the density for ternary systems obtained from MD simulations.

| System | **Number (*N*)** | | | **Mole fraction (*x*)** | | | **Density $\rho$ (g cm$^{-3}$)** | |
|---|---|---|---|---|---|---|---|---|
| | $H_2O$ | MDEA | IL | $H_2O$ | MDEA | IL | Calculated | Experiment |
| *a* | 267 | 27 | 9 | 0.88 | 0.09 | 0.03 | 1.09106 | 1.05531* |
| *b* | 267 | 46 | 13 | 0.82 | 0.14 | 0.04 | 1.11032 | 1.11781* |
| *c* | 267 | 56 | 24 | 0.77 | 0.16 | 0.07 | 1.16493 | - |
| *d* | 267 | 66 | 33 | 0.73 | 0.18 | 0.09 | 1.19577 | 1.18699* |
| *e* | 267 | 79 | 47 | 0.68 | 0.20 | 0.12 | 1.23134 | - |

* data taken from Sairi et al. (2015)

This can be done by randomly placing the [gua][OTf], MDEA and water molecules in a cubic box and by performing relatively long simulation (Micaelo et al., 2006) using PACKMOL (Martínez & Martínez, 2003; Martinez et al., 2009) at the known overall mixture density at 298.15 K. The numbers of molecules were distributed in random positions and orientations in a cubic box defined by the maximum coordinates of *x, y, z* = (27, 27, 27) Å (Appendix G). All systems were simulated at 298.15 K, a temperature for which experimental (Sairi et al., 2015) data on density properties are available (Table 3.2).

### 3.4.3 Absorption $CO_2$ in MDEA + [gua][OTf] aqueous solution

MDs simulations for five ternary systems (system I-V) were performed using GROMACS (van der Spoel et al., 2010) version 4.5.5 software package at 298.15 K. The composition of all systems is the main issue for any studies involving simulation of alkanolamine, IL and water especially in our case, where we wanted to study the intermolecular interactions involved in mechanisms governing the absorption of $CO_2$. Table 3.3 represents the composition for all systems.

**Table 3. 3:** Terms and conditions used for MDs simulation at 298.15 K.

| System | Number, *N* | | | | | Mole fraction, *x* | | | | |
|---|---|---|---|---|---|---|---|---|---|---|
| | **MDEA** | **IL** | **$H_2O$** | **$CO_2$** | **$CH_4$** | **MDEA** | **IL** | **$H_2O$** | **$CO_2$** | **$CH_4$** |
| I (ternary mixture) | 51 | 7 | 1970 | | | 0.1416 | 0.0347 | 0.8237 | | |
| II (ternary mixture + 536 $CO_2$ (l) | 51 | 7 | 1970 | 536 | | 0.1416 | 0.0347 | 0.8237 | | |
| III (ternary mixture + 127 $CO_2$ (g) | 51 | 7 | 1970 | 127 | | 0.1416 | 0.0347 | 0.8237 | | |
| IV ($H_2O$(l) + 7 $CH_4$(g) + 153 $CO_2$ (g) | | | 2135 | 7 | 153 | | | | 0.11 | 0.89 |
| V (ternary mixture + 7 $CH_4$ (g) + 153 $CO_2$ (g) | 51 | 7 | 1970 | 7 | 153 | 0.1416 | 0.0347 | 0.8237 | 0.11 | 0.89 |

When setting up a system for MD simulation, some precautionary steps need to be followed such as avoiding the possibility of simulating a system trapped in local minima due to an initially imposed artificial ion ordering. This can be done by randomly placing the $[gua]^+$, $[OTf]^-$, MDEA and water molecules in a rectangular box and by performing relatively long simulation (Micaelo et al., 2006). These ternary systems were simulated by building an initial molecular system using PACKMOL (Martínez & Martínez, 2003; Martinez et al., 2009) (Appendix H). At the beginning of the simulation, the simulation cell contained two building blocks with different phases set side-by-side. The first phase consisted of acid gas components ($CO_2$ and/or $CH_4$) in either a gas or liquid phase, whereas the second block consisted of ternary mixture solution (see Figure 3.3).

The time evolution of the five described systems was studied in detail and compared to identify the special effects of system composition. The systems were not expected to achieve equilibrium in the global thermodynamics sense, but they were run for a sufficiently long time and expected to be stable in terms of molecular simulations. For these reasons, the ensemble average values were only used for some properties and features, while the rest analysis depending on visual observations using VMD package (Humphrey et al., 1996).

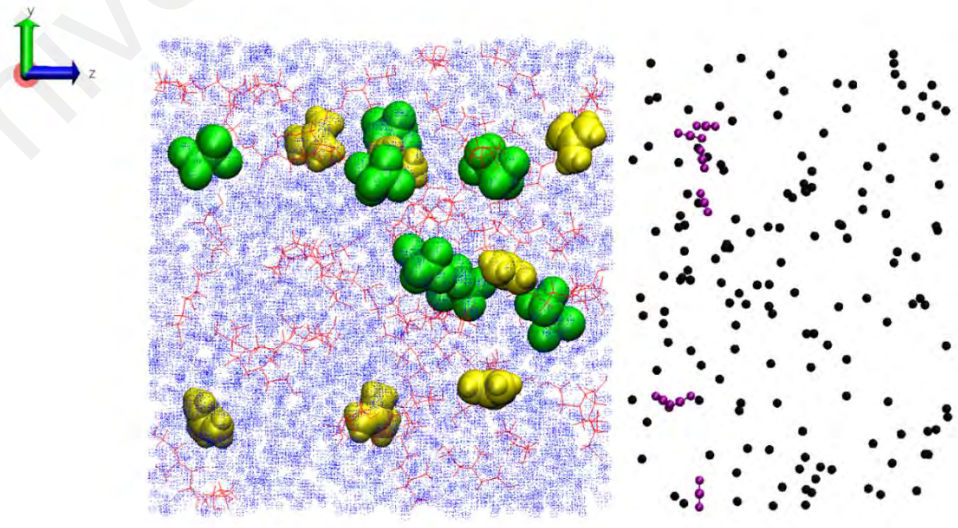


**Figure 3. 3**: Connected purple spheres represent $CO_2$ molecules; black dotted are is methane molecules, blue dotted area is aqueous phase; red lines show MDEA; large yellow and green connected balls molecules stand for $[gua]^+$ and $[OTf]^-$

### 3.5 Computational details for all systems

Initial configurations for all systems were minimized to 1,000,000 steps using the steepest descent method until the minimization was converged (Appendix I-K). These energy minimization step was functioned to remove close contacts between the MDEA, water molecules cation and anion in their initial random configuration (Kuo et al., 2004). Maximum step size and tolerance allowed were between 0.01 nm and 0.1 kJ $nm^{-1}$ $mol^{-1}$, respectively. The simulations were first initialized under canonical ensemble (NVT) to establish initial equilibration as well as proper orientation of the molecules/ions involved (Appendix L-N). Next, it was equilibrated as an isothermal-isobaric ensemble (NPT) (see Appendix O-Q) at selected pressures and temperatures in order to ensure full equilibration of all systems properties (checked through constant temperature and pressure graphs, respectively). An additional of 3-5 ns runs under the previous condition enabled liquid densities.

Finally, the simulations were adjusted to maintain average densities and continued to be equilibrated in NVT (Appendix R-T). Trajectories of 6 ns (ternary systems), 10 ns (binary systems) and 24 ns (absorption $CO_2$ in ternary system) with NVT were carried out for data collection and analysis, respectively. A time step of integration of 2 fs was used. Pressure was controlled using Berendsen barostat (Berendsen et al., 1984) with a reference pressure of 1 atm, a relaxation time of 1.0 ps, and isothermal compressibility of $4.5 \times 10^{-5}$ $bar^{-1}$. Temperature was maintained by the V-rescale thermostat (Bussi et al., 2007). Cations, anions, and MDEA (and water in cases where solvent is included) were separated using heat baths with temperature coupling constant of 0.1 ps. In this case, lengths of all bonding were constrained using the LINCS algorithm (Hess et al., 1997), while its neighbor searching was done up to 9 Å and updated at every 10 steps. Long-range electrostatic interactions were cut off at 12.0 Å using the combination of Particle Mesh Ewald (PME) method (Essmann et al., 1995) and a fourth-order interpolation.

The distance for the Coulomb cut-off radius and the van der Waals potential cut-off radius were calculated explicitly up to 9 Å.

### 3.6 Analysis of ionic liquids properties

All the thermodynamics properties and density of the structure during the simulation were computed. The analysis was calculated using the *g_energy* tool in GROMACS (van der Spoel et al., 2010) version 4.5.5 except for spatial distribution function which was performed using PyMol (DeLano, 2002) to visualize of a particular file type. The physical state of ILs was determined by observing the radial distribution function plot. The RDF calculations were performed using *g_rdf* tool. This RDF represents the probability of finding two molecules separated by a distance from a particular point. In GROMACS, the RDF between two types of particle *A* and *B* was calculated as based on Equation 3.2:

$$g_{AB} = \frac{\langle \rho B(r) \rangle}{\langle \rho B \rangle_{local}} = \frac{1}{\langle \rho B \rangle_{local}} \frac{1}{N_A} \sum_{t \in A}^{N_A} \sum_{i \in B}^{N_B} \frac{\delta\,(r_{ij} - r)}{4\pi r^2} \qquad (3.2)$$

with $\langle \rho B(r) \rangle$ the particle density of type *B* at a distance *r* around particles *A*, and $\langle \rho B \rangle_{local}$ the particle density of type *B* averaged over all spheres around particles *A* with radius $r_{max}$ the value for $r_{max}$ was half of the box length (van der Spoel et al., 2010).

The mean square displacement was performed using *g_msd*. This mean square displacement also contains information on the diffusion of atoms. Therefore, the slope of the mean square displacement is called the self-diffusion coefficient. According to Allen & Tildesly (1989), the Einstein relation shown in Equation 3.3 was used to determine the self-diffusion coefficient of the ionic liquid (Allen & Tildesley, 1989).

$$\lim_{t \to \infty} \langle \| r_i(t) - r_i(0) \|^2 \rangle_{i \in A} = 6 D_A t \qquad (3.3)$$

where $D_A$ is the self-diffusion coefficient of particle A. For molecules with more than one atom, $\boldsymbol{r}_i$ can be taken as the center of mass. $\boldsymbol{r}_i(t)$ is the position of atom *i* at a specific time and $\boldsymbol{r}_i(0)$ is the position of atom *i* at initial time.

The average density was performed using *g_density*. This average density used to compute partial densities across the box. This is useful for looking at the distribution of groups or atoms across the interface (van der Spoel et al., 2010).

# CHAPTER 4: RESULTS AND DISCUSSIONS

Classical MD simulations were performed to understand the phase equilibrium behaviour of aqueous [gua][OTf] IL solution (binary solvents) at 7 different molar fractions of water ranged from 0.1 to 0.7 at 440.15 K and ternary aqueous mixtures containing [gua][OTf] IL and water mixed with MDEA in different function composition at 298.15 K. For binary solvents, the simulations measured changes in different physical properties such as density, structural, bonding properties (radial distribution function, water clustering and hydrogen bonding) and dynamic property (diffusion coefficient). While for ternary solvents, the analysis of structural and dynamic properties showed that the molecular level of ternary mixtures is slightly affected by the presence of MDEA and [gua][OTf ] molar fractions.

Based on their physical properties such as viscosities, these ternary solvents can be applied in the natural gas industry, such as removing carbon dioxide using aqueous MDEA and IL at high pressure. Later, MD simulations were performed at a constant temperature of 298.2 K for five systems to provide insight into molecular distribution in the ternary solution and to enhance understanding of absorption mechanisms on the molecular scale. When $CO_2$ is present, it forms a dense layer on the surface, and the cation-anion associations at the interface are disrupted. The continuous increase of $CO_2$ does not affect the structure of the ionic liquid, but $CO_2$ molecules are always captured by the cavity of guanidinium cation.

## 4.1 Microstructures, interactions and dynamics properties studies of aqueous [gua][OTf] IL

### 4.1.1 Pure ILs

#### 4.1.1.1 Validation of the force field

To validate the force field used to model [gua][OTf], the densities of pure ILs were examined and compared against existing experimental data. Table 4.1 shows the simulated densities at different temperatures for 10 ns [gua][OTf] isothermal-isobaric ensemble. It was also observed that the density is decreased inversely the temperature. In addition, the deviations of simulated density values reported by Russell et al. (1994) were the same as current simulations *i.e* in the range of 1-5%. From the results, good agreement of approximate density values for both simulation and experiment is observed.

**Table 4. 1:** Density for pure [gua][OTf] ionic liquid obtained from MDs simulations as a function of temperature.

| Temperature (K) | Density (g cm$^{-3}$) | |
|---|---|---|
| | Calculated | Experimental |
| 297 | 1.671 | 1.661* |
| 325 | 1.667 | - |
| 354 | 1.597 | - |
| 383 | 1.595 | - |
| 412 | 1.618 | - |
| 440 | 1.598 | - |

* data taken from Russell et al. (1994)

#### 4.1.1.2 Radial distribution functions

RDF analysis was used to describe the probability distribution of cations or anions around a given reference group (Sun et al., 2010). Figure 4.1 shows the RDF, *g(r)*, between the centre of mass (COM) of cation-cation ($g(r)_{cc}$), cation-anion ($g(r)_{ca}$) and anion-anion ($g(r)_{aa}$) at 440 K. All solvation peaks extend beyond ~20 Å in the same figure, which is approximately the half-length of the simulation box.

Cation-anion peaks are well-defined, sharper and located at shorter distances compared to the cation-cation and anion-anion ion pairs. The most dominant and sharp first peak belongs to cation-anion ($g(r)_{ca}$) and it occurs at r ~4.7 Å with a $g(r)$ of 3.48. It is obvious, that a strong electrostatic attraction exists between each cation-anion association. The RDF value falls and passes through a minimum value around r ~7 Å. The possibilities of finding a cation-anion pair with this separation are the lowest and structural correlation is long-ranged which indicates that molten salts are strongly coupled ionic systems which are characterized by strong solvation peaks in the RDF properties (Del Pópolo & Voth, 2004; Keblinski et al., 2000). On the contrary, the first peak of cation-cation and anion-anion RDFs are significantly weaker than that of the cation-anion. A closer observation shows that the first peak of cation-cation RDFs is broader than anion-anion RDF.

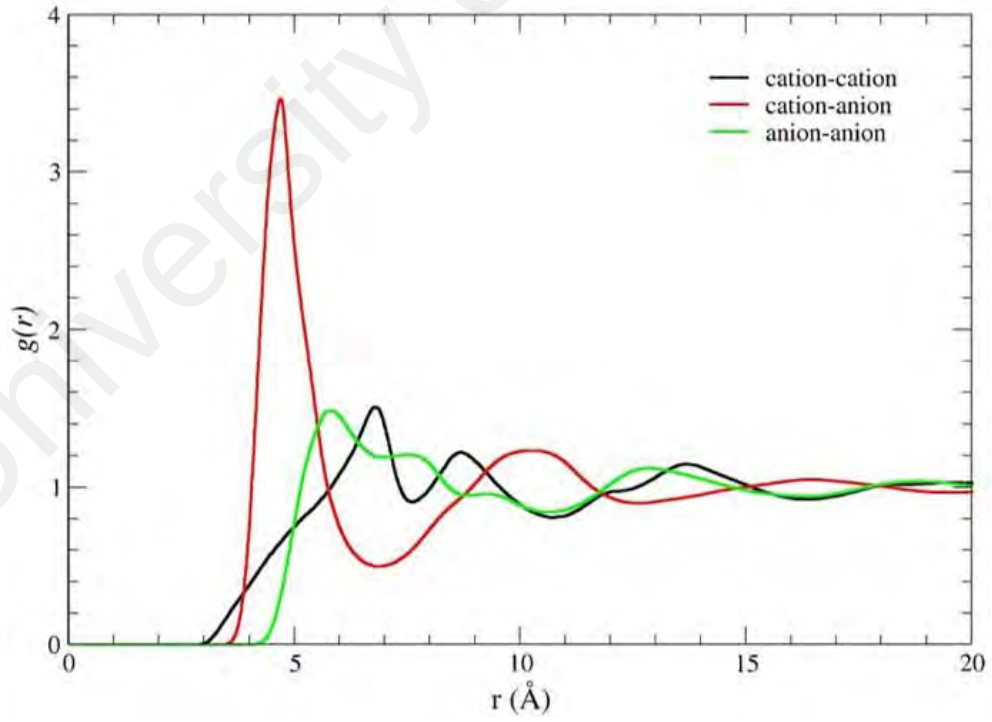


**Figure 4. 1**: RDF of the center of mass for $[gua]^+[gua]^+$, $[gua]^+[OTf]^-$ and $[OTf]^-[OTf]^-$ at 440 K

This is because of the orientational correlation between the cations itself due to the smaller sizes and molecular weight when compared to anions. The findings suggest that the structure of IL depend strongly on their chemical compositions. This is supported by similar observations performed by Chang *et al.* for *N*,*N*-diethyl-*N*-methylammoniumtriflate (Chang et al., 2010). Figure 4.2 exhibits the atomic RDFs decomposition between the N and H atoms of $[gua]^+$ and the F and O atoms of $[OTf]^-$ at 440 K. These RDFs have shown signs of complex features that we consider as molecular orientational correlations.

The most prominent characteristic is its first sharp peak between the H atoms of cations and the O atoms of the anions which occur at r~1.7 Å. The trending is similar to those observed in other literature (Chang et al., 2010). Conversely, the first RDF peak for H atoms in the cation and the F atoms in the anion is much weaker and occurs at a much larger separation. In the same figure, *i.e* Figure 4.2, H atoms of $[gua]^+$ ions have a strong affinity towards the O atoms over F atoms of $[OTf]^-$. This is due to the negative charges, which are attached to the sulfonate groups, yielding interactions that are stronger than the interactions with electrophilic fluorines (Chang et al., 2010). Therefore, the RDFs suggest that cation-anion local structural arrangement preferred the H atoms to be bonded to the sulfonate group.

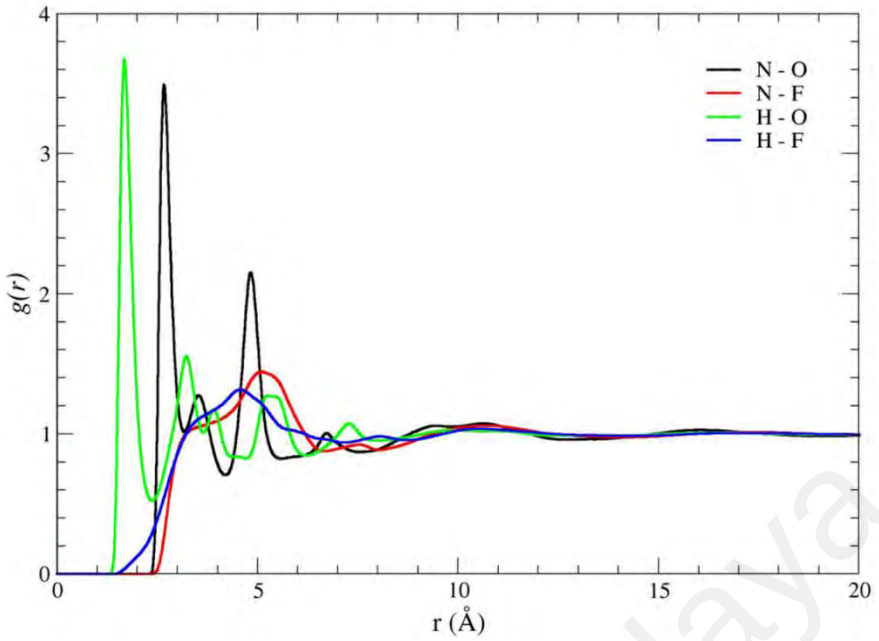


**Figure 4. 2**: RDF of the atomic pair correlation between the $[gua]^+$ and $[OTf]^-$. The data points correspond to N of cation-O of anion, N of cation-F of anion, H of cation-O of anions. H of cation-F of anion, respectively

#### 4.1.1.3 Spatial distribution functions

Spatial distribution functions compute the probability of finding a molecule in three-dimensional space around a centre molecule. It provides an intuitive vision of the whole systems allowing the studied of cations and anions interactions to be performed. In this work, SDFs are visualized using a software package called PyMOL (DeLano, 2002). Figure 4.3 presented the SDFs of ILs cations (blue cap) around the anion region (sulfonate group). An additional clarity, only C atoms of the cations are depicted in this work. The strongest peak in RDFs graph (refer to Figure 4.2) is an indication of preferred distance for the centre of mass of the cations around the anions centres. SDFs has shown cations are strongly localized around the oxygen region site of anions, which proved the high charge density anions strengthens these cation-anion interactions. Thus, explains why cations are seen to be found around the oxygen region rather than fluorine. Highly-fluorinated ILs with delocalized anions charges tend to form hydrophobic ILs that are immiscible with water (Kohno & Ohno, 2012).

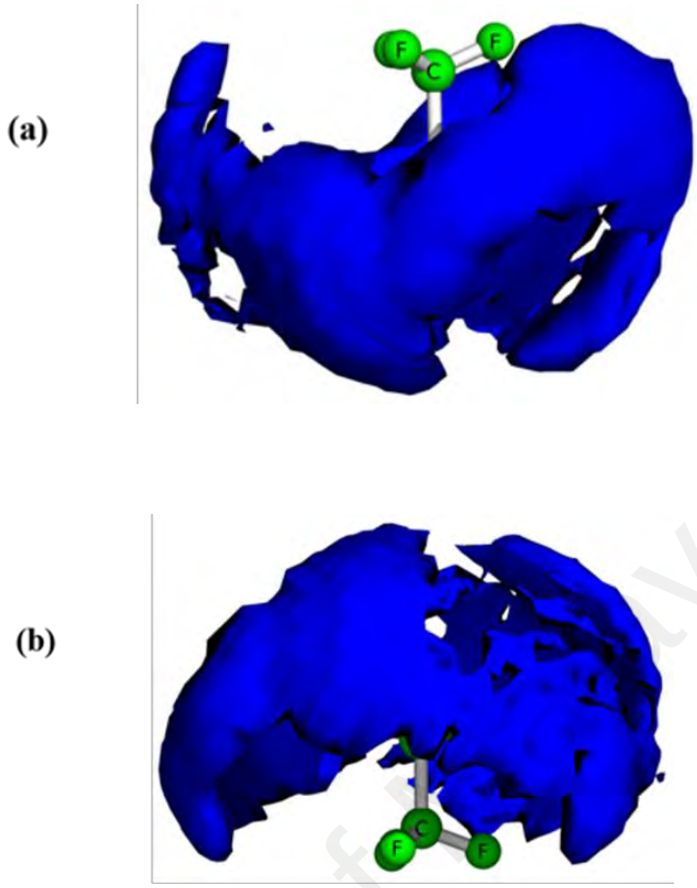


**Figure 4. 3**: SDF of cations (blue surfaces) around $[OTf]^-$ anion

### 4.1.2 Aqueous IL mixtures

#### 4.1.2.1 Thermodynamics

Seven different aqueous-IL mixtures were studied with varying water molar fractions, $x_w$ = 0.1, 0.2, 0.3, 0.4, 0.5, 0.6, 0.7 (34, 77, 131, 204, 256, 384, 597) water molecules for 306 ion pairs in the simulation respectively (refer to Table 3.1). In the same 10 ns isothermal-isobaric ensemble of [gua][OTf] MD simulations, both calculated densities of aqueous-IL mixtures (Figure 4.4) and excess molar volume ($V_m$) of mixing as a function of $x_w$.

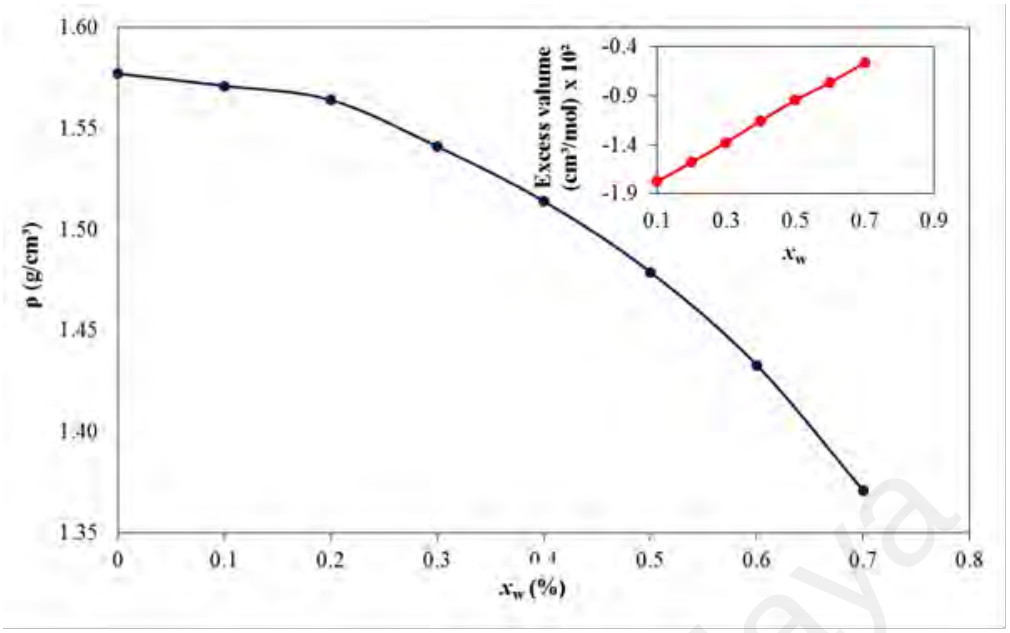


**Figure 4. 4**: The calculated density of aqueous [gua][OTf] IL as a function of $x_w$. Displayed in the inset are the $V_m$

Although at low $x_w$, the solution densities varied slightly of one another, there were different characteristics observed during this simulation. For example, at $x_w$=0.1, water tends to form its own monomers (Figure 4.5(a)), while the dimers occurred at $x_w$ =0.2 and above (Figure 4.5(b)). The later then intercalated between anions and cations creating hydrogen bond network with ILs. As $x_w$ increases, aqueous IL mixtures densities decrease rapidly to match bulk water densities. The calculated $V_m$ show non-steady linear increase with decreasing $x_w$ and negative $V_m$ are recorded 0.1 to 0.7 molar fractions of water. These negative $V_m$ values are the results of specific interactions between aqueous IL include the partial charge transfer, formation of hydrogen bond, CH-π bond, π-π stacking, and n-π bond interaction (Anantharaj & Banerjee, 2011). Therefore, ILs with sulphur/nitrogen atoms mixtures have stronger hydrogen bond interactions that lead to negative $V_m$ as compared to IL-IL, thiophene-thiophene (Anantharaj & Banerjee, 2011) or pyrrole-pyrrolea (Anantharaj & Banerjee, 2011) interactions.

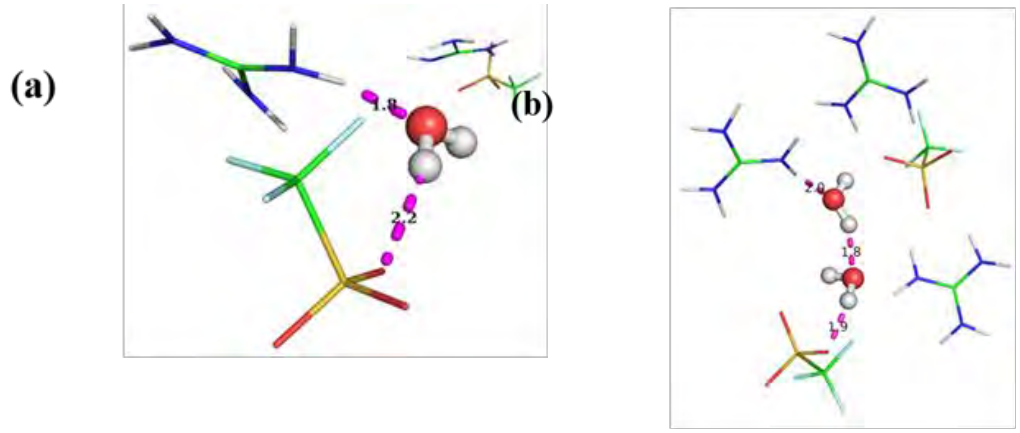


**Figure 4. 5:** (a) A water monomer intercalated between $[gua]^+$ $[OTf]^-$; (b) water dimer intercalated between $[gua]^+$ $[OTf]^-$

#### 4.1.2.2 Radial distribution function

To study the structural properties of aqueous IL system, we calculated the RDF for aqueous IL based on $x_w$ given in Table 3.1. Figure 4.6 shows the RDF between the COM of $g(r)_{cc}$, $g(r)_{ca}$ and $g(r)_{aa}$ for several $x_w$. There are two main points to be discussed in details. For aqueous-IL mixture, RDFs studies based on Figure 4.6, are the sharp and well-defined peaks observed RDFs at high water molar fractions, which suggested persistence long-range spatial correlations between these ions. Second, are the roles of water in altering aqueous-IL mixture structures.

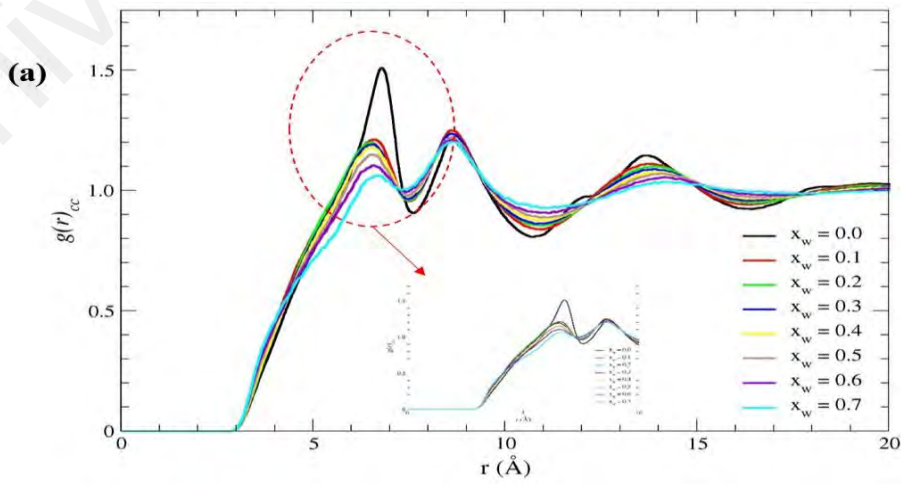

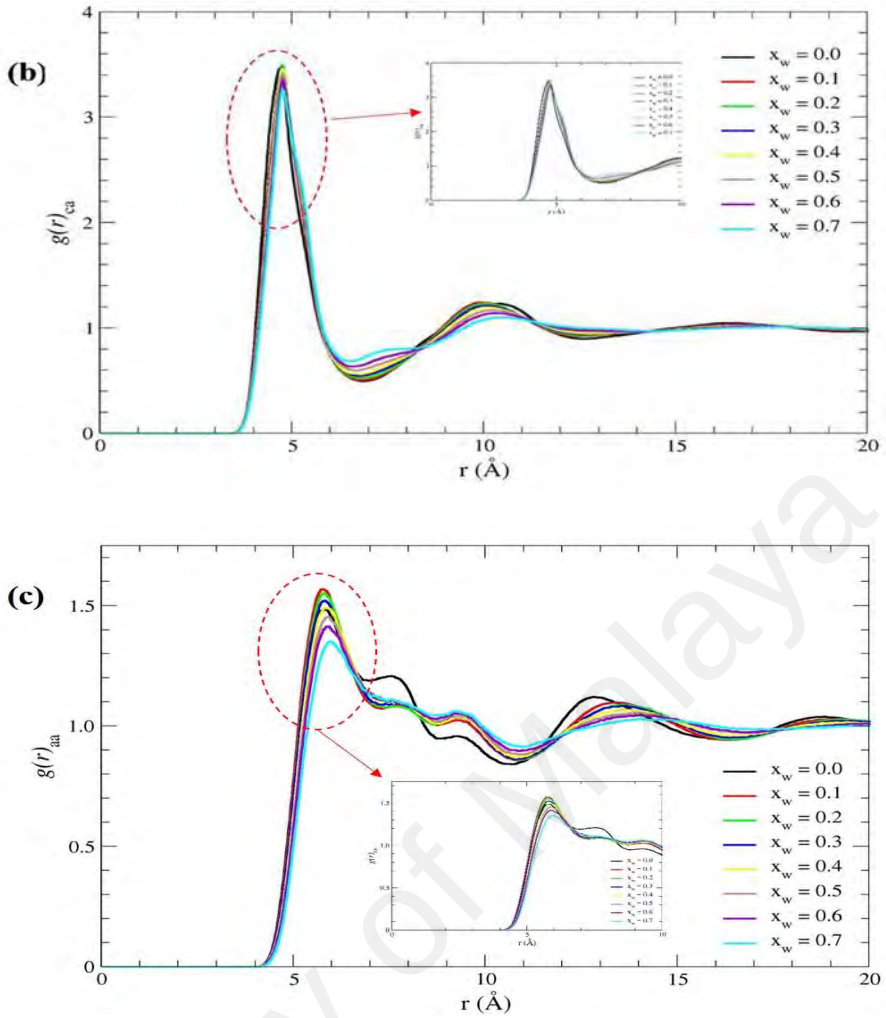


**Figure 4. 6:** RDF of the COM: (a) $[gua]^+[gua]^+$, (b) $[gua]^+[OTf]^-$ and (c) $[OTf]^-[OTf]^-$ at 440 K

Figure 4.7 shows the snapshots, of $x_w$ = 0.1, 0.2, 0.3, 0.4, 0.5, 0.6 and 0.7 (Figure 4.7 (a)-(g)), respectively. Water molecules existed in the form of monomers at low $x_w$ (Figure 4.7 (a), (b), (c)). It intercalated between anions and cations (Figure 4.7(a)), in the form of dimers (Figure 4.7(b)) and finally as small clusters (Figure 4.7 (c), (d)). These changes in structures continued until a water network at medium $x_w$, started to develop together with a percolated water network at high $x_w$ (Figure 4.7 (e), (f), (g)). The increase in $x_w$ broaden peaks and shifts in RDFs. For cation-cation interactions, the strongest clustering of ion pairs in the pure IL appeared at r~ 6.8 Å. By introducing water molecules into ILs, it broadened the cation-cation peaks (Figure 4.6(a)), suggesting that the strong cation-cation associations are weakened by the presence of water molecules.

As for cation-anion RDFs (Figure 4.6(b)), its first peak occurs at r~ 5.0 Å, an indication of strong cation-anion associations is at a high molar fraction of water. On the other hand, the first peak of anion-anion RDF (Figure 4.6(c)) broadened and shifted to a smaller separation gap. These behaviours indicate that water molecules have reduced the anion-anion correlations.

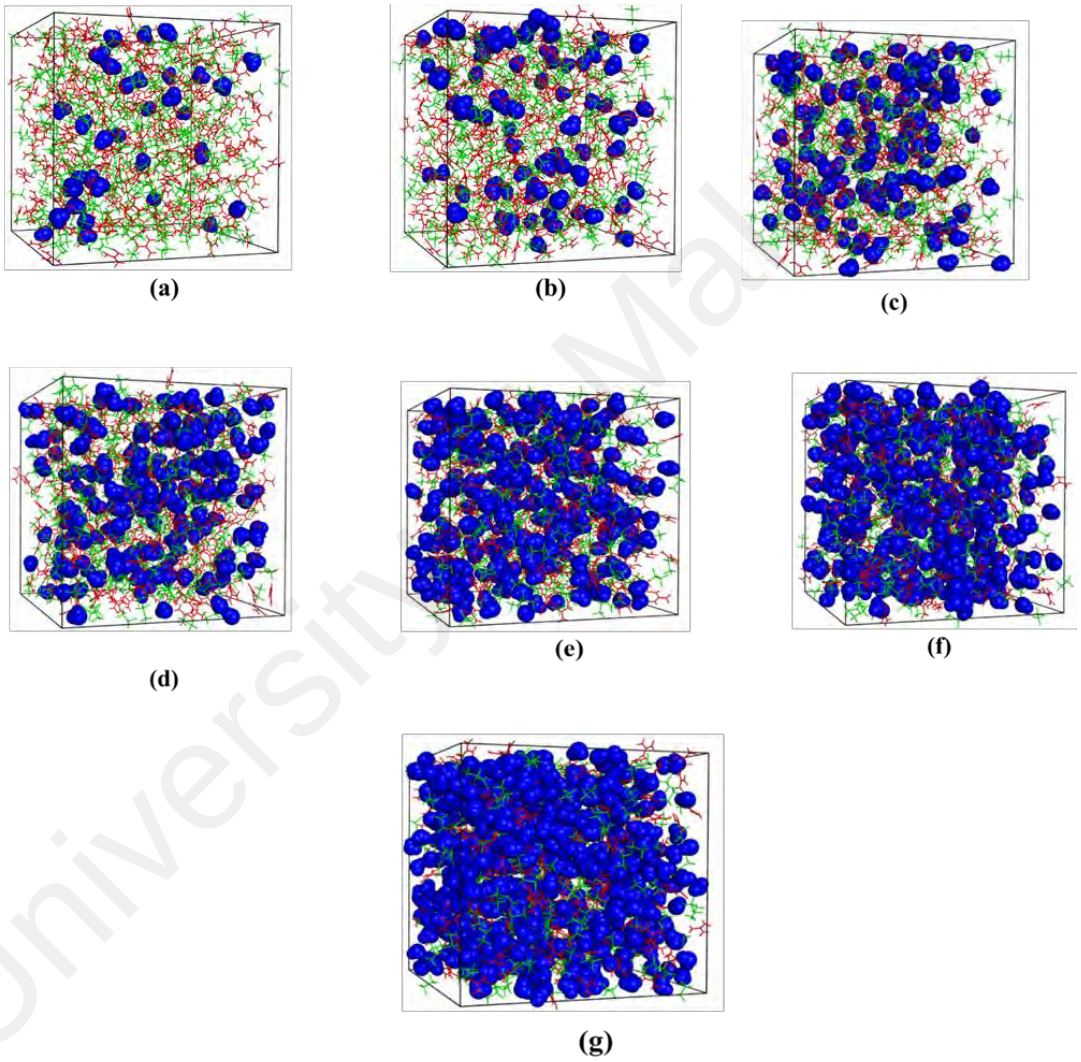


**Figure 4. 7**: Snapshots of $[gua]^+$ ,$[OTf]^-$ and water mixtures for $x_w$ (a)-(g) where $x_w = 0.1$, 0.2, 0.3, 0.4, 0.5, 0.6, 0.7, respectively. Besides, to show the structure of the water network, the snapshots reveal the layered structure of the IL with the red colour representing the $[gua]^+$ cations separated by green colour representing the $[OTf]^-$ anion and blue colour representing water molecules.

Displayed in Figure 4.8 are the RDFs for the atomic pair from the atomic pair collection RDFs between $[gua]^+$- $H_2O$ and $[OTf]^-$-$H_2O$. H(N) atoms of $[gua]^+$ are selected to represent cations and O(S) atoms of the $[OTf]^-$ are selected to represent the anions, while H(W) and O(W) atoms represent water. These atomic RDFs exhibit distinctive features, presenting of the presence of well-defined solvation structures. The pronounced first peaks of the H(N) – O(W) of $[gua]^+$ and O(S) – H(W) of $[OTf]^-$ RDFs were recorded at r ~ 1.8 Å due to direct interactions between water and above-mentioned ions. The heights of these peaks decrease inversely $x_w$, an indication of strong water-ion interactions within dilute solutions. This observation highlights the tendency of water to intercalate in first coordination shells of $[gua]^+$ and $[OTf]^-$ ions.

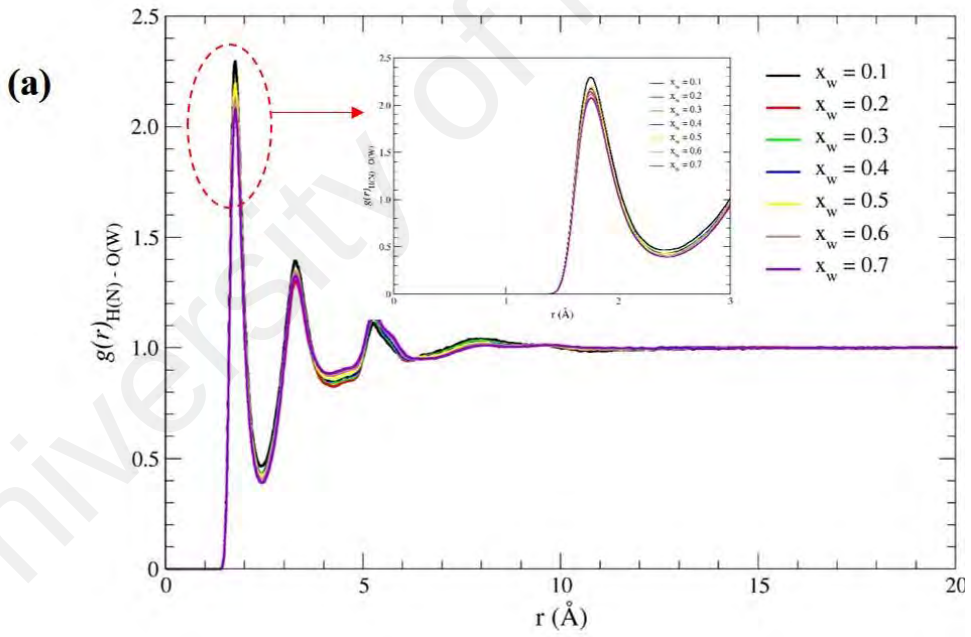


**Figure 4. 8:** RDF of the atomic pair correlation between the $[gua]^+$-$H_2O$ and $[OTf]^-$-$H_2O$. The RDFs between (a) O of water and H (attached to N) of cations; (b) H of water and O of anions

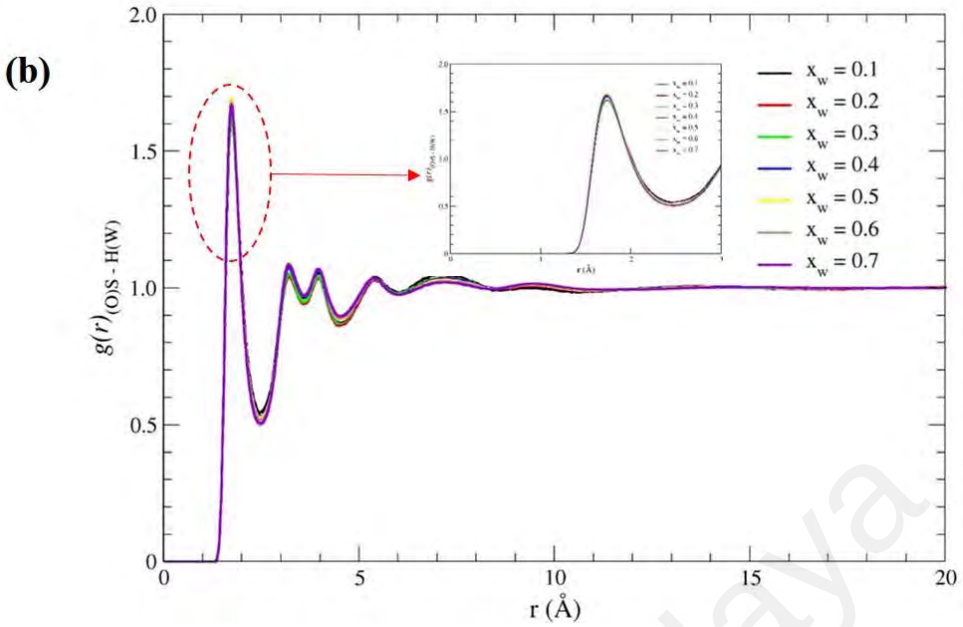


**Figure 4.8,** continued.

#### 4.1.2.3 Spatial distribution function

SDFs between water and ions in aqueous-ILs mixtures were investigated. IL-water and the results are presented in Figure 4.9. Based on the figures (Figure 4.9 (a), (b)), water molecules (blue caps) and anions (red caps) are sharing the same spatial regions around $[gua]^+$ ion (above and below). Even at low (Figure 4.9(a)) and high (Figure 4.9(b)) $x_w$, all the anions are strongly localized around cations as compared to water molecules, thus it is proven that water molecules have no effects on the cation-anion interactions. Similar to Figure 4.3(b), SDFs verified the cause of sharp peaks in RDFs graph, but it also identified the preference of water molecules to develop hydrogen bonding with anions rather than being localized simultaneously around cation. In the simulation of [OTf] ions for sulfonate groups, Figure 4.9 ((c), (d)) show how water molecules (blue caps) and cation (red caps) occupy the regions around these anions. When $x_w$ (Figure 10(d)) increased, its molecules strongly localized around sulfonate groups compared to cations, a concrete evidence of reduction in water molecules and anions (fluorination and aromatization) interactions (Khan et al., 2014).

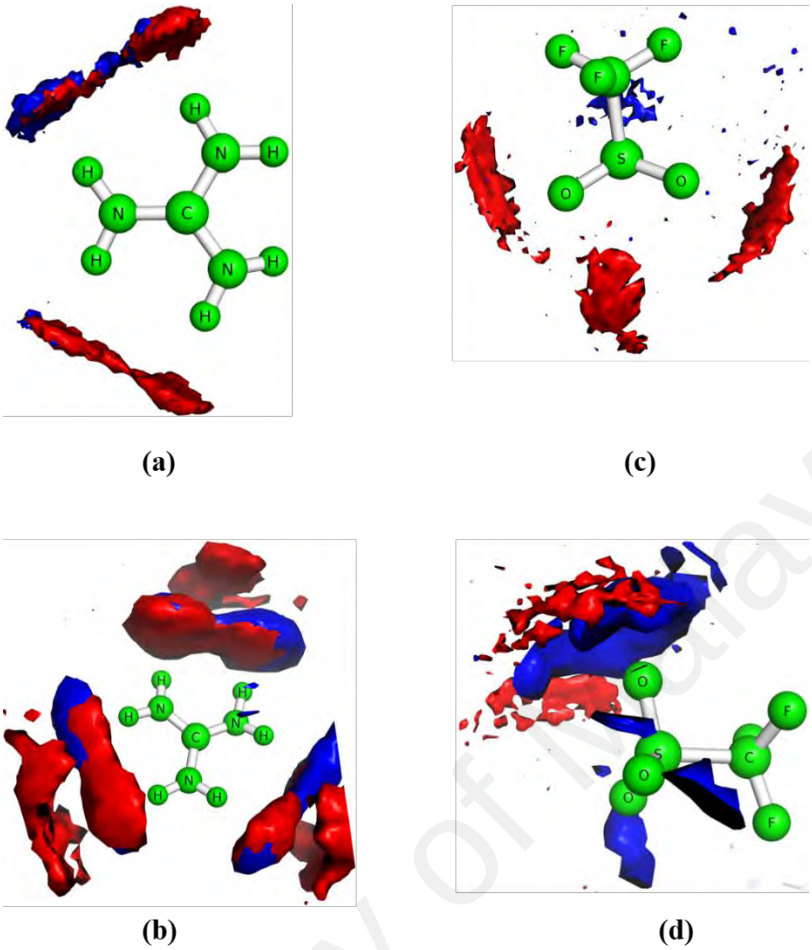


**Figure 4. 9**: Spatial distribution functions of (a) water (blue color), $[OTf]^-$ anions (red color) around $[gua]^+$ cation at $x_w = 0.10$; (b) water (blue color), $[OTf]^-$ anions (red color) around $[gua]^+$ cation at $x_w = 0.70$; (c) water (blue color), $[gua]^+$ cations (red color) around $[OTf]^-$ anion at $x_w = 0.10$; (d) $[gua]^+$ cations (red color) around $[OTf]^-$ anion at $x_w = 0.70$

The high charged densities at the oxygen site for anions strengthened ions-water molecules interactions (Bhargava et al., 2011). This explained the tendency of ILs with highly-fluorinated and charged delocalized anions, for example bis(trifluoromethanesulfonyl)imide anion, $[Tf_2N]^-$ and hexafluorophosphate anion ($PF_6^-$), forming hydrophobic ILs that are immiscible with water (Kohno & Ohno, 2012). According to the highest RDFs for the atomic pairs, cations prefer to develop hydrogen bonding with water molecules rather than localized around anions. These SDFs verified the broadening of cation-cation peaks (Figure 4.6(a)) and anion-anion peaks (Figure 4.6(c)).

#### 4.1.2.4 Ion-water structure and interactions

We have examined the formation of hydrogen bonds between water-water molecules, water-cations as well as water-anions pairs at varying $x_w$. There are two bases of geometric definitions for hydrogen bonds. First, if the radial distance between the labelled hydrogen and an acceptor atom is equal to or shorter than 2.45 Å and second if the angle of acceptor-donor hydrogen is equal to or shorter than 30° (refer Figure 4.10). However, the distance between acceptor and donor atoms should be less than 3.5 Å. For water-anion pairs, hydrogen atoms of water molecules act as the donors and oxygen atoms of anions are the acceptors. However, for water-cation pairs, donors are the nitrogen atoms of cations and oxygen atoms from water molecules are the acceptors. In general, the average number of cation-water and anion-water hydrogen bondings per water molecule increase with the amount of $x_w$ as given in Figure 4.11. Although both interactions give an indistinctive number of hydrogen bonds values from low to high $x_w$ cation-water pairs have the most hydrogen bonds. Therefore, it can be concluded that both ions have succeeded to form hydrogen bonds with water molecules.

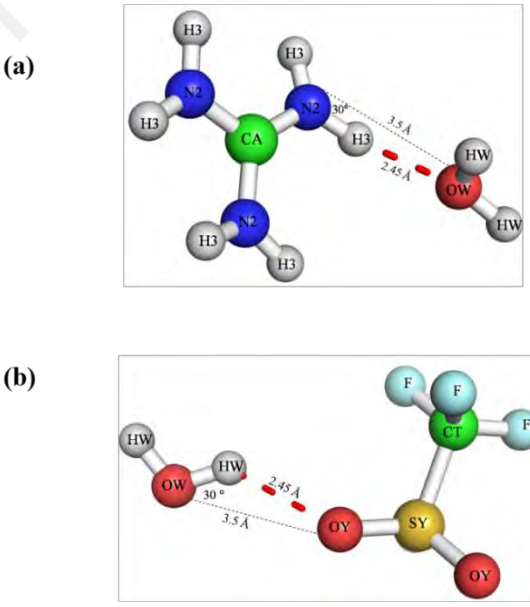


**Figure 4. 10**: Geometric criteria used in this work for the calculation of a number of hydrogen bonds formed between (top) water-$[gua]^+$ and (bottom) water-$[OTf]^-$ pairs

A closer look into the ion-water structures found more water molecules reside in their coordination shells, which is similar to the trend in anions. However, the ability for anions to form more hydrogen bonds are highly electronegative atoms (oxygens and fluorines), inhibited by the presence of highly-fluorinated and charged delocalize anions which prefer to form hydrophobic ILs even though they have high electronegative atoms (oxygen and fluorine atoms).

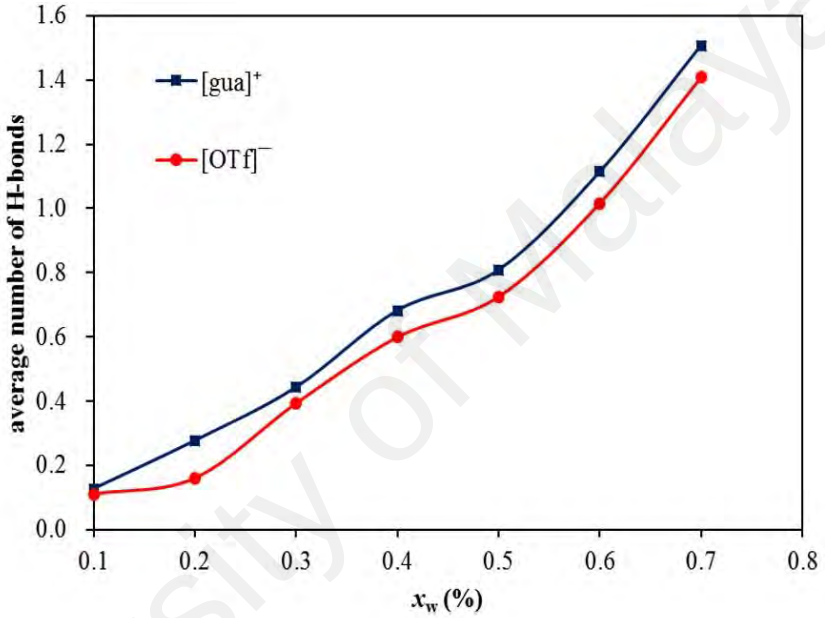


**Figure 4. 11:** Average number of hydrogen bonds per water molecule against $x_w$

#### 4.1.2.5 Dynamic/transport properties

Water molecules effects on the dynamic properties of ILs mixtures are calculated using $D$ and orientational autocorrelation function of $[gua]^+$ and $[OTf]^-$ ions, based on water molar fractions given in Table 3.1. For this work, $D$ was obtained through a linear fitting of the slope in the region ranging from 8 to 10 ns of mean square displacement curves for all simulated systems. The results are given in Table 4.2. In general, $D$ increased with $x_w$, since water molecules displaced easily than the ILs. There was a significant increase in the $D$ as water concentration increased.

Because of the sizes and structures of [OTf]- anions in water, the diffusion rate constants of $[OTf]^-$ anions in water were higher than that of $[gua]^+$ cation.

Both ions exhibited a quite similar diffusivity over the $x_w$ range, suggesting interrelated motions between the ions and also among ILs-water pairings (Chang et al., 2010; Fraser et al., 2007; Moreno, et al., 2008; Rollet et al., 2007).

**Table 4. 2:** *D* of $[gua]^+$, $[OTf]^-$ and water in aqueous IL as a function of $x_w$.

| $x_w$ (%) | $D$ x $10^9$ ($m^2s^{-1}$) | | |
|---|---|---|---|
| | **Water** | **$[gua]^+$** | **$[OTf]^-$** |
| 0 | - | 0.28 ± 0.073 | 0.23 ± 0.10 |
| 0.1 | 1.4 ± 0.49 | 0.50 ± 0.15 | 0.43 ± 0.15 |
| 0.2 | 1.6 ± 0.65 | 0.64 ± 0.15 | 0.49 ± 0.14 |
| 0.3 | 1.6 ± 0.74 | 0.83 ± 0.25 | 0.54 ± 0.25 |
| 0.4 | 1.9 ± 0.67 | 0.93 ± 0.39 | 0.80 ± 0.12 |
| 0.5 | 1.6 ± 0.87 | 1.0 ± 0.19 | 0.82 ± 0.30 |
| 0.6 | 1.7 ± 1.1 | 1.3 ± 0.25 | 1.2± 0.18 |
| 0.7 | 1.5 ± 1.5 | 1.5 ± 0.42 | 1.6 ± 0.44 |

Water facilitates the translational motion of both ions as determined by the larger diffusion rate constant at a higher level of hydration. Water molecules shielded the electrostatic attractions between ions and weakened the structural organizations of these IL-water mixtures. Impact on the dynamics of ion pairs contact formation by water was examined using the time correlation function, *R(t)*. As hydration level increased, the ion pairs contact weakened, leading a shorter time scale for ion dissociations. Spohr & Patey (2010) observed the physical reason for water's impact on transport properties in ILs. They found that the dominant effect of water was dynamical in origin and influenced by the type of ILs when more water molecules were added into the ILs, it replaced the heavier counterions from the solvation shells, decreased the effects of caging and lead to increasing of mobility. Our results are in agreement with their conclusion. We also studied how the rotational motion of $[gua]^+$ and $[OTf]^-$ ions being affected by the presence of water molecules. The reorientation of $[gua]^+$ and $[OTf]^-$ in aqueous solution was examined using Equation 4.1 for the orientational autocorrelation functions.

$$C_l(t) = \left\langle P_l\left[\ \vec{u}(0)\cdot\vec{u}(t)\right]\ \right\rangle \qquad (4.\ 1)$$

$P_l$ denotes the *l*th Legendre polynomial and $\vec{u}(t)$ is the body-fixed unit vector along any specified axis at time *t*. Average orientational autocorrelations functions, $C_l(t)$, from the N-H bond vector of $[gua]^+$ ions (Figure 4.12 (a)) and O-S bond vector of $[OTf]^-$ ions (Figure 4.12 (b)) were computed for several water fractions. It can be estimated using exponential decay functions after an initial behaviour occurred within 1 ps. A slow decay of these correlation functions was witnessed and such results were expected due to strong intermolecular attractions in these IL-water mixtures that hindered rotational motions of particular ions. These rotational time scales are slightly larger than those reported for imidazolium-based IL (Chang & Dang, 2008; Kelkar & Maginn, 2007). It is clear that water molecules have a substantial impact on the rotational motion of ions. By intercalated in the solvation shell, ions experienced a diminished caging effect and able to rotate freely. The water molecules rotated much faster than those of ions, which meet our expectation due to its smaller steric hindrance values.

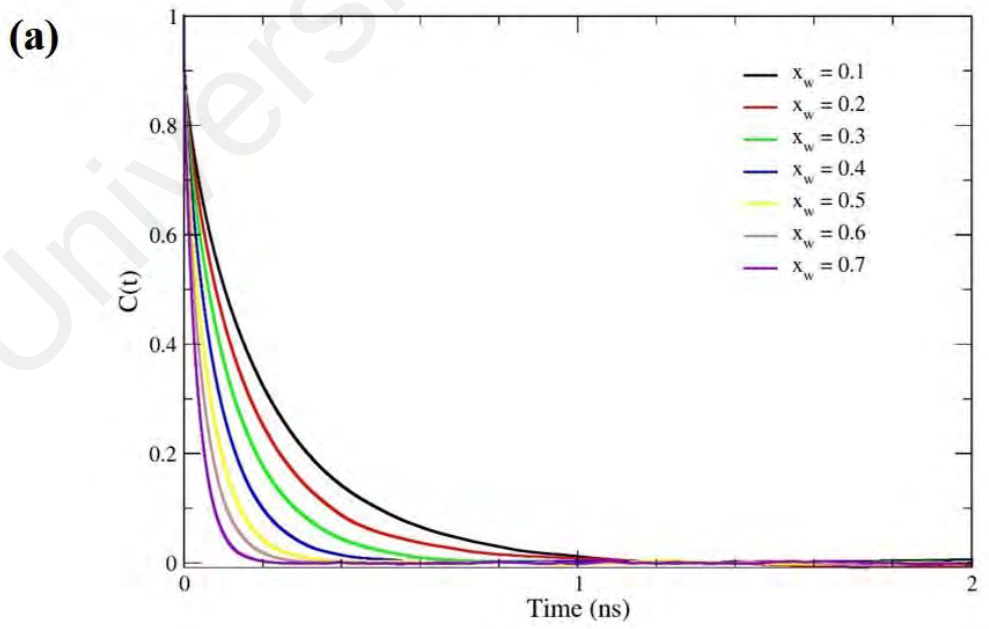


**Figure 4. 12**: The normalized rotational autocorrelation functions in IL-water (a) the N-H vector of $[gua]^+$; (b) the O-S vector of $[OTf]^-$.

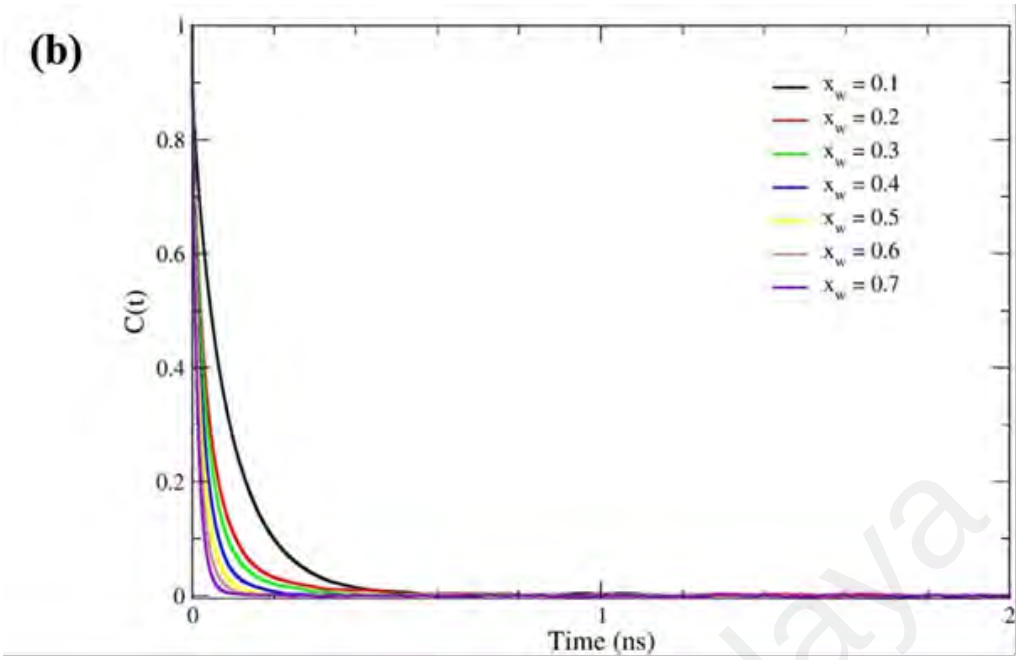


**Figure 4. 12,** continued.

## 4.2 Microstructures, Interactions and Dynamics Properties Studies of MDEA+ [Gua][Otf] + Water Tertiary System at Standard Temperature

### 4.2.1 Validation of the Force Field For Mixture Densities

To validate the force field used to model the ternary systems, the $\rho$ of mixtures were examined and compared against available experimental data. Table 4.3 present the densities for five ternary systems, as obtained experimentally (Sairi et al., 2015) and by our simulations (averaged over 6 ns isothermal-isobaric ensemble). The deviations of simulated densities values from experimental data reported by Sairi et al. (2015) is in the range of 1-5%. From the result, good agreement of approximate density values for both simulation and experiment is observed.

**Table 4. 3:** Density for [gua][OTf] +MDEA+ water systems at 298.15 K obtained from MD simulations.

| System | $x_{mdea}$ | $x_{IL}$ | $\rho$ (g cm$^{-3}$) | |
|---|---|---|---|---|
| | | | Calculated | Experimental |
| *a* | 0.09 | 0.03 | 1.09106 | 1.05531 |
| *b* | 0.14 | 0.04 | 1.11032 | 1.11781 |
| *c* | 0.16 | 0.07 | 1.16493 | - |
| *d* | 0.18 | 0.09 | 1.19577 | 1.18699 |
| *e* | 0.20 | 0.12 | 1.23134 | - |

* data taken from Sairi et al. (2015)

### 4.2.2 Solute-water interactions

MDs simulations allow us to determine the structure of substance over the RDF. The RDF calculations were performed using *g_rdf* tool. This RDF represents the probability of finding two molecules separated by a distance from a particular point. This function shows the number of neighbouring atoms, *Y* around a central atom, *X* in a defined volume (Orozco et al., 2014). We first analyze the RDFs of the effect of water in [gua][OTf] ion pair and the effect of water in MDEA molecules. In this part, due to a large number of atoms, it is required to define the following symbolization: $O_W$ and $H_W$ refer to oxygen and hydrogen belonging to water, $O_N$ and $H_N$ refer to the oxygen and hydrogen atoms of the hydroxyl group, $N_N$ refers to nitrogen atom of amino group of the MDEA molecule, H and N represents the hydrogen and nitrogen atoms of $[gua]^+$ ion, while O represent as oxygen of the sulfonate group as well as F atoms refer to fluorine atoms of $[Otf]^-$ ion, respectively.

### 4.2.3 Interaction and structures studies of aqueous [gua][OTf] in amine media

To study the special effects of water on [gua][OTf] liquid structure, the radial distribution function, *g(r)*, between the COM of $g(r)_{cation\text{-}cation}$, $g(r)_{\text{cation-anion}}$ and $g(r)_{\text{anion-anion}}$ were calculated for five different *x* of [gua][OTf], MDEA and water and shown in Figure 4.13. Two key ideas are noticeable from these figures. First, well defined RDF peaks are observed in cation-anion even at a low molar fraction of [gua][OTf], proposing the persistence of long-range spatial correlations between these ions. Second, as molar fraction of [gua][OTf] increases, the broadening of RDF peaks and the shifts in the peak positions of these RDFs proved that water molecules have shown an important character in modifying the [gua][OTf] structure. By presenting water molecules into the [gua][OTf], the cation-cation RDF (Figure 4.13(a)) interactions become suggestively less frequent even at high [gua][OTf] *x*.

Suggesting that the strong cation-cation association is weakened by the presence of water molecules. While the first peak of the anion-anion RDF (Figure 4.13(c)) interactions broaden and shift into smaller separations. These show that water molecules have reduced the cation-cation correlations and broadening the anion-anion RDF peak even at high *x* of [gua][OTf], respectively. Conversely, both cation-cation and anion-anion pairs are consistently distributed, and the RDF peaks at r~12 Å fades as molar fraction of [gua][OTf] increases. However, as shown in Figure 4.13(b), the two maxima peaks between the cations and anions can be clearly identified located at r~4.7 and 5.3 Å, which may be due to the tendency of water molecules localizes around [gua] cation plane (Figure 4.15(a)). However, the strong cation-anion association is not weakened by the absence of water molecules although at a low molar fraction of [gua][OTf] in amine media. This behaviour suggesting that the existence of water molecules cannot affect the strong association between cation-anion even at a low molar fraction of [gua][OTf].

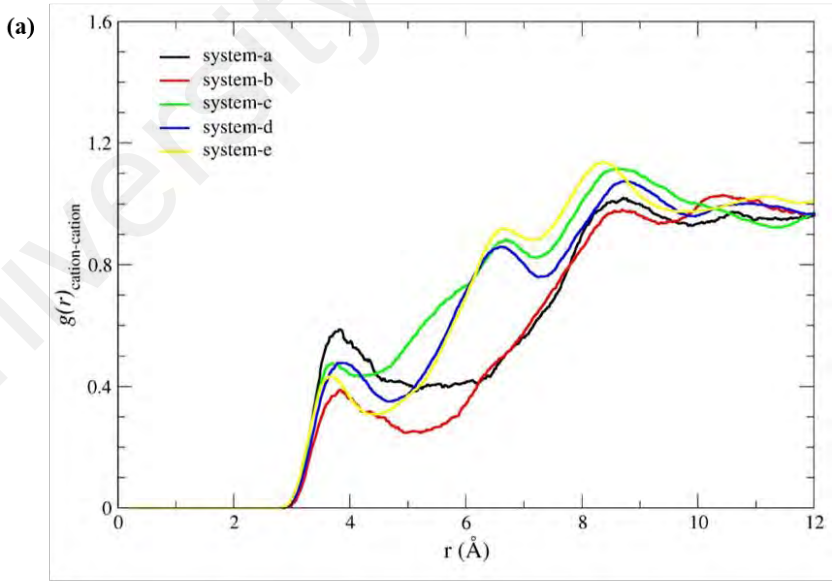


**Figure 4. 13:** RDFs of tertiary system: (a) $g(r)_{\text{cation-cation}}$, (b) $g(r)_{\text{cation-anion}}$; (c) $g(r)_{\text{anion-anion}}$.

(b)

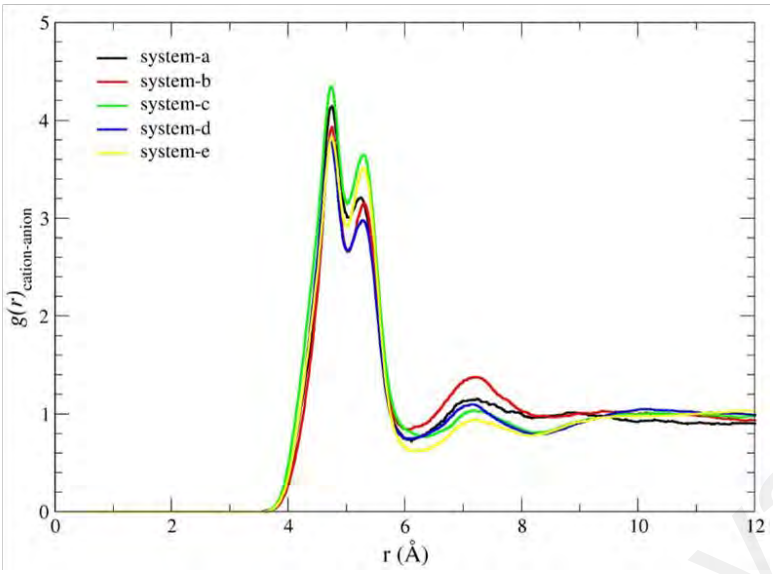


(c)

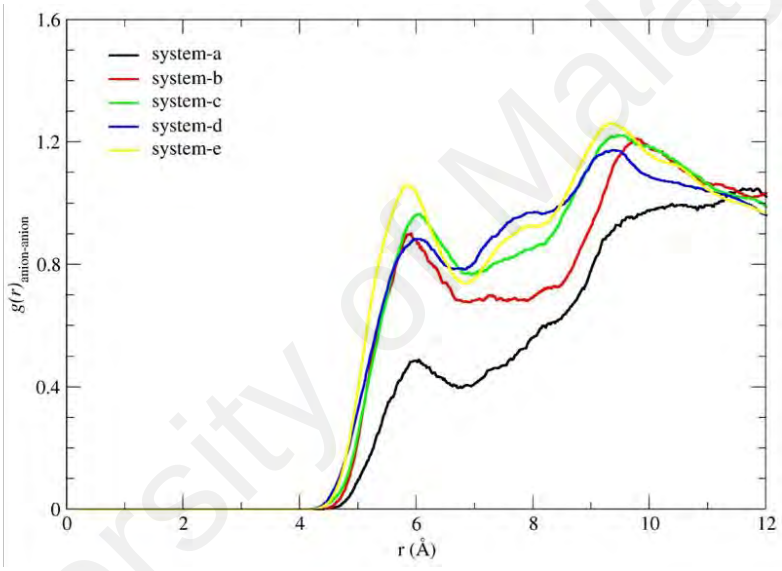


**Figure 4.13,** continued.

Figure 4.14 shows the atomic RDFs characters of complex features that we consider as molecular orientational correlations. Figure 4.14(a) corresponds to the pair distribution functions between hydrogen atoms of $[gua]^+$ with the oxygen atom of water ($g(r)_{O_w\text{-}H}$). It can be seen that the existence of hydrogen bonds between $[gua]^+$ ion and water molecules is confirmed with a very well define and sharp peak identified around r ~1.72 Å. This is due to direct interactions between water molecules with $[gua]^+$ ion.

Moreover, the heights of these peaks are found to decrease significantly decreasing [gua][OTf] molar fraction, again suggestive of strong water-ion interactions in dilute situations. It can be seen that the $g(r)_{\text{N-H}}$ (Figure 3(b)), even at a high molar fraction of [gua][OTf], the first solvation shell is unclear and so there is no proof of hydrogen bonds have taken place within cation-cation interaction. As shown in Figure 4.14(c), a very well defined and sharp RDF peaks located at r~1.7Å show that there is clear evidence present of hydrogen bonds between oxygen atoms from sulfonate group of $[OTf]^-$ and hydrogen atoms of water molecules, in which a very well defined and sharp peak.

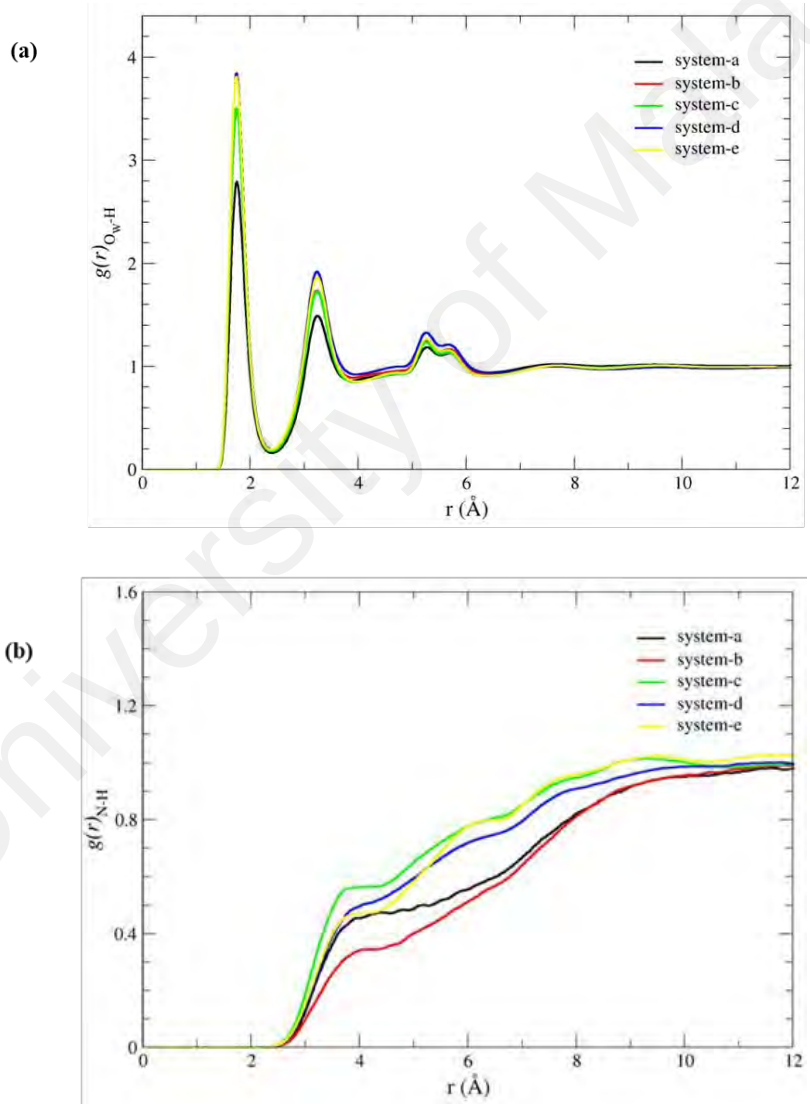


**Figure 4. 14**: RDF of the atomic pair correlation between the $[gua]^+$-$H_2O$ and $[OTf]^-$-$H_2O$. The RDFs between (a) oxygen atoms of water and hydrogen atoms of $[gua]^+$ ion; (b) nitrogen atoms of $[gua]^+$ ion and hydrogen atoms of $[gua]^+$ ion; (c) hydrogen atoms of water and oxygen atoms of $[OTf]^-$ ion; (d) hydrogen atoms of water and fluorine atoms of $[OTf]^-$ ion.

(c)

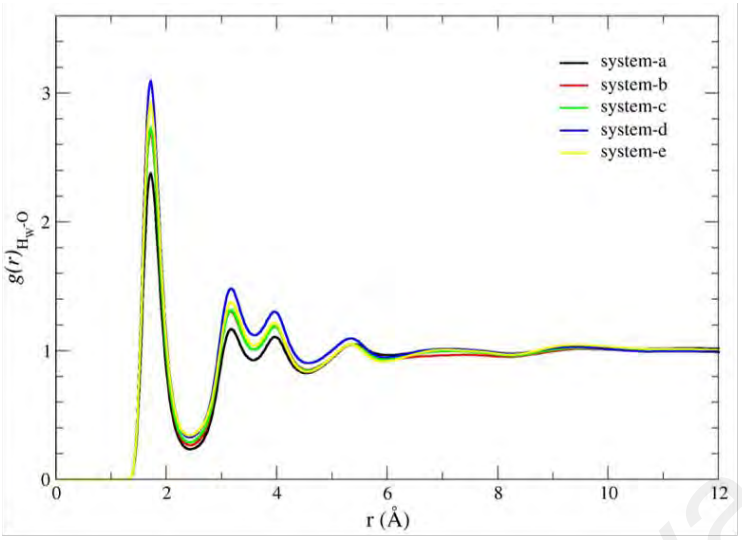


(d)

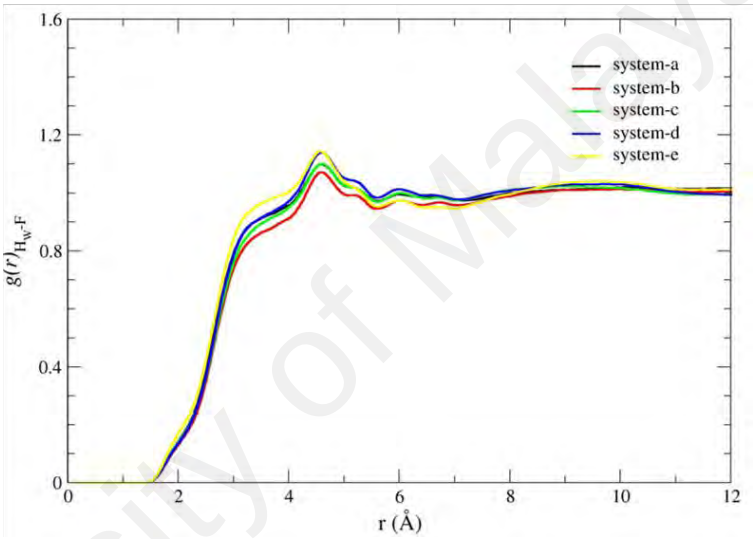


**Figure 4. 14,** continued.

However, from Figure 4.14(d) it can be seen that the broadening of the peaks and the shifts in the positions of the peak occur at RDFs. Therefore, since there is little tendency for fluorine atoms from $[OTf]^-$ ions to be hydrogen-bonded to water molecules in the first solvation shell, and because of the sign of a hydrogen bond between sulfonate group and water, we can conclude that sulfonate group are surrounded by water even at low or high molar fraction of [gua][OTf], respectively. This is due to the negative charges, which attached to the sulfonate groups, yielding interactions that are stronger than the interactions with electrophilic fluorines (Chang et al., 2010).

This suggests that anion-water local structural arrangement preferred with the hydrogen atoms bonded to the sulfonate group rather than fluorine atoms. This observation evidently points to the tendency of water to switch the counterions in the first coordination shell of the $[gua]^+$ and $[OTf]^-$ at a low or high molar fraction of [gua][OTf]. The SDF which computes the probability of finding a molecule in three-dimensional space around a centre molecule provides a more intuitive visual picture of the systems. In this work, the SDF is visualized by the software package PyMOL (DeLano, 2002). Figure 4.15 shows selected spatial distributions of waters (blue cap) around cation around $[gua]^+$ as well as waters (blue cap) around anion (sulfonate group of $[OTf]^-$). For clarity, only the COM of the water is depicted.

The strongest peak at RDF graph in Figure 4.14(a) is an indication of preferential distance for the COM of the water molecules around cation centre. SDF in Figure 4.15(a) shown that oxygen region site of water molecules are strongly localized around the hydrogen region site of the cation. It is probable to assume that the functional group responsible for hydrogen bonds, not the C=NH group but the $NH_2$ group of $[gua]^+$. While Figure 4.15(b), shows that the high charge density at the oxygen sites of the anion strengths the anion-water interaction. Therefore, water molecules are preferentially found around oxygen region site rather than fluorine region site of $[OTf]^-$. Besides, ILs with highly-fluorinated and charge-delocalized anions, tend to form hydrophobic ILs and are immiscible with water (Kohno & Ohno, 2012).

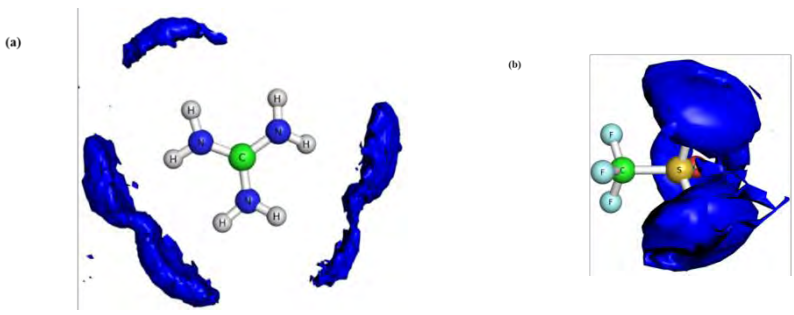


**Figure 4. 15**: SDFs: (a) waters (blue surfaces) around $[gua]^+$ ion; (b) waters around $[OTf]^-$ ion.

### 4.2.4 Interaction and structures studies of aqueous MDEA in [gua][OTf] media

MDEA is a ternary amine, contains two hydroxyl groups and there is no hydrogen associated with the amino group. Figure 4.16 shows the effects of MDEA in aqueous [gua][OTf]. Figure 4.16 also shows a well-defined primary solvation shell with their maxima located around r~3.18 Å at five different molar fractions of MDEA. This agrees that MDEA can associate between water due to their hydroxyl and amino groups. Figure 4.17, shows the atomic RDFs characters of MDEA with water as molecular orientational correlations. The first peak of the $g(r)_{N_N\text{-}N_N}$ in aqueous solution RDF (Figure 4.17(a)) broadens and shifts to smaller separations. Therefore, we can conclude that the first solvation shell is unclear and so there is no proof of intermolecular hydrogen bonding between amino groups of MDEA and appear to be relatively weak features even at a high molar fraction of MDEA. Figure 4.17(b) shows the behaviour of the amino group with water in term of $g(r)_{H_W\text{-}N_N}$ pair distribution function. It can be seen that these graphs are more intense and sharper than the $g(r)_{H_W\text{-}N_N}$ peaks. Thus, the presence of hydrogen bonds between amino groups of MDEA with water molecules is confirmed, with a maximum located around r~1.9 Å.

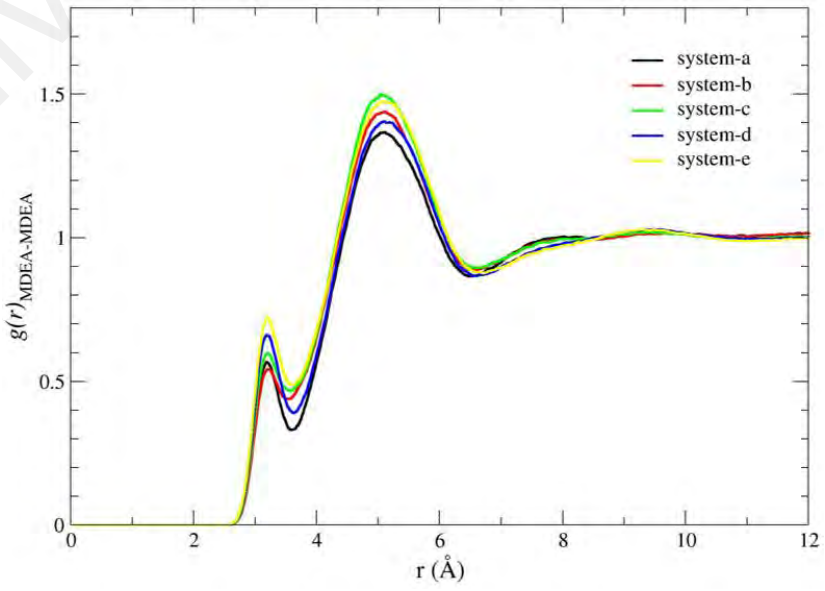


**Figure 4. 16:** RDF between COM of MDEA with water.

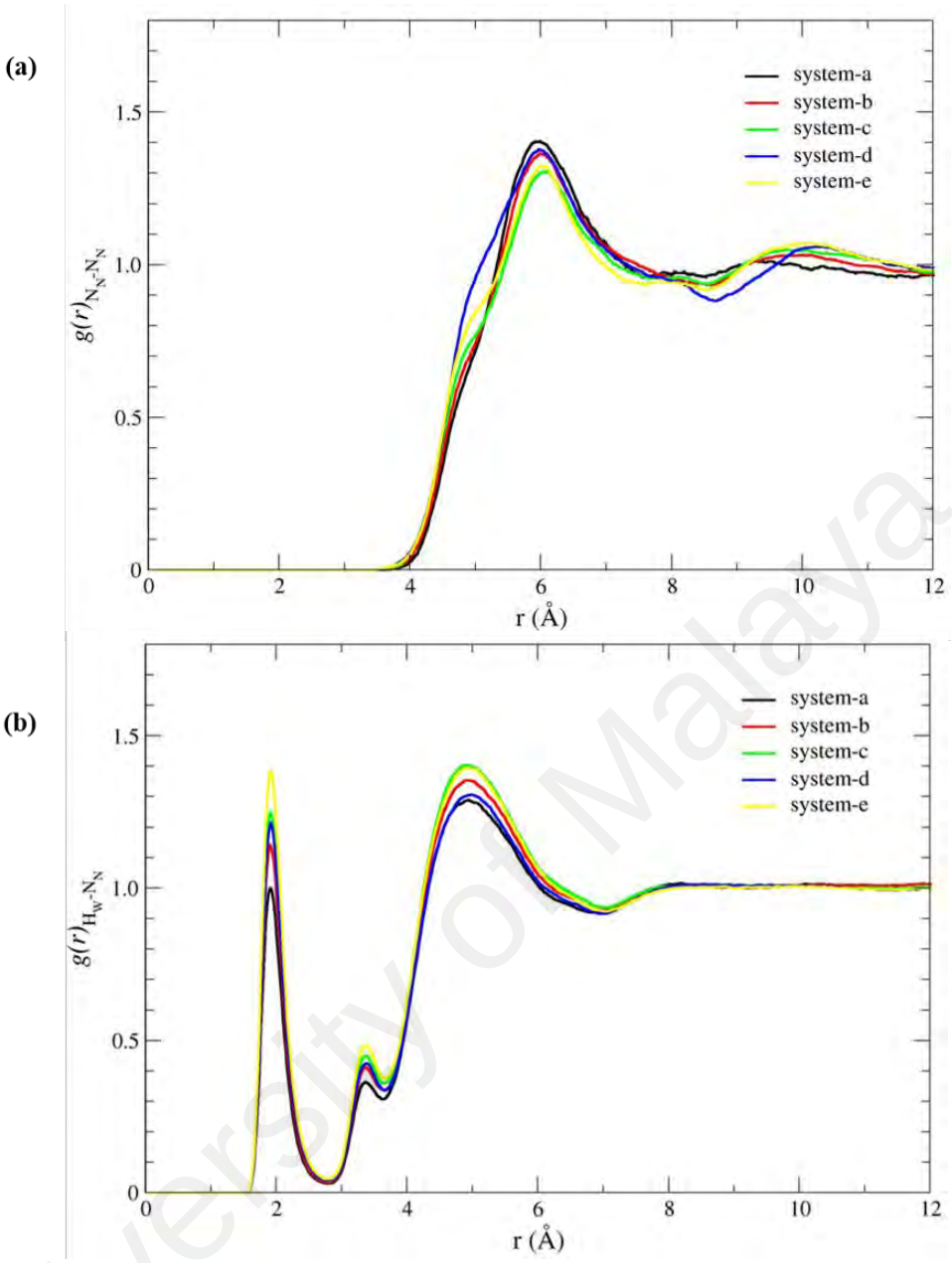


**Figure 4. 17:** RDFs of the atomic pair correlation between the MDEA-$H_2O$.The RDFs between (a) nitrogen atoms from amino group of MDEA; (b) hydrogen atoms of water and nitrogen atoms from amino group of MDEA; (c) hydrogen atoms of water and oxygen atoms from hydroxyl group of MDEA; (d) oxygen and hydrogen atoms from hydroxyl group of MDEA.

**(c)**

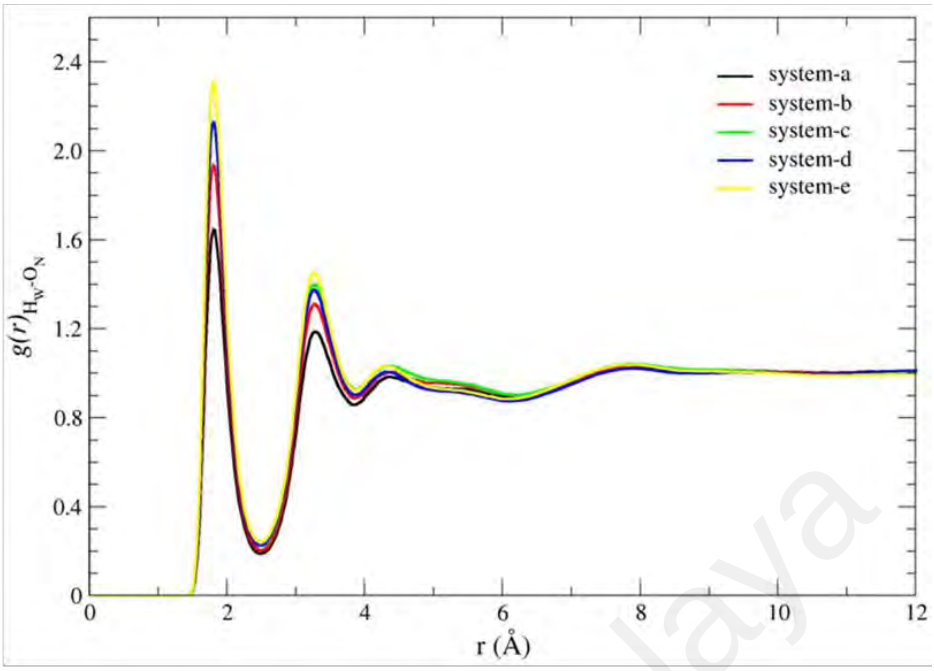


**(d)**

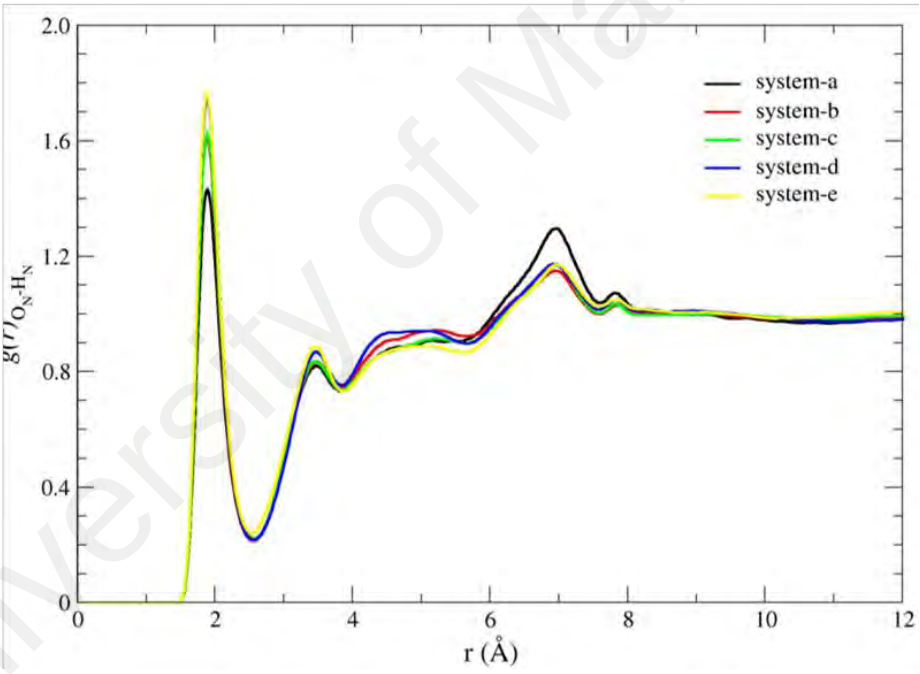


**Figure 4. 17,** continued.

Nevertheless, it is possible to see that the highest peaks correspond to the pair distribution function between the hydrogens belonging to water and with hydroxyl group of MDEA molecules in $g(r)_{H_W\text{-}O_N}$ (Figure 4.17(c)) with a maximum located around r~1.8 Å, indicating the presence of a hydrogen bond. In all cases their intensities are higher than the other RDF graphs. While, the presence of intermolecular hydrogen bonds between two hydroxyl groups of MDEA is confirmed with the results obtained for $g(r)_{O_N\text{-}H_N}$ showed in Figure 4.17(d), in which a very well defined around r~1.86 Å. Summarizing, association between MDEA with water is possible through the hydroxyl and amino groups. The hydroxyl group appears to have a stronger association rather than amino group. Orozco et al. (2014) also observed the same trend for aqueous solutions of amines and alkanolamine.

A more detailed picture of the spatial arrangement of the involved molecules may be obtained from spatial distribution function in Figure 4.18. Figure 4.18 show selected spatial distributions of waters (blue cap) around MDEA. For clarity, only COM of the water is depicted. The strongest peak at RDF graph in Figure 4.17(c) is an indication of preferential distance for the COM of the water molecules around MDEA molecules. This SDF in Figure 4.18 shown that, oxygen region site of water molecules are strongly localized around hydroxyl group region site of MDEA strengths the MDEA-water interaction. While, the charge density are also found around nitrogen atom from at the amino sites of the MDEA. Thus, it is probable to assume that the functional groups of MDEA responsible for hydrogen bonding between water molecules.

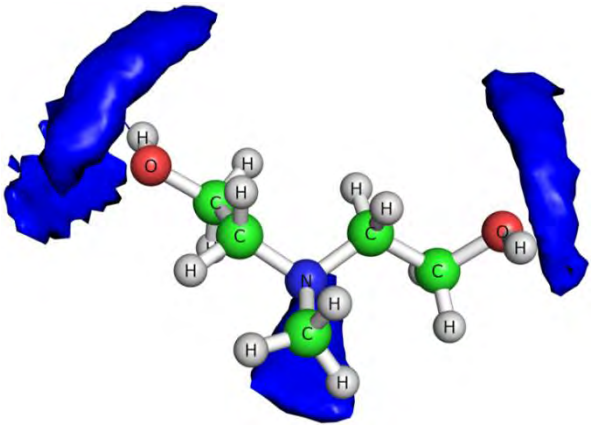

**Figure 4. 18**: SDFs of waters (blue surfaces) around MDEA molecules

### 4.2.5 IL-MDEA interactions

Figure 4.19 shows the RDFs calculated between the COM of $[gua]^+$, $[OTf]^-$ and MDEA of the system *a* where the mole fraction of water is the highest among all systems. Water plays a major role in altering the [gua][OTf] microstructure. As shown in Figure 4.19(a), one visible maximum sharp and well-defined peak can be clearly identified for the $g(r)_{\text{cation-anion}}$ function located around r~4.74 Å indicates that, $[gua]^+$ appears to favor interaction with the MDEA rather than with water. This behaviour indicates that there is persistence of long-range cation-anion correlations between these ions. For MDEA-MDEA and water-water distribution, the sharp initial increase of the water-water RDF, compared with the broadening MDEA-MDEA curve, suggests a more specific $[OTf]^-$ also appears favor interaction with the MDEA rather than with water. As can be seen, the structural behaviour for the other systems is found to be similar (in Appendix U) and there is no big differences can be appreciated. The coordination number (CN) for Figure 4.19(a) are shown in Appendix V in appendix section. Based on Figure 4.19(b), it is clearly shows that the slightly stronger interaction of water-water is observed when increasing the concentration of IL.

(a)

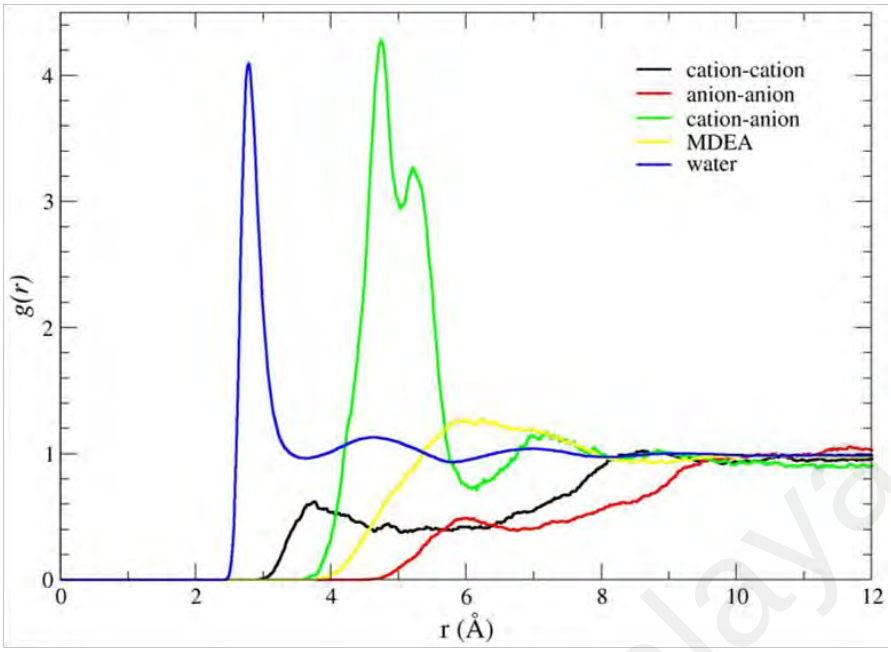


(b)

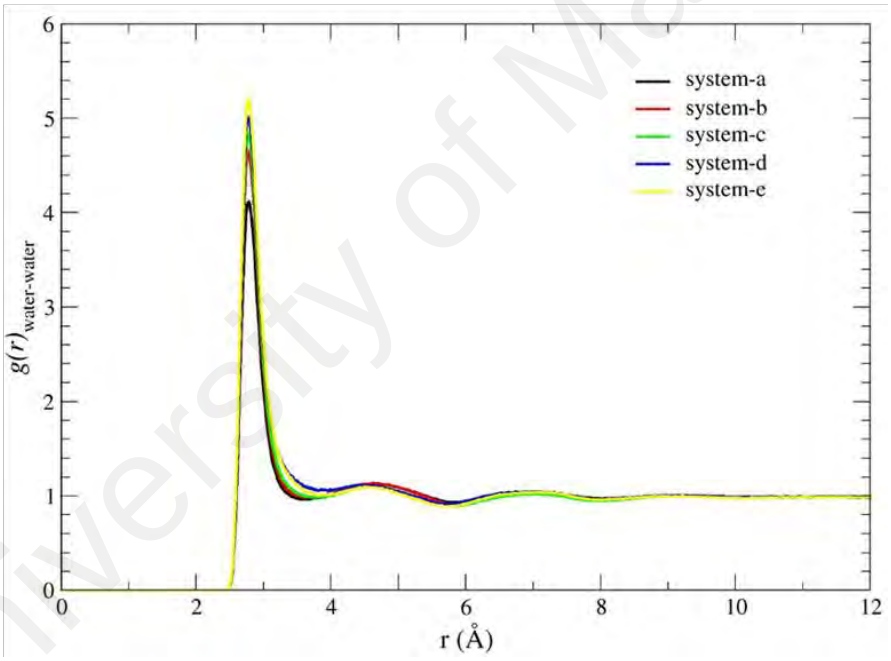


**Figure 4. 19:** Center of mass RDF of system *a* with mol fraction of water, MDEA, IL are 0.88, 0.09, 0.03, respectively: (a) MDEA/water, cation and anion around central cation, anion around anion central ; (b) $g(r)_{\text{water-water}}$ for different $x_{\text{IL}}$

More specific interaction between water molecules and [gua][OTf] even at high *x* of [gua][OTf] can be found. In addition, the relevant calculated RDFs are reported in Figure 4.20. The behaviour of Figure 4.20 is quite similar to that for water-[gua][OTf] and water-MDEA interaction systems (Figure 4.14 and 4.17): IL-MDEA structuring effected by addition molar fraction of [gua][OTf] in which little tendency for fluorine atoms from $[OTf]^-$ ion to be hydrogen bonded to MDEA in the first solvation shell (Figure 4.20(b)), while strong hydrogen bond between MDEA with sulfonate group (Figure 4.20(a)) is observed.

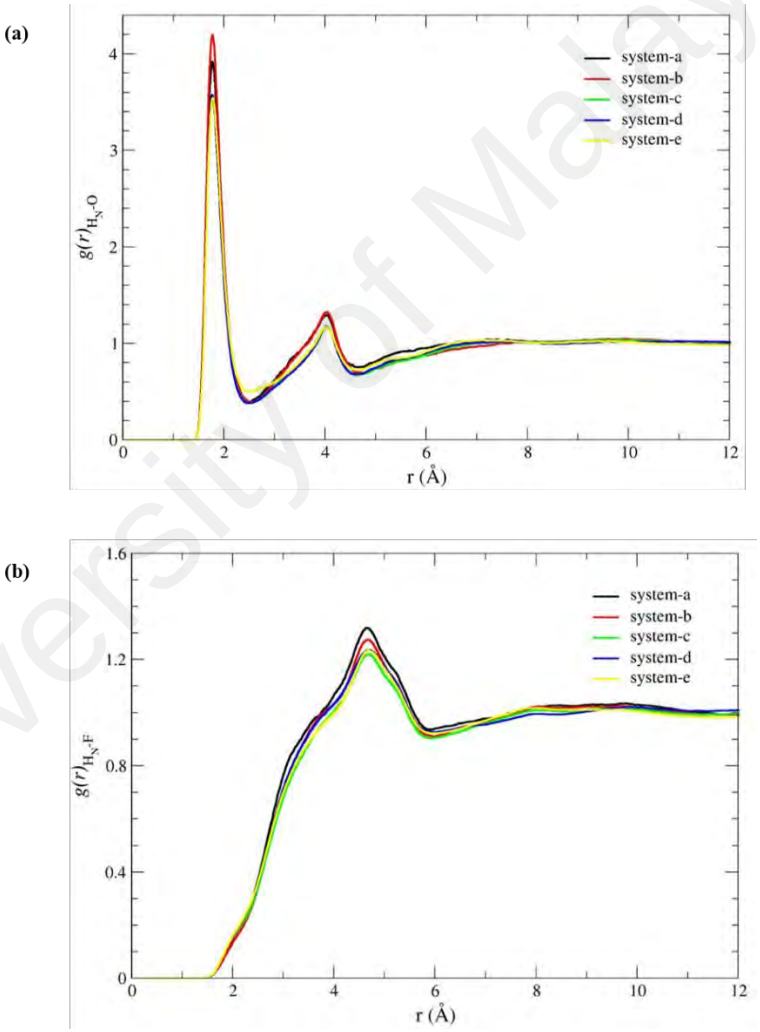


**Figure 4. 20:** RDF of the atomic pair correlation between the MDEA-IL: (a) hydrogen atoms from hydroxyl group of MDEA and oxygen atoms of $[OTf]^-$ ion; (b) hydrogen atoms from hydroxyl group of MDEA and fluorine atoms of $[OTf]^-$ ion; (c) hydrogen atoms of $[gua]^+$ ion and oxygen atoms from hydroxyl group of MDEA; (d) ) hydrogen atoms of $[gua]^+$ ion and nitrogen atoms from amino group of MDEA

(c)

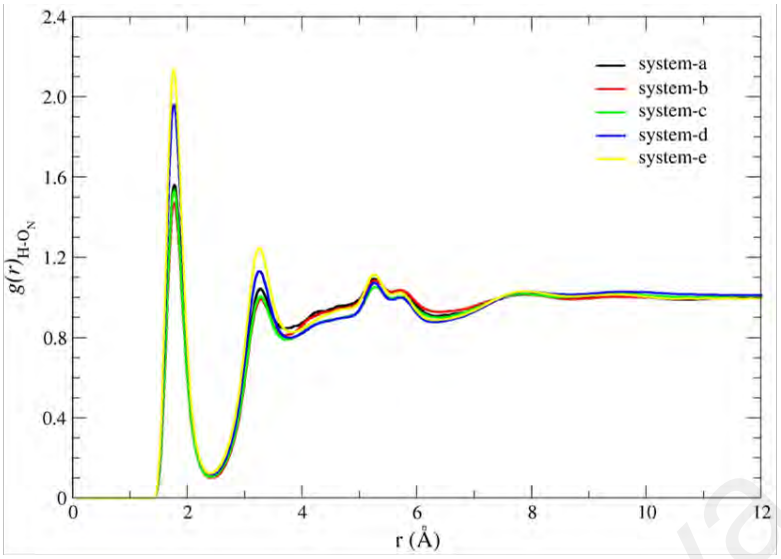


(d)

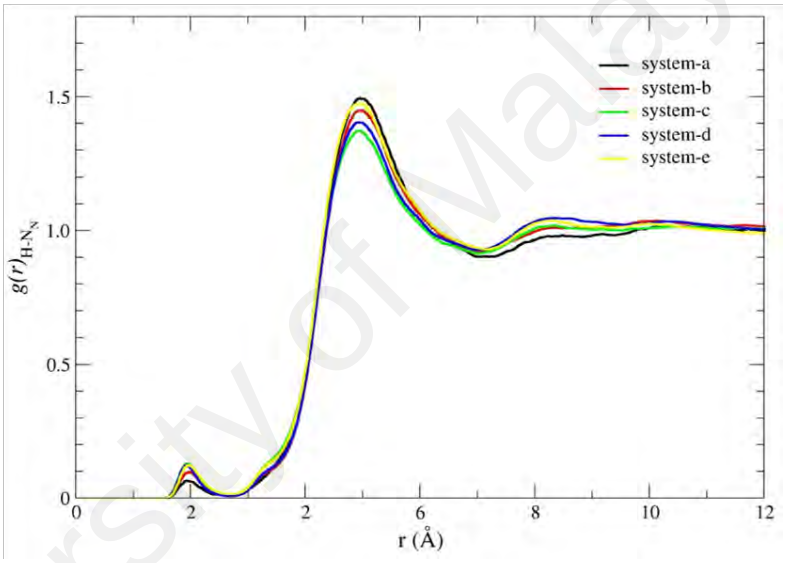


**Figure 4. 20,** continued.

There are also intramolecular interactions between two hydroxyl groups of MDEA molecules, which can form hydrogen bonding. SDF for COM distribution of MDEA-IL interaction are reported in Figure 4.21(a), structuring $[gua]^+$ ions (red cap) and $[OTf]^-$ ions (yellow cap) around MDEA molecule. Figure 4.21(a) proved that, the cations and anions preferred localized around hydroxyl groups rather than amino group. While, Figure 4.21(b) and Figure 4.21(c) shows more specific MDEA appears favor interaction with the $[gua]^+$ and $[OTf]^-$ ions. MDEA around $[gua]^+$ ion is characterized by hydroxyl groups of MDEA (green cap) around $[gua]^+$ ion (Figure 4.21(b)). While, Figure 4.21(c) is characterized also by hydroxyl groups (green cap) of MDEA around $[OTf]^-$ ion. In figure 4.21, the MDEA of alkyl chain can rotation in the mixing phase with water. Therefore, the mobility of MDEA and the rotation of MDEA's alkyl chain may be also one of the factors.

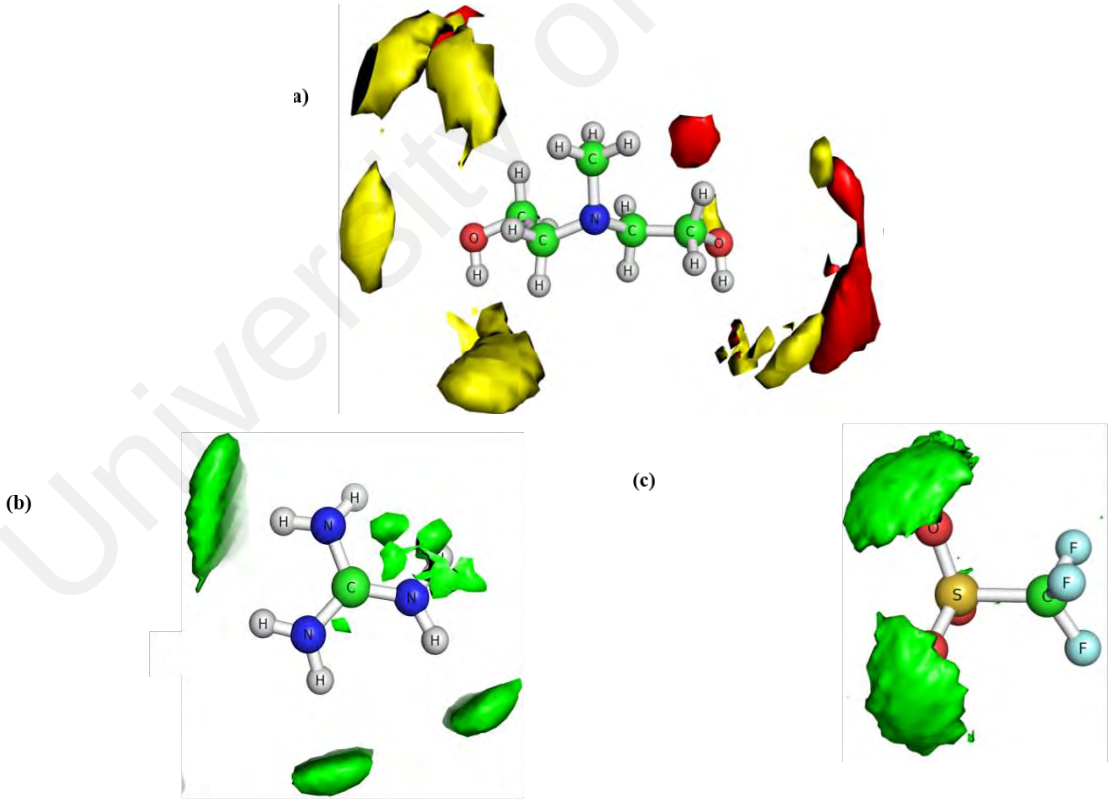


**Figure 4. 21:** SDFS: (a) $[gua]^+$ ions (red cap) and $[OTf]^-$ ions (yellow cap) around MDEA molecule; (b) MDEA (green surfaces) around $[gua]^+$ ion; (c) MDEA (green surfaces) around $[OTf]^-$ ion.

The previous paper by Cesare Marincola et al., (2012) reported that ammonium of alkyl chain is difficult to rotate in the pure ionic liquid and the alkyl chain can rotate in the mixing the ionic liquid with water by NMR spectroscopy. We have investigated the dihedral angle of MDEA's NT-CT-CT-OH and CT-CT-OH-HO changing in between the pure ionic liquid and the mixing ionic liquid with water. Based on the composition, system *a* have the highest composition of water and lowest composition of ionic liquid ($x_{water}$=0.88 and $x_{IL}$=0.03), whereas the lower composition of water is observed for system *e* ($x_{water}$=0.68 and $x_{IL}$=0.12). As expected, we have found that system *e* in higher IL concentration has the NT-CT-CT-OH torsion of -5.60 ± 20.10 and CT-CT-OH-HO of -0.04 ± 15.74 which indicated the smaller rotation compare to the system *a* (NT-CT-CT-OH torsion of 11.57 ± 30.21 and CT-CT-OH-HO of 0.83 ± 4.11.

The main chain NT-CT-CT-OH in higher IL concentration cannot rotate much where the end chain CT-CT-OH-HO has not much significant difference in the torsion distribution for two compositions. Therefore, NT-CT-CT-OH and CT-CT-OH-HO are difficult to rotate in pure ionic liquid and easily rotate in the mixing ionic liquid with water. In addition, the motional freedom of the whole molecule has been increased at higher water contents. Based on Figure 4.21(c), an examination of the specific spatial distribution of $H_N$ around the anion shows that hydrogens atoms from hydroxyl group in MDEA are positioned near the high charge density at the oxygen sites of the anion rather than fluorine region site of the $[OTf]^-$. While, as we can see $O_N$ from hydroxyl group in MDEA are positioned near the H atom from cation rather than the nitrogen atom of $[gua]^+$ ion.

### 4.2.6 Viscosity and diffusion coefficient

The main obstacle of using ILs in the industry is to improve the transport properties by reducing its viscosity and improving its diffusion coefficient while preserving its chemical stability as well as their excellent solvent properties. It is beneficial to the applications in the natural gas industry such as removing $CO_2$ using ILs as a solvent. On the other hand, the viscosity of the ternary systems increases by increasing the molar fraction of [gua][OTf] and MDEA and it is valuable to the industry applications for removal $CO_2$ at high pressure. For instance, Sairi et al., (2011) have studied the solubility of $CO_2$ in aqueous MDEA and IL systems at the pressure ranged from 500 to 3000kPa. Tian et al. (2012) have reported the phase behaviour of IL mixtures and the solubility of $CO_2$ at elevated pressures. They have made an impact to improvement of the research on coupling $CO_2$ with ILs, but, neither of them has stated the *D* of IL-$CO_2$ at high pressure. Therefore, we are interested to explore the diffusion using the molecular dynamics simulation. Usually, due to the strong hydrogen bonds interaction, the diffusion coefficient of the ILs is very low (Dong et al., 2006).

For this work, the *D* is obtained by linear fitting of the slope in the region from 4 ns to 6ns of MSD curves against time for all simulated systems. The results are given in Table 4.4. It can be seen that the *D* of both [gua][OTf] and water decrease with the increasing of the mole fraction of MDEA in the liquids phase while the diffusion coefficients of both MDEA and [gua][OTf] increase with increasing of the mole fraction of water. Aparicio & Atilhan (2012) stated that a decrease in the average diffusion rate of the mixed fluid should lead to an increase in viscosity. When MDEA mole fraction is 0.09, the dynamics of the ternary system is characterized by diffusion heterogeneity, with water molecules diffusing faster than [gua][OTf] and MDEA. Water would be expected to increase the rate of diffusion. Therefore, the addition of water molecules leads to an increase in the diffusion rate for all the involved molecules.

The structure of MDEA molecules has to significantly change in order to accommodate more [gua][OTf] and water molecules, which has an obvious impact on the transport properties of the ternary system.

**Table 4. 4**: *D* for [gua][OTf] + MDEA+ water systems at 298.15 K obtained from MD simulations.

| System | $x_{IL}$ | $x_{MDEA}$ | $D$ x $10^9$/m$^2$ s$^{-1}$ | | |
|---|---|---|---|---|---|
| | | | water | IL | MDEA |
| *a* | 0.03 | 0.09 | 1.1± 0.030 | 0.28 ± 0.018 | 0.29 ± 0.047 |
| *b* | 0.04 | 0.14 | 0.64 ± 0.020 | 0.13 ± 0.027 | 0.11 ± 0.018 |
| *c* | 0.07 | 0.16 | 0.44 ± 0.026 | 0.083 ± 0.027 | 0.10 ± 0.014 |
| *d* | 0.09 | 0.18 | 0.27 ± 0.0048 | 0.031 ± 0.0033 | 0.051 ± 0.0024 |
| *e* | 0.12 | 0.20 | 0.16 ± 0.043 | 0.024 ± 0.0062 | 0.035 ± 0.00060 |

The viscosity (*η)* analysis was performed employing the periodic perturbation method (Allen & Tildesley, 1989) as shown in Table 4.5. This method has been reviewed in the 2000s by Hess (2002). Increasing of [gua][OTf] and MDEA and decreasing of water molar fraction can significantly increase the viscosity of ternary systems, respectively. This aspect can be described by hydrogen bonding existing in pure IL and between IL with solvents too. The addition of distilled water during the IL mixture preparation reduced to a large extent the aqueous mixture viscosity due to the water low viscosity. Decrease of the viscosity is due to the presence of the water molecules which reduces the electrostatic attractions between the ions. Therefore, the overall cohesive energy of the system is decreased and consequently, viscosity is decreased as well.

**Table 4. 5:** Viscosity for [gua][OTf] + MDEA+ water systems at 298.15 K obtained from MD simulations.

| System | $x_{MDEA}$ | $x_{IL}$ | $x_{water}$ | $\eta$ (mPa.s) |
|---|---|---|---|---|
| *a* | 0.09 | 0.03 | 0.88 | 1.20 |
| *b* | 0.14 | 0.04 | 0.82 | 3.97 |
| *c* | 0.16 | 0.07 | 0.77 | 7.40 |
| *d* | 0.18 | 0.09 | 0.73 | 27.45 |
| *e* | 0.20 | 0.12 | 0.68 | 44.37 |

Whereas, Figure 4.22 shows the snapshots for all ternary systems. At low *x* of MDEA and [gua][OTf] (system a-c), water molecules start to intercalate between MDEA molecules and [gua][OTf] ion pairs to produce hydrogen bonding between themself. However, at high *x* of MDEA and [gua][OTf] (system d-e), interaction between MDEA molecules in Figure 4.17(b) and 4.17(c), [gua][OTf] in Figure 4.14(c) and 4.14(d) with water molecules becomes stronger as in because they increase the intermolecular and intramolecular hydrogen bonds, making it more resistant to flow since both nitrogen and oxygen atoms are strongly electronegative. Therefore, those substances which are capable of forming hydrogen bonds tend to have a higher viscosity than those that do not.

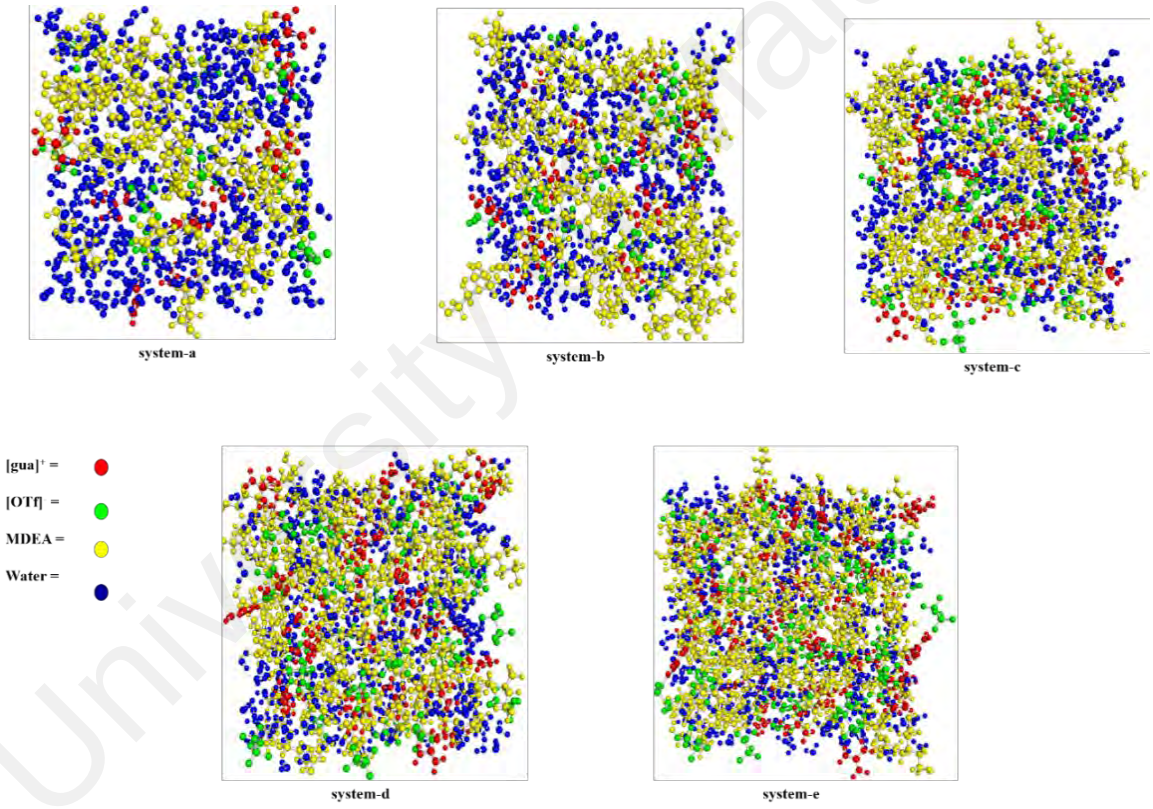


**Figure 4. 22**: Snapshots of [gua] [OTf]-MDEA- water mixtures for all systems to showing the structure of strong hydrogen bonding between molecules.

Substances which have the possibility for multiple hydrogen bonds exhibit even higher viscosities. Thus, increasing of [gua][OTf] and MDEA and decreasing of $x_w$ can significantly increase the viscosity of ternary systems, respectively. The simulating results indicate that the microstructures of systems have been changed a little while the viscosity can be quite high when adding IL. However, from the experimental results, the viscosity of ILs significantly decreases with the addition of $CO_2$ while maintaining its chemical stability and excellent solvent properties. The volumes of the mixtures increase slightly even though a large amount of $CO_2$ is dissolved in the IL liquid phase (Lu et al., 2003; Shiflett & Yokozeki, 2005; Tomida et al., 2007). Further exploration in the microstructure for the effect of adding $CO_2$ should be further investigated. A possible explanation is that $CO_2$ could form the strong interaction with amino group, which could accelerate the removal rate or hydroxyl group in a similar situation as water in void space at higher concentration of water which is found to be bound stronger at amino or hydroxyl group in MDEA or ILs.

## 4.3 Absorption Carbon Dioxide in MDEA + [Gua][Otf] Aqueous Solution

### 4.3.1 Ternary Mixture Solution (System I)

System I is known as a ternary solution, which contains aqueous [gua][OTf] IL including MDEA molecules. This system was set up using only a single building block with dimensions 40 x 40 x 40 Å, which contained 51 molecules of MDEA, 7 [gua][OTf] IL and 1970 water molecules. The overall density was 1118 $kgm^{-3}$, density value reported from literature (Sairi et al., 2015). Figure 4.23 showed that the system displayed a non-uniform pattern after ~0.5 ns in *X* direction. The solution started to form MDEA-free cavities so that $[gua]^+$ and $[OTf]^-$ stayed in the water while at the same time, MDEA stayed away from water.

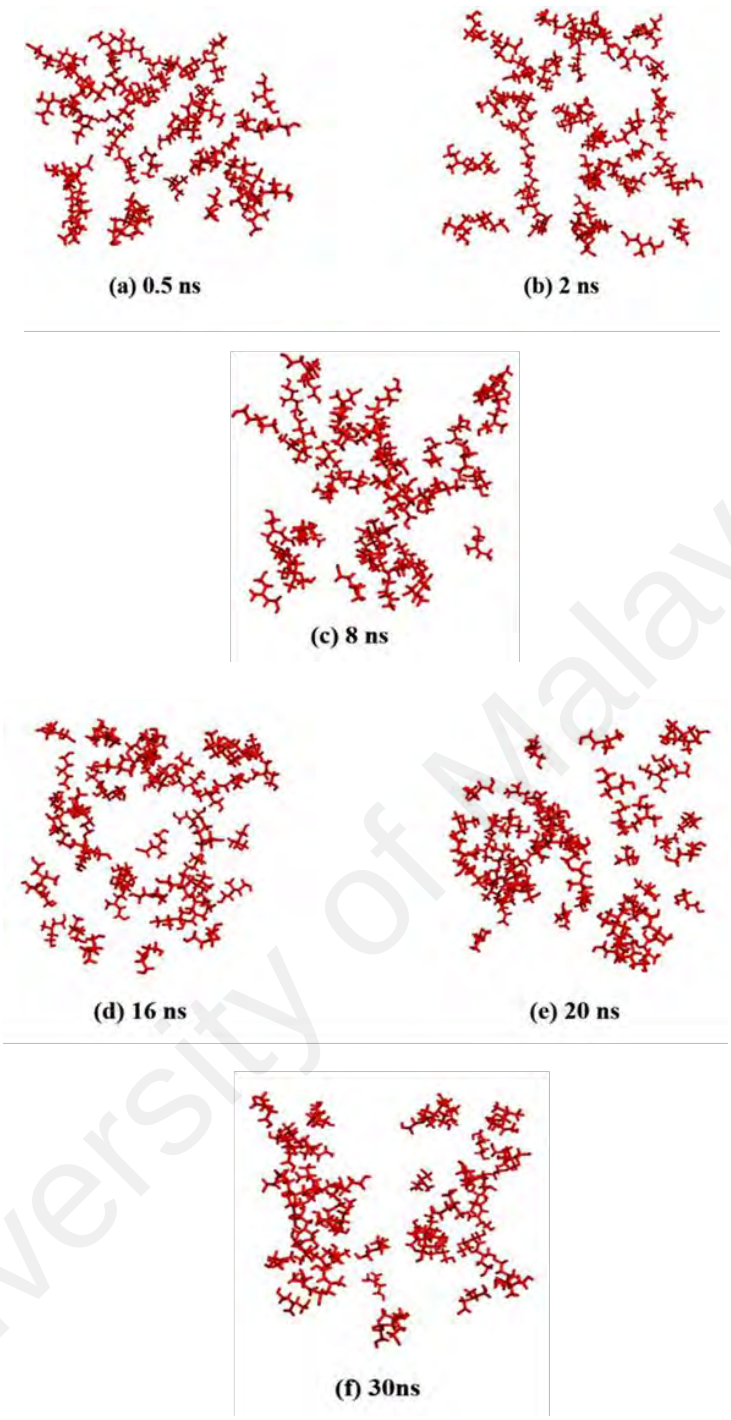


**Figure 4. 23**: Evolution of MDEA-free cavities leading to phase separation in *X* direction (only MDEA molecules are shown)

The main factor affecting the distribution of molecules in System I is caused by the characteristic solutes of hydrophobic and hydrophilic (Farmahini et al., 2011). The dominant solvent in the ternary solution is water, which is 82% of the existing molecules. Therefore, water has a strong dipole moment in the system and the implication of hydrophobic-hydrophilic behaviour was expected. $[gua]^+$ and $[OTf]^-$, which carried formal positive and negative charges respectively, preferred to stay inside the polar solvent (water), while neutral charge (MDEA) exhibited a marked hydrophobic behaviour.

Hence, MDEA and water molecules repel each other. This leads to the formation of the MDEA free cavities inside the ternary solution. These two dominated waters and dominated MDEA phases were separated by an almost static interface. By this static, it means that the shape of the interface did not change significantly over time. These cavities evolved over the simulation time so that, they gradually formed two separate phases after 20ns. In Figure 4.23, the illustration of IL is excluded but they are presented in Figure 4.24.

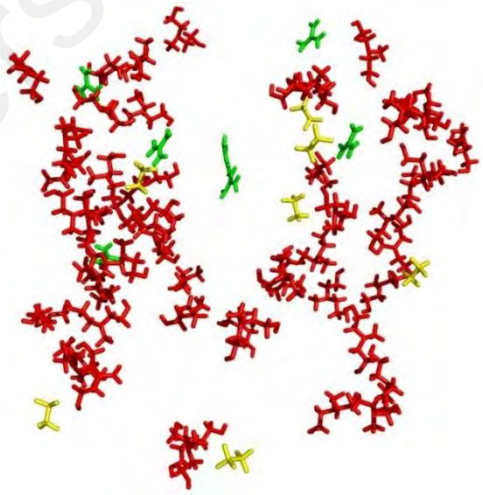

**Figure 4. 24**: Evolution of MDEA-free cavities leading to phase separation in X direction. Red lines show MDEA; yellow and green lines stand for $[OTf]^-$ and $[gua]^+$ ions.

To obtain more insight into the interaction between water, MDEA molecules and IL, the RDF, between the COM of $[gua]^+$, $[OTf]^-$ and MDEA molecules for System I are shown in Figure 4.25. Haron et al., (2015) reported that water plays a major role in altering the [gua][OTf] microstructure. As shown in Figure 4.25, the most dominant and sharp first RDF peak are clearly identified for $g(r)_{water}$ function located around $r \sim 2.76$ Å, which indicates that $[gua]^+$ and $[OTf]^-$ appears to favour interaction with the water molecules (hydrophilic character) rather than with MDEA molecules. This behaviour indicates that there is a persistence long-range cation-anion correlations between these ions. Besides, the existence of water molecules affects the strong hydrogen bonds between ions. This is due to direct interactions between water molecules (oxygen atoms) with $[gua]^+$ ion (hydrogen atoms) as well as water molecules (hydrogen atoms) with $[OTf]^-$ (Haron et al., 2015). The phase separation becomes virtually complete after about 20 ns from the RDF and density profile.

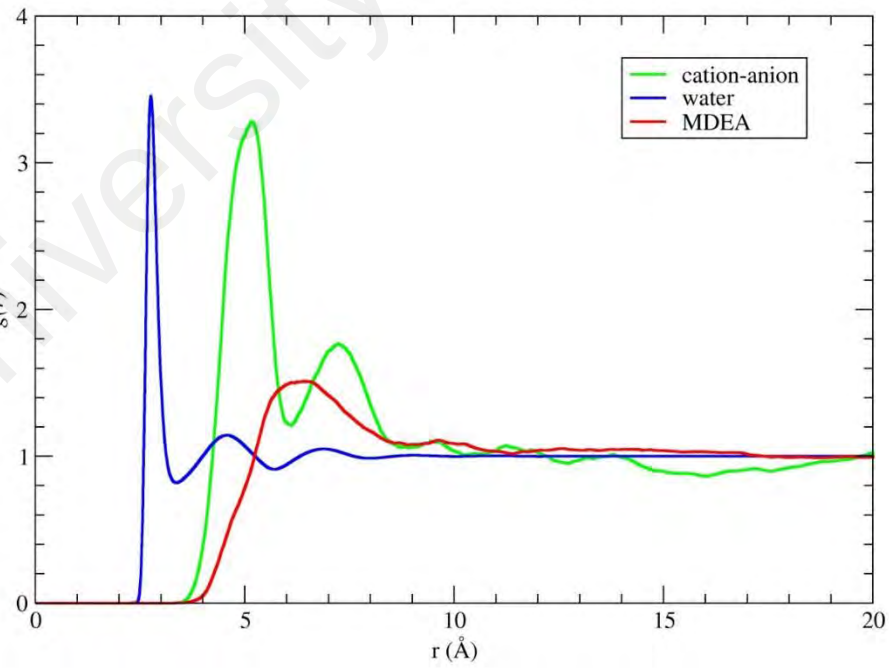


**Figure 4. 25**: RDF between COM of cation, anion, water and MDEA molecules

Figure 4.26 presents the density profile of the system along the *X* direction averaged over the last 0.2 ns of the simulation. It becomes evident when comparing Figure 4.23 and Figure 4.24 that the system's density profile stays consistent with the molecular distribution illustrated. The density profile in Figure 4.26 shows a dramatic decrease in the concentration of water (between ~20-35 Å) with the corresponding rise in the concentration of MDEA. As discussed before, $[gua]^+$ and $[OTf]^-$ mostly stayed inside the polar phase showing their hydrophilic character.

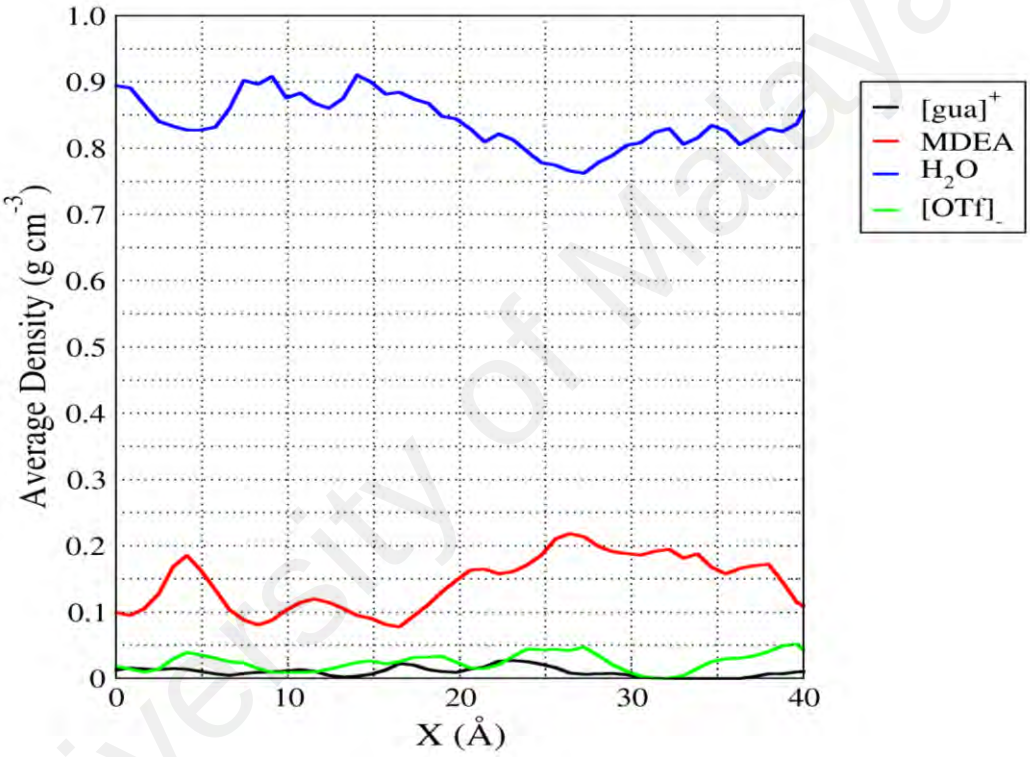


**Figure 4. 26**: Density profile of System I averaged over the last 0.2 ns of the simulation.

Table 4.6 shows the relative contribution of different species to hydrogen bond network. These results explain the preference of $[gua]^+$ and $[OTf]^-$ stayed at the water phase. All of them appear to have successfully formed hydrogen bonds with surrounding water even in the low concentration system (7 IL pairs). Therefore, water will be a favourable environment for the IL, and they will strongly prefer to stay inside the water bulk in this system. Farmahini et al., (2011) also reported that ionic piperazines strongly stayed inside the water bulk in MDEA solution.

**Table 4. 6**: Average number of hydrogen bonds per simulation frame.

| Molecular pair | $H_2O$-$[gua]^+$ | $H_2O$-$[OTf]^-$ | MDEA-$[OTf]^-$ | MDEA-$[gua]^+$ |
|---|---|---|---|---|
| Number of H-bonds per species | 4.71 | 4.71 | 0.09 | 0.27 |

### 4.3.2 Ternary Mixture Solution and Liquid Carbon Dioxide (System II)

System II contains a ternary solution contacted with liquid carbon dioxide at a density corresponding to the pressure of 100 bar and temperature 298.2 K (536 molecules). The ternary solution used was identical to system I. Since water will be present in a real $CO_2$ capture operation, the interaction between water and IL is also of interest. At the beginning of the simulation, the two separate $CO_2$ and ternary solution building blocks were placed side by side. Once the simulation was initiated, these two phases were allowed to interact with one another. Similarly, to System I, the molecular distribution of the system was strongly affected by the hydrophobic-hydrophilic characteristics of different species.

Given the relatively hydrophobic nature of carbon dioxide presents as a separate phase in this system, it would be favourable for the other hydrophobic species to move away from the aqueous phase into the carbon dioxide bulk, and this was exactly the behaviour observed in this system. At the start, the ternary solution and carbon dioxide phase were completely separated, but as the simulation progressed, MDEA started to move out of the water phase and dissolve into the liquid carbon dioxide, while $[gua]^+$ and $[OTf]^-$ preferred to stay inside the water. Instantaneously, we observed a small degree of carbon dioxide dissolution in water. Figure 4.27 shows the time evolution of the system and emerging molecular distribution patterns. The connected purple spheres represent carbon dioxide molecules; the blue dotted area is an aqueous phase; red lines show MDEA; large yellow and green connected balls molecules stand for $[gua]^+$ and $[OTf]^-$.

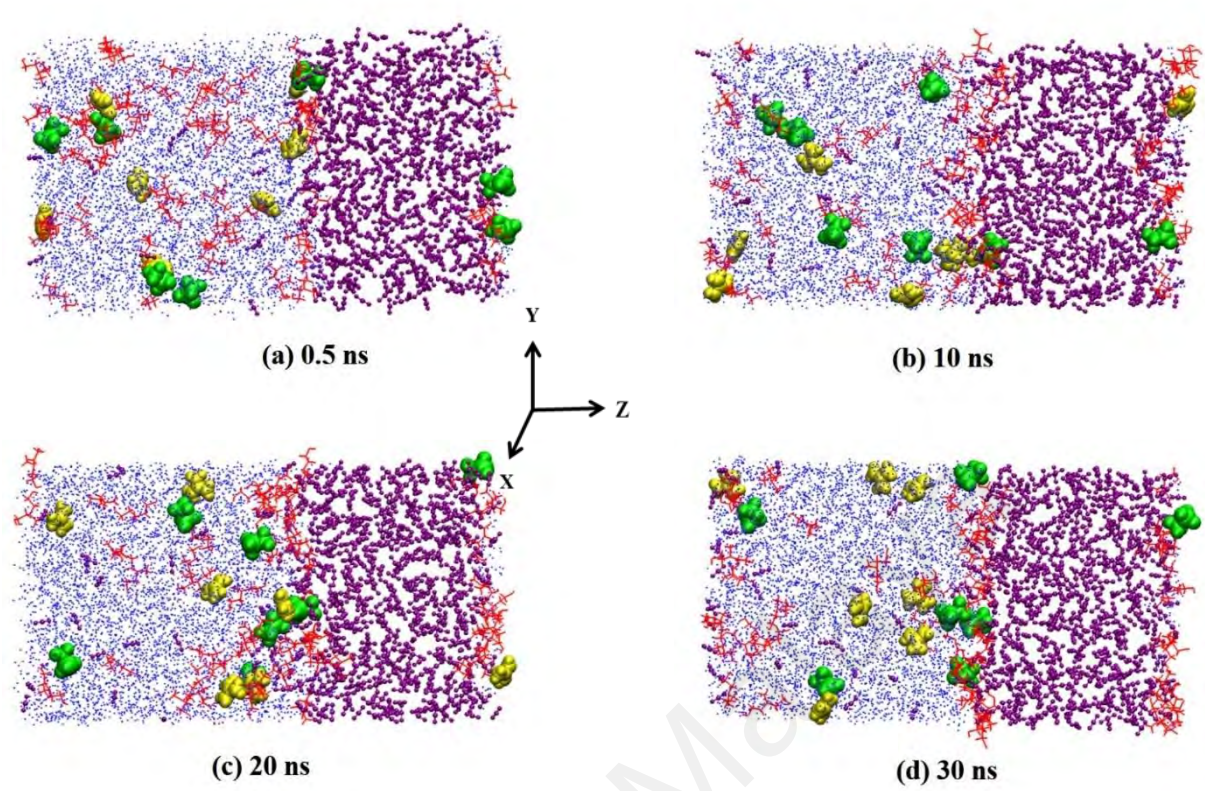


**Figure 4. 27**: *Z* direction of System II as it evolves with time. Connected purple spheres represent carbon dioxide molecules; blue dotted area is aqueous phase; red lines show MDEA; large yellow and green connected balls molecules stand for $[gua]^+$ and $[OTf]^-$.

To obtain more insight $CO_2$ go into guanidinium cavities, we calculated the radial distribution function between COM of cation-anion, cation-cation, anion-anion, water, MDEA and $CO_2$ molecules for System II over the last 0.2 ns of the simulation (Figure 4.28). The most dominant and sharp RDF peak is clearly identified for $g(r)_{\text{cation-anion}}$ around r ~ 4.5 Å, which indicates $CO_2$ molecules (purple line) appears to favour interaction with cation (black line) at r ~ 6.1 Å and MDEA molecules (red line) at r ~ 5.8 Å rather than anion molecules (green line) at r ~ 5.0 Å. This behaviour indicates that guanidinium IL provide some cavities in which $CO_2$ gas molecules mainly exist (Liu et al., 2014). Some of the researchers found that the cavities are closely associated with the capture process of $CO_2$ (Cadena et al., 2004; Huang et al., 2005; Liu et al., 2014). Huang et al., (2005) simulated the system of imidazoles ionic liquids and $CO_2$.

The addition of $CO_2$ molecules didn't influence the imidazoles structure of ionic liquids. They noticed there are some cavities in the IL, which enable the $CO_2$ molecules not to destroy the microscopic structure of the IL when they enter into the cavities. The presence of F atoms in poly(ionic liquid)s is not a significant factor for improved $CO_2$ sorption (Privalova et al., 2013; Tang et al., 2005). The phase separation becomes virtually complete after about 30 ns.

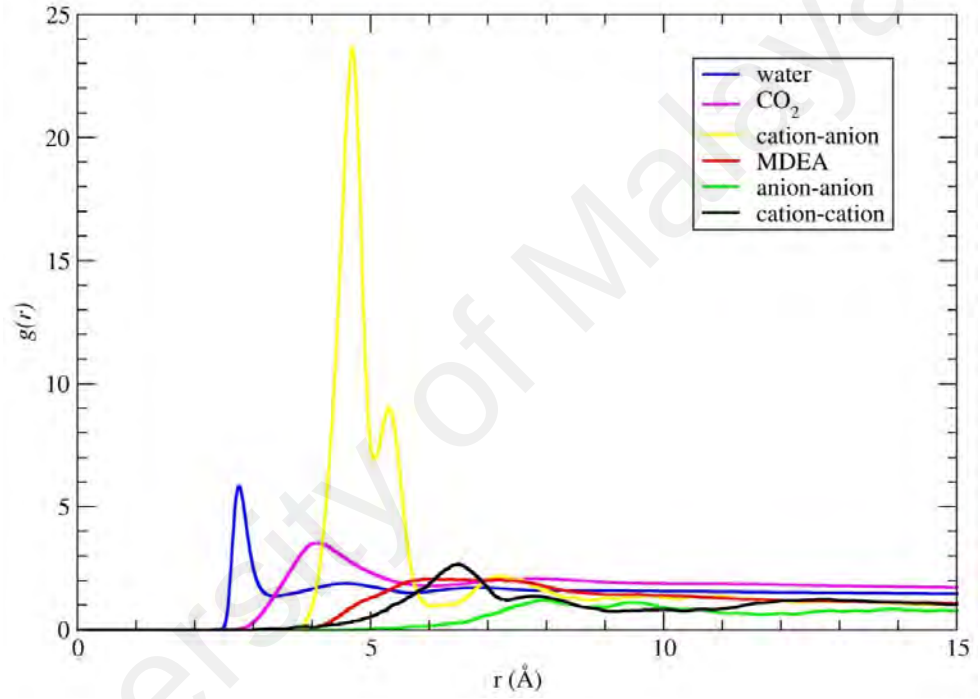


**Figure 4. 28**: RDF between COM of cation, anion, cation-anion, water, MDEA and $CO_2$ molecules.

Figure 4.29 showed the density profile of the System II along the *Z* direction averaged over the last 0.2 ns of the simulation. The most interesting observation here concerns the carbon dioxide affinity for MDEA (2-10 Å), which the high concentrations of these two components always coincided. High loading capacity of MDEA has potential to remove $CO_2$. Thus, it was important to determine how MDEA will perform when it comes in contact with carbon dioxide. During the simulation of System II, we obtained clear visual indications for such an affinity.

As the simulation progressed, we started to observe some of the cavities in the guanidinium cation, which enable the $CO_2$ molecules to enter into the cavities. This is evident in Figure 4.30 which shows the system after 30 ns of simulation and the interaction of $CO_2$ around -$NH_2$ of $[gua]^+$ in the black circle.

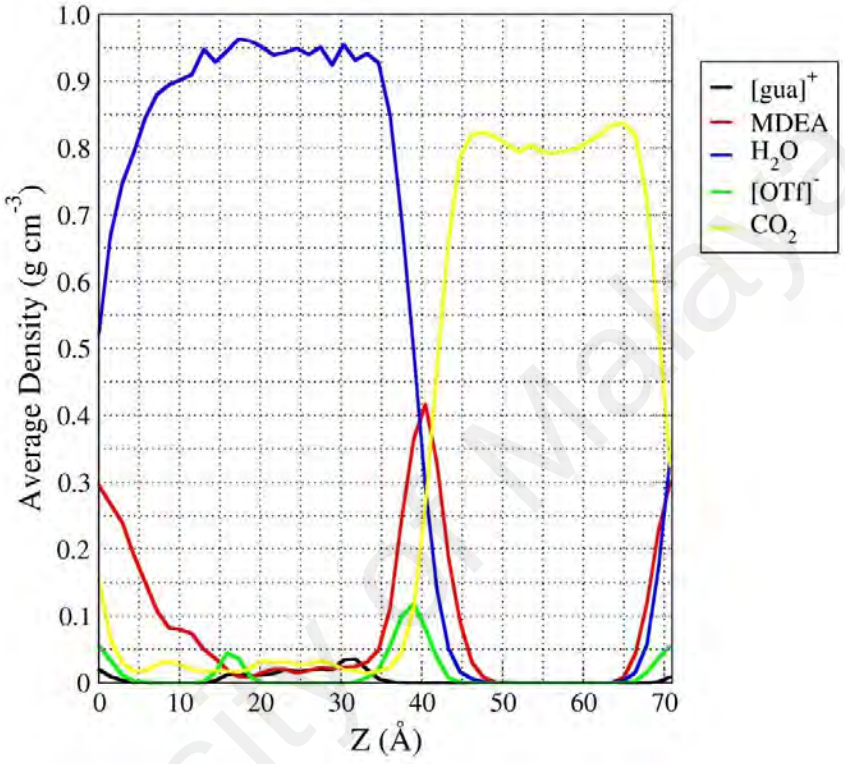


**Figure 4. 29**: Density profile of System II averaged over the last 0.2 ns of the simulation.

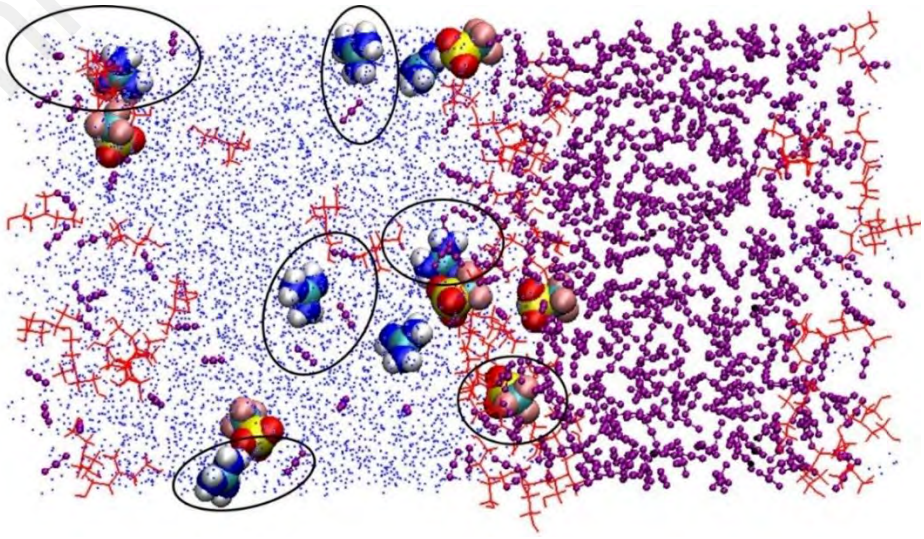

**Figure 4. 30**: $CO_2$ molecules enter the IL cavities. $CO_2$ around -$NH_2$ of $[gua]^+$ molecules.

### 4.3.3 Ternary Mixture Solution and Gaseous Carbon Dioxide (System III)

In this system, a block of pre-equilibrated gaseous $CO_2$ at density corresponding to 60 bar and 298.2 K (127 molecules) was exposed to the original ternary solution of System I. We expected to observe detectable absorption of $CO_2$ by given the affinity of $CO_2$ with IL and MDEA molecules in System II, as well as availability of gaseous carbon dioxide in the current system. The simulation was run for 30 ns, with the absorption process monitored and illustrated in Figure 4.31. Figure 4.31 showed that, once the simulation was initiated, carbon dioxide molecules started to attack the interface where a high concentration of amine and IL molecules is available to them (Figure 4.31 (a)). During the simulation, the $CO_2$ try to find the cavities in $[gua]^+$ and at the same time, try to react with MDEA molecules in the water phase (Figure 4.31(b)). After 20 ns of simulation, $CO_2$ molecules starting to cluster around IL molecules and try to enter into $[gua]^+$ cavities.

$CO_2$ molecules showed a clear affinity towards the reaction between $CO_2$ and tertiary amine (MDEA) indicates that MDEA does not react directly with $CO_2$. Instead, tertiary amine acts as bases, which catalyze the hydrogen of $CO_2$. Carbon dioxide absorption was observed, with the $CO_2$ molecules enter into $[gua]^+$ molecules (similar to System II). A significant amount of $CO_2$ was thus absorbed by the amine solution and remained inside the MDEA phase. This is a very informative observation consistent with theories of carbon dioxide absorption and in line with experimental results obtained (Ahmady et al., 2011; Blauwhoff et al., 1984; Derks et al., 2011; Feng et al., 2010; Ramachandran et al., 2006). $CO_2$ absorption by MDEA will be the rate-limiting process so that $CO_2$ molecules behind the gas-liquid interface on the gas side will ‘‘queue up’’ to enter the interface (Figure 4.31(a)).

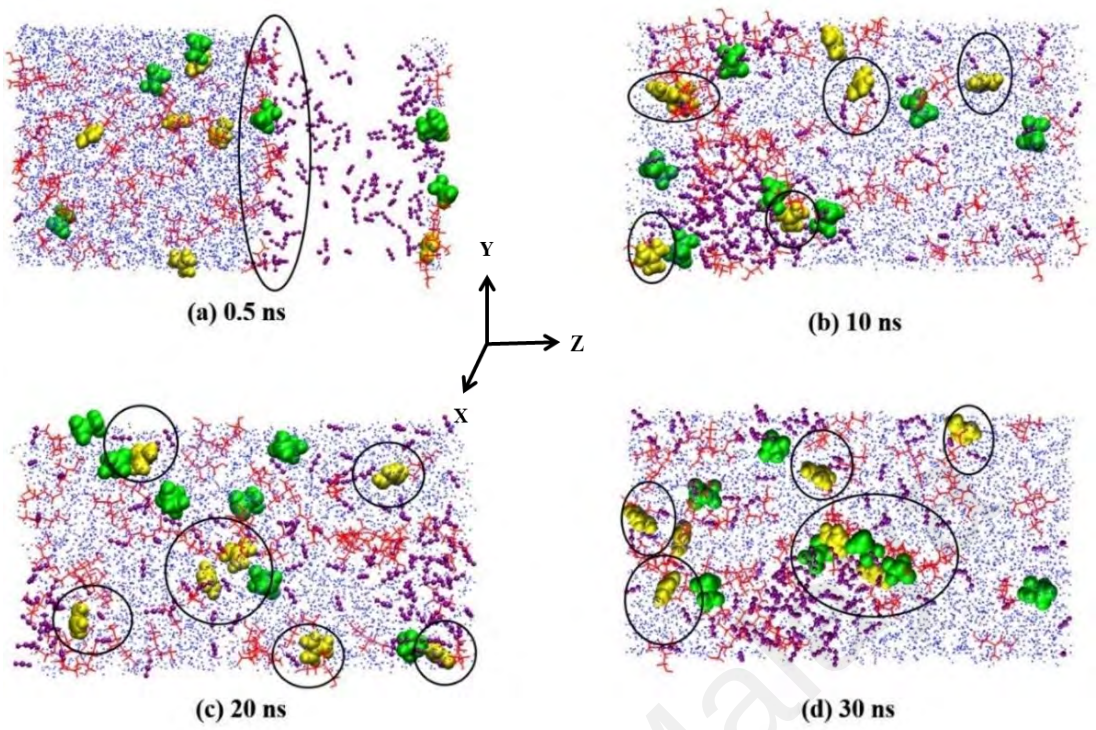


**Figure 4. 31**: *Z* direction of System III evolution during $CO_2$ absorption. The same color scheme is used as is shown in System II.

Based on Donaldson & Nguyen (1980), the reaction between MDEA and $CO_2$ is a base-catalyzed hydration reaction presumably hydrogen bonding between amine and water, which weakens the H-O bond and increases the nucleophilic reactivity of the water toward $CO_2$. This mechanism is shown below (Equation 4.2):

$$\mathbf{R_3N + H - O - H + O = C = O \Leftrightarrow\ R_3NH^+ +\ + HCO_3^+} \qquad (4.\ 2)$$

Thus, MDEA will remove $CO_2$ molecules (in the form of $HCO_3^-$) from the interface and carry them away into the liquid bulk. This process will occur in parallel with the diffusion of carbon dioxide into the interface and further into bulk. The conversion to carbamate ($CH_2NO_2^-$) is exothermic and thus will have an immediate effect of expanding the local environment to accommodate the newly formed (larger and more complex) carbamates. The high concentration of $CO_2$ molecules behind the inter-face is obvious in Figure 4.31(a).

Additionally, we observed carbon dioxide tend to localize around cation throughout the entire simulation (indicated by black circles in Figure 4.31 (b)–(d)). As seen in Figure 4.31(d), at the end of the simulation time (30 ns), a number of $CO_2$ molecules had dissolved in water molecules is small rather than absorbed in MDEA. Furthermore, it has been emphasized by experimentalists (Böttinger et al., 2008; Samanta & Bandyopadhyay, 2009) that MDEA has a high stoichiometric loading capacity for the removal of $CO_2$. Figure 4.32 shown the RDF between COM of cation, anion, cation-anion, water, MDEA and $CO_2$ molecules.

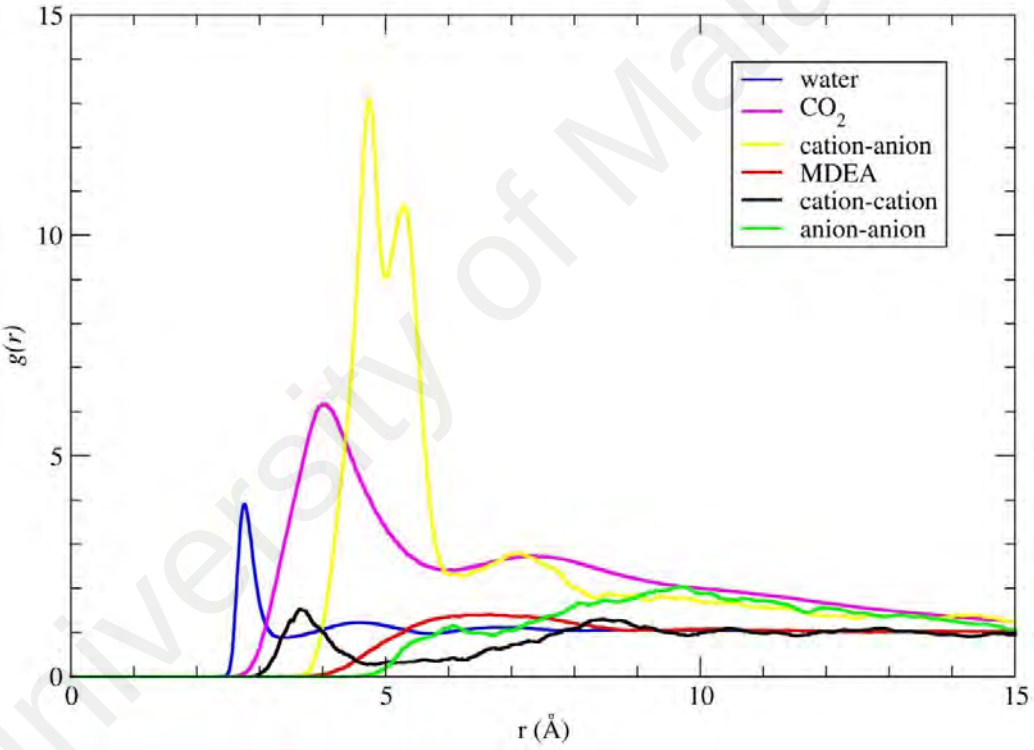


**Figure 4. 32**: RDF between COM of cation, anion, cation-anion, water, MDEA and $CO_2$ molecules

Similar to RDF for System II, the highest and sharp peak are clearly identified for $g(r)_{\text{cation-anion}}$ around r ~ 4.7 Å, which indicates $CO_2$ molecules (purple line) appears to favour interaction with cation (black line) and MDEA molecules (red line) at r ~ 3.2 – 5.1 Å, rather than anion molecules (green line) at r ~ 5.8 Å. This behaviour indicates that guanidinium ion has some cavities which $CO_2$ can enter. Density profile of the system for the last 1000 configurations of simulation over 0.2 ns is presented in Figure 4.33. It emphasizes the high loading capacity of MDEA in bulk removal of carbon dioxide and confirms our observations pertaining to the molecular distribution in the bulk and at the interface. As seen in Figure 4.33, the high concentration of carbon dioxide coincides with high MDEA concentrations in the areas covering 16–30 Å and 52–60 Å of the simulation box, representing the high loading capacity of MDEA for $CO_2$.

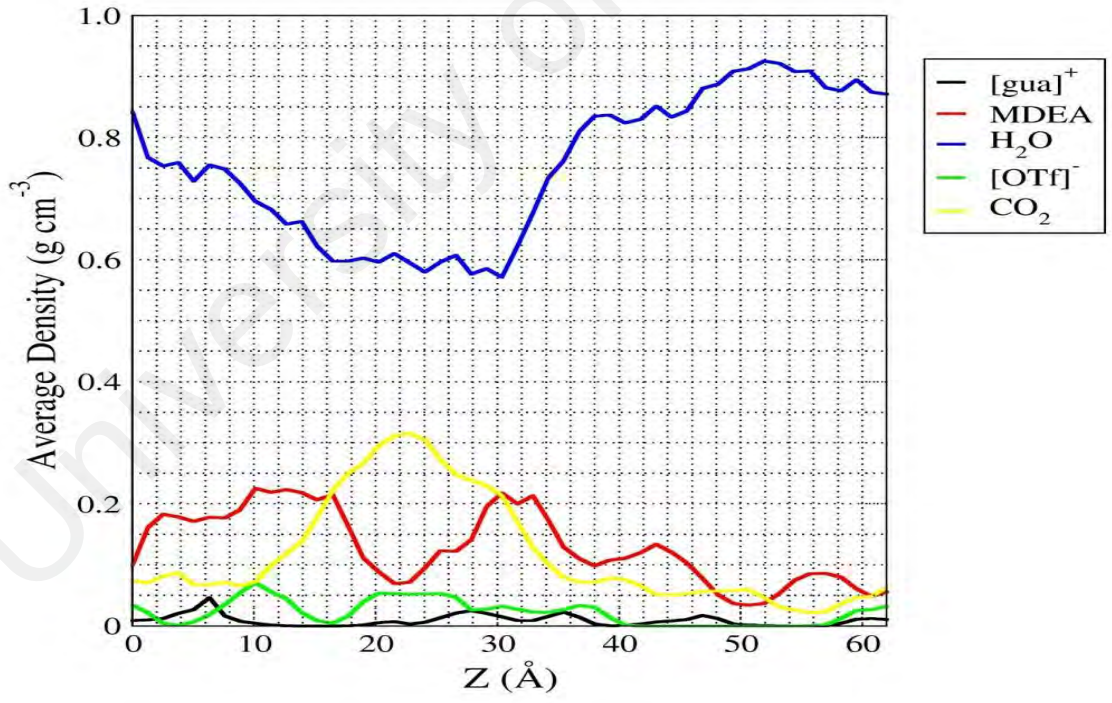


**Figure 4. 33:** Density profile of System III averaged over the last 0.2 ns of the simulation.

### 4.3.4 Pure Water and Gaseous Mixture of $CH_4$ and $CO_2$ (System IV)

The main purpose of System IV was to test the suitability of the OPLS one-site $CH_4$ model for the simulation of aqueous phases. This system did not contain a ternary solution, with the liquid phase originally having only 2135 water molecules at 999.92 $kgm^{-3}$ density. The gas box consisted of a pre-equilibrated 11–89 mol% mixture of $CO_2$ and $CH_4$ (153 and 7 molecules, respectively). Thermodynamic conditions used were similar to System V (T = 298.2 K, P = 100 bar) to assist the comparison of the $CO_2$ and $CH_4$ in water solubility. This comparison verified the positive effect of ternary solution for the absorption of carbon dioxide by improving the $CO_2$ solubility in water and an emphasized the negative effect of undesired trapping of $CH_4$ in the ternary solution. The time evolution of System IV is presented in Figure 4.34.

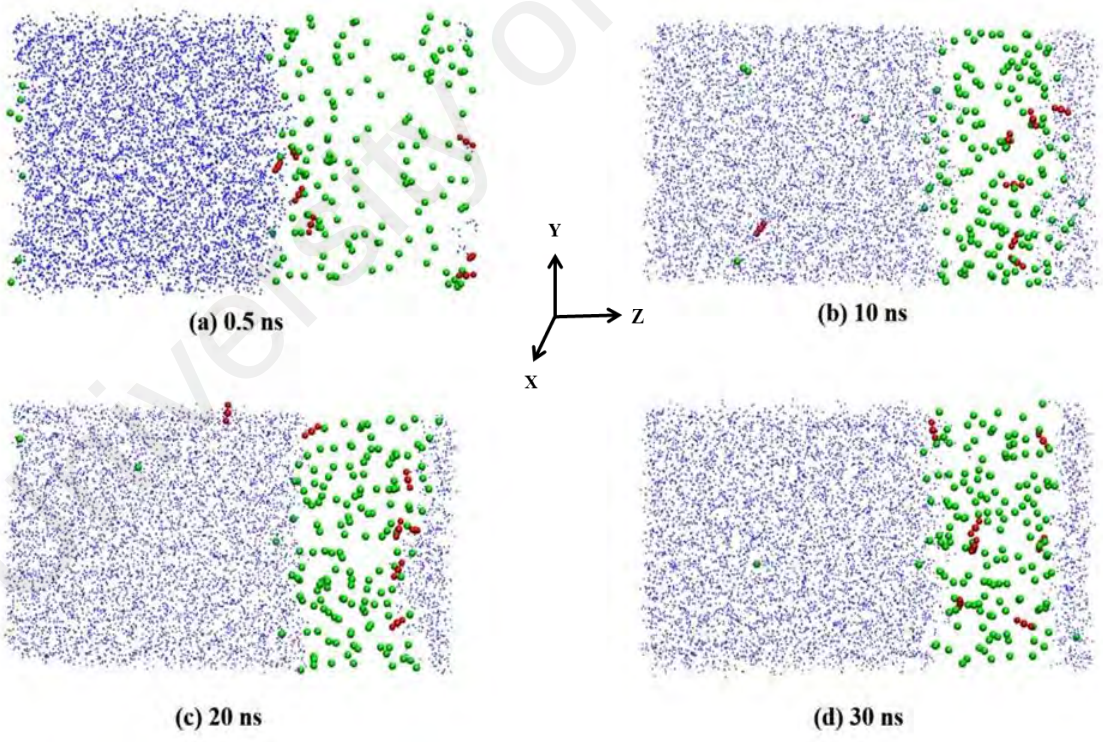


**Figure 4. 34**: *Z* direction of System IV as it evolves with time. One site $CH_4$ molecules are indicated as green balls. Connected red spheres represent carbon $CO_2$; and blue dotted area is bulk water.

Figure 4.35 showed the RDF between COM of $CO_2$, $CH_4$ and water molecules. Based on RDF, $CO_2$ molecules appears to be more soluble in water (r ~ 3.2 Å) rather than $CH_4$ molecules (r ~ 3.5 Å). Figure 4.36 presents the density profile of this system calculated for the last 1000 configurations of the system to compute the solubility of the gaseous components inside the water solution using the one-site methane model. This figure is in a good agreement with the experimental data (Adisasmito et al., 1991; Duan & Sun, 2003; Wiebe & Gaddy, 1940; Wiebe & Gaddy, 1939), $CO_2$ and $CH_4$ exhibited low solubility in pure water under the thermodynamic conditions of interest, with $CH_4$ solubility much lower than that of $CO_2$. The average density of $CH_4$ is less than in $CO_2$ in 0-40 Å region. Farmahini et al., (2011) also observed the same trend for the solubility of $CO_2$ and $CH_4$ molecules in pure water.

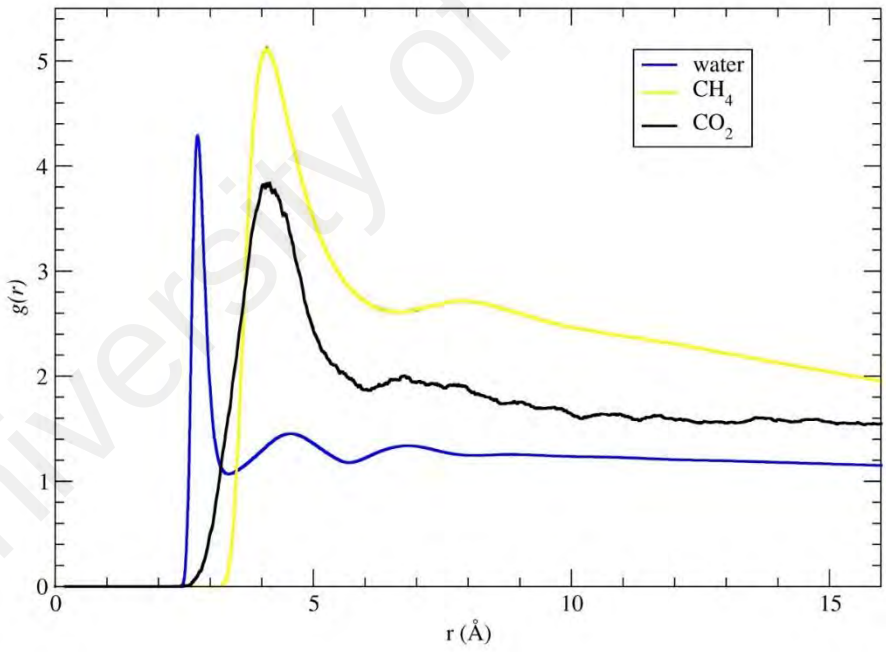


**Figure 4. 35**: RDF between COM of water, $CH_4$ and $CO_2$ molecules

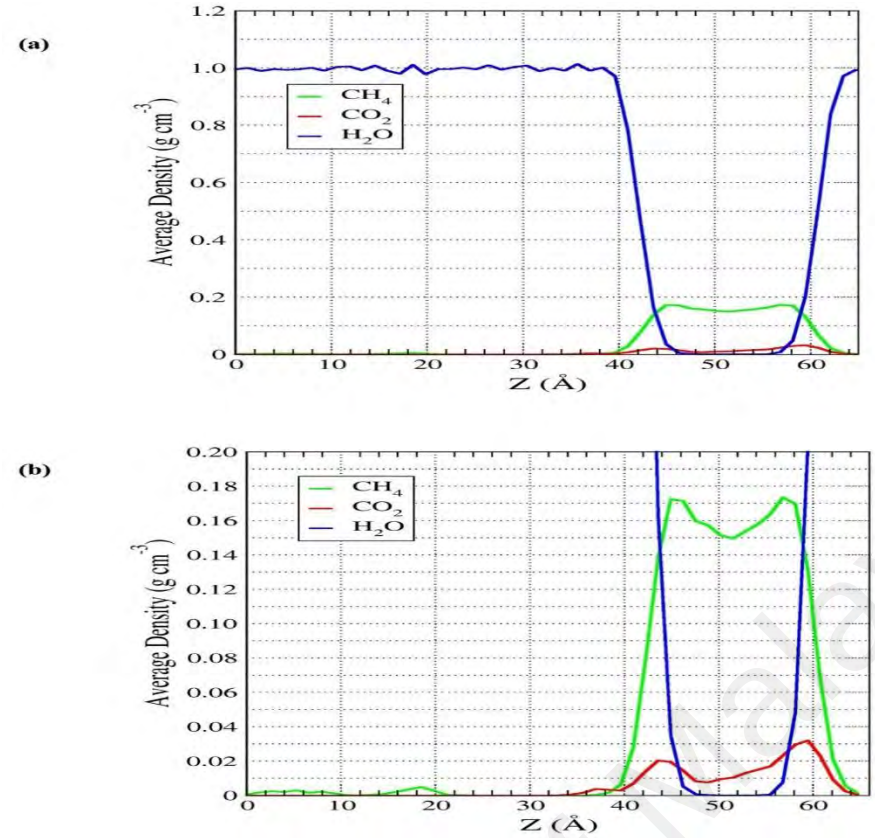


**Figure 4. 36**: Density profile of the System IV. (a) overall view and (b) magnified view

### 4.3.5 Ternary mixture solution and a gaseous mixture of $CH_4$ and $CO_2$ (System V)

System V was the primary system investigated in this study of phenomena occurring during industrial $CO_2$ absorption from natural gas. As a side goal, we also aimed to investigate the undesired trapping of methane molecules during this process. Thus, we brought the ternary solution at T=298.2 K (identical to that of System I) into contact with a pre-equilibrated gaseous mixture of 11 mol% $CO_2$ and 89 mol% $CH_4$ (one of the building blocks used in System IV). This system was run for 30 ns in total. The time evolution of the system is illustrated in Figure 4.37. The colour conventions denoting molecular representations are similar to Figure 4.27 and Figure 4.34 for Systems II and IV, respectively.

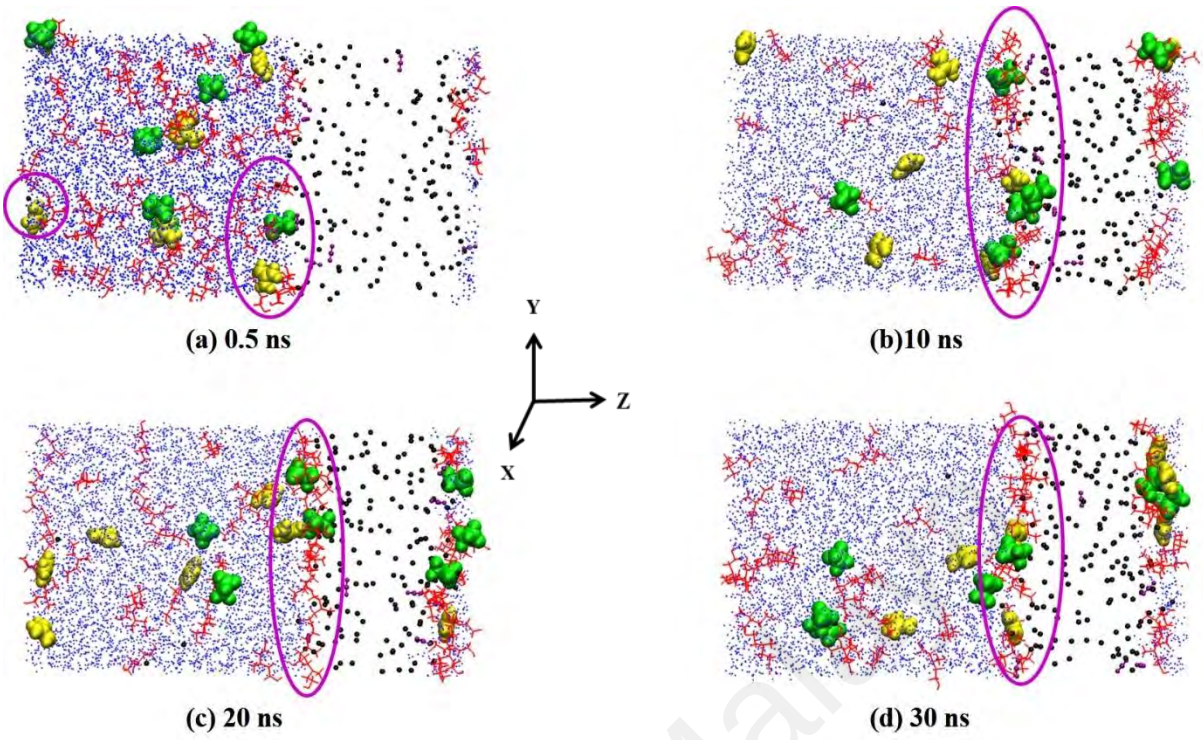


**Figure 4. 37:** *Z* direction of System IV evolution during $CO_2$ absorption. One site $CH_4$ molecules are indicated as green balls. Connected red spheres represent $CO_2$ molecules and blue dotted area is bulk water.

From figure 4.37, this system has undergone a phase separation between water and MDEA similarly to Systems I, II and III. The distribution pattern agreed well with their hydrophobic (MDEA molecules) hydrophilic ($[gua]^+$ and $[OTf]^-$) natures. Visual observations made during the last 30 ns of simulation demonstrated that essentially the same process of carbon dioxide absorption as in System III (see Figure 4.31 (a)–(d)). The only difference lies in a much lower concentration of $CO_2$ due to methane being the main constituent of our natural gas mixture. Again, MDEA demonstrated its high loading capacity for removal of $CO_2$, since a large amount of carbon dioxide absorbed into the MDEA phase during the simulation. To quantify the molecular distribution of the liquid phase, the density profile of the system was calculated for the last 1000 configurations of the simulation (Figure 4.38).

The magnified view of the density profile plotted in Figure 4.38 (b) clearly illustrates a distinct preference of $[gua]^+$ (black line) and $[OTf]^-$ (green line) to remain either inside the MDEA-water interface (0–46 Å and 60-70 Å), demonstrating the strong hydrophilic characteristic between water and ionic liquid. While $[gua]^+$ (black line) also remain inside the gas-liquid interface (40-62 Å), indicates that guanidinium cation has some cavities in which $CO_2$ gas molecules mainly exist. At the same time, the density profile of the system shows a high capacity of MDEA for $CO_2$ loading between 0–48 Å and 58–70 Å (red line). One of the more significant observations made in the course of this simulation was the evidence of methane trapping by the ternary solution. This phenomenon was easily detectable both through visual observations of the system (Figure 4.37 (a)–(d)) and its density profiles (Figure 4.38). The violet curve ($CH_4$ concentration profile) shows the high concentration of methane observed inside the MDEA bulk (40–50 Å) and provides the concrete evidence for trapping of methane into the IL phase. Considering the aforementioned explanations, we concluded that MDEA not only has a high loading capacity for removal of $CO_2$ but possesses a similar ability to retain $CH_4$ inside the solution.

The trapping of $CH_4$ is an undesired industrial phenomenon, making it technically and economically very important in gas treating plants. However, the mechanism responsible for this process is not understood yet. Nevertheless, these values emphasize a higher relative absorption of carbon dioxide in comparison with the trapping of methane in each system. A more comprehensive understanding of the trapping mechanism would require an independent study. However, in this work, we attempted to provide a clearer view of the problem, never discussed in the literature but know industrially, and tried to present certain insights which may be used for further investigations. The existence of already absorbed carbon dioxide inside the ternary solution may increase diffusivity and mobility of methane in the system, with the higher diffusivity promoting the trapping of methane.

One may hypothesize that methane molecules will follow the carbon dioxide into the MDEA. While in Figure 4.39 shown the RDF for system V. Based on the RDF $CO_2$ molecules appears delocalized around cation (r~2.7Å) and favour interaction with MDEA molecules. While $CH_4$ molecules easily trapped in the IL.

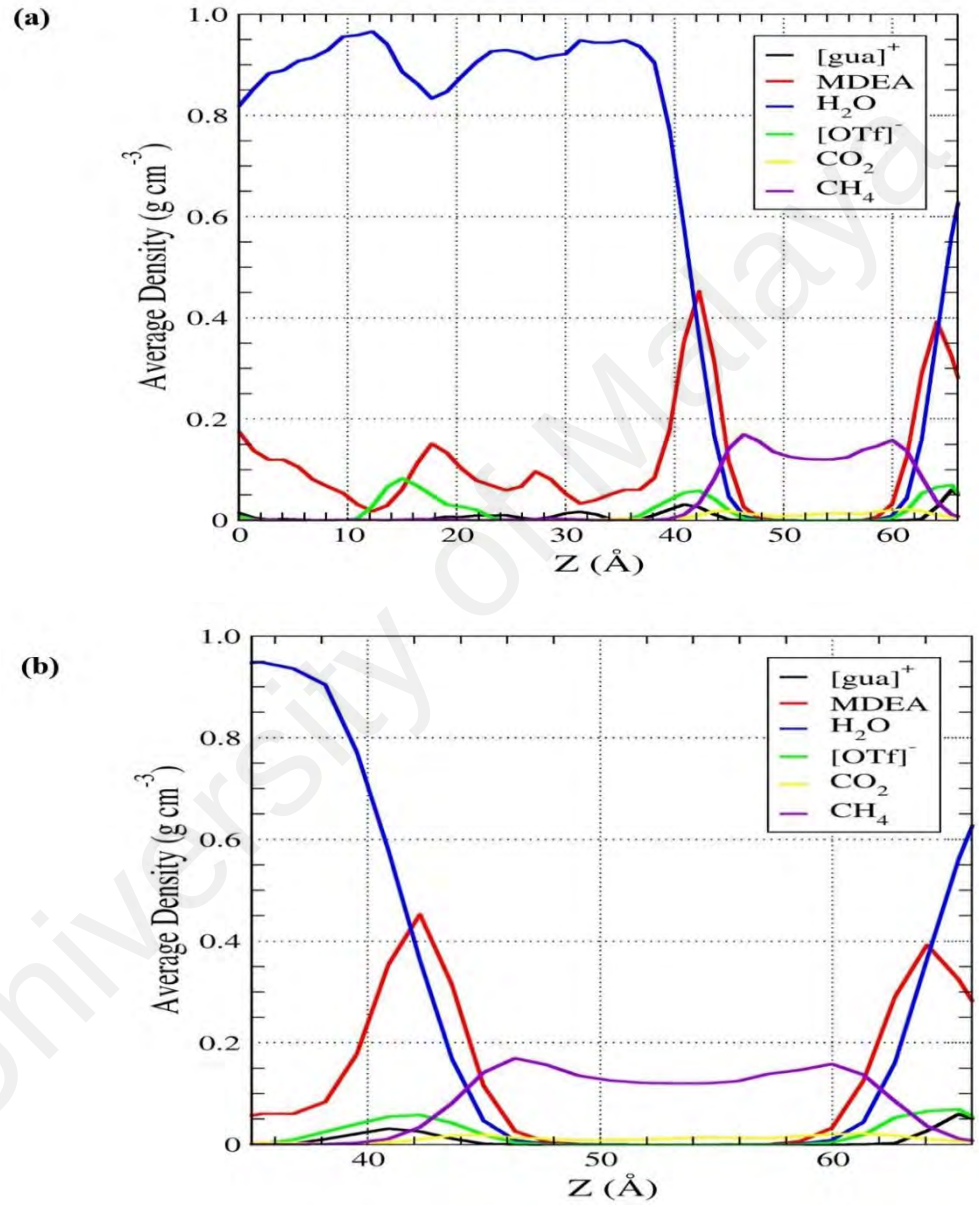


**Figure 4. 38**: Density profile of the System V. (a) overall view and (b) magnified view.

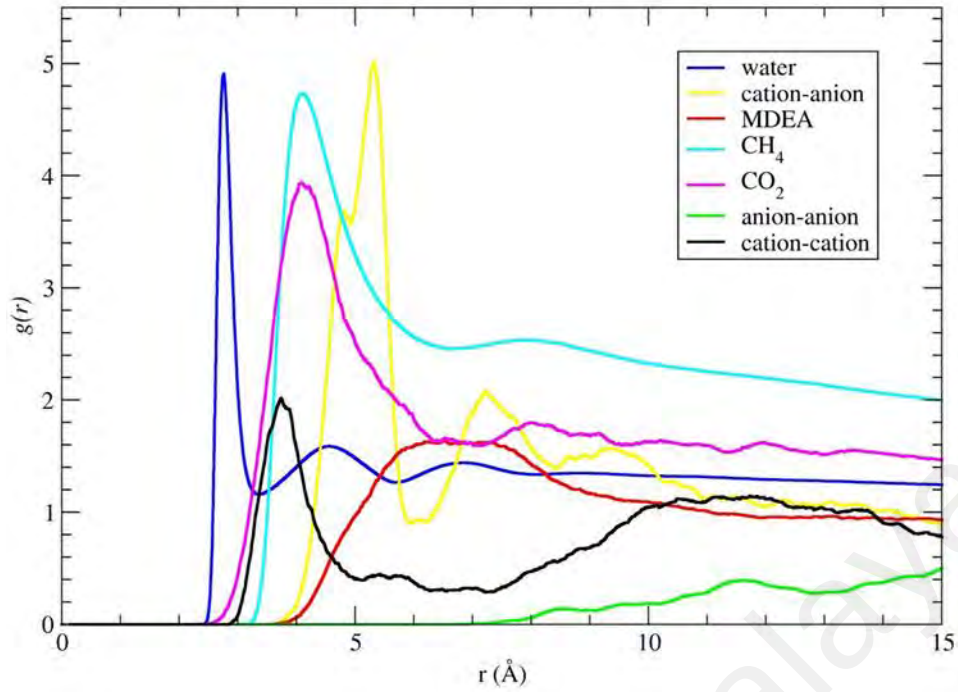


**Figure 4. 39**: RDF between COM of cation, anion, cation-anion, water, MDEA, $CH_4$ and $CO_2$ molecules

# CHAPTER 5: CONCLUSIONS AND RECOMMENDATIONS

Here, we investigated the equilibrium behaviours, interactions and structures, microstructures, dynamical and transport properties aqueous [gua][OTf] IL (binary solvents) and MDEA + [gua][OTf] + water (ternary solvents) at different compositions and temperatures using classical MD simulation techniques. For binary solvents, it was observed that the molecular structures are consistent with other ILs investigated by previous researches, which exhibited well-defined structures. The cation-anion associations were found to be unyielding based on the IL-water mixture RDFs even at a high molar fraction of water. $[OTf]^-$ ions diffused faster than $[gua]^+$ ions and improved both translational and rotation motions of the ions mentioned significantly, whereby, as water molar fraction increased, the translational motion of both ions increased. In hydrogen bond analysis, the number of hydrogen bonds per water increased consequently with water molar fractions. Water molecules were likely to be isolated at a low water molar fraction but started to cluster with each other and formed a large network at a higher value of water molar fraction.

Current studies have shown no common cations or anions between different mixtures of ILs, making the elucidation of trends more challenging in ionic liquids industry. For all systems for ternary solvents, we found that the densities increase when increasing [gua][OTf] and MDEA of molar fractions and decreasing water molar fraction. We found a good consistency between the calculated densities with experimental values reported previously. From a structural point of view, structured solute-water interactions and MDEA-[gua][OTf] interactions have also observed by our RDFs analysis. Their molecular structure is consistent with other solute-water interactions and [gua][OTf]-MDEA interactions investigated in the literature, which exhibited well-defined structures.

A preferred long-range structural correlation between these ions resulting from charge ordering has been observed in high mole fraction of water. RDFs analysis is similar in all systems with slightly stronger interaction of water with water or MDEA or [gua][OTf] when adding IL. For *D*, the water molecules diffuse faster when [gua][OTf] and MDEA molar fraction increases. As water molar fraction increases, the translational motion of [gua][OTf] and MDEA molecules decreases. From RDFs, we observed that the water molecules form a distinct solvation shell around the cations and anions with weakened electrostatic interactions and their mutual association between ions. These trends are the same as MDEA-water interaction and MDEA-[gua][OTf]. Meanwhile, increasing of [gua][OTf] and MDEA and decreasing of water molar fraction can significantly increase the viscosity of ternary systems. These ternary solvents can be applied in the natural gas application such as removing carbon dioxide using aqueous MDEA and IL at high pressure. Hence, these findings are important evidence to prove the effectiveness of the new suggested IL-based solvents for $CO_2$ absorption.

Based on physical properties of binary and ternary solvents, the existing data are crucial for newly suggested ILs-based solvents application in acid gases absorption such as $CO_2$ and $SO_2$ especially in a natural gas process where the usage of aqueous ILs at high temperature has its utmost potential. For the absorption mechanism of $CO_2$ into ternary systems, we concluded that MDEA molecules showed a tendency to separate from the aqueous phase. It was found that the ionic nature of $[gua]^+$ and $[OTf]^-$ made them soluble in water, with this phase separation shown to be energetically favourable. High loading capacity of MDEA for removal of carbon dioxide was observed in all systems containing this gaseous component. Specifically, we have demonstrated a high affinity of carbon dioxide for the amine and alcohol groups of MDEA. Each MDEA molecule possesses three functional groups with high $CO_2$ affinity, the noticeable capacity of MDEA for the absorption of $CO_2$ was found to be conclusive.

A complete process of $CO_2$ absorption was observed. Considering this pattern, we concluded that $[gua]^+$ will have an important effect on the absorption of carbon dioxide at both low and high loading. Moreover, we have shown for the first time that this solution will also have a great affinity for undesired trapping of methane. Two hypotheses were suggested to explain the trapping mechanism. We have found certain indications that pointed to the possibility of such a structure formation. At the same time, we have shown that the amine groups in MDEA molecules are mainly responsible for both the absorption of carbon dioxide and entrapment of methane.

## 5.1 Recommendations for future studies

ILs have currently been applied as promising solvents in media for gas and liquid separations and chemical separation. The presence of water modified the characteristics of ILs including alteration of fundamental properties such as density, viscosity, and heat capacity. When ILs and amines are combined together *i.e.* ternary solvents, they give a better performance than amine-functionalized ILs. Researches have turned out their interest with this kind of ternary solvent as a solvents for $CO_2$ capture and acid gas removal rather than aqueous amine solvents itself (Akhmetshina et al., 2017; Ju et al., 2018; Sairi et al., 2015; Sheridan, et al., 2018; Yang et al., 2014). These attractive properties could lead the way to clean gas separation technologies that eliminate emissions of the harmful gases into the atmosphere. Further research could be carried out to improve the understanding of the properties of this ternary solvent as well as their applications in the future. At the present moment, this class of [gua][OTf] is poorly characterised from a molecular point of view, and new insights will provide the groundwork for future development and have great potential to be used in the absorption of acid gases, such as $SO_2$ and $CO_2$. Thus, new perspectives from molecular dynamic simulations research will provide the groundwork for future development.

A few suggestions are as below:

1) Prolong the simulation time in order to have good conformational sampling for radial distribution function and spatial distribution function.
2) Further study can also be done using different size of the box in order to investigate the relationship between structure and physical properties of binary and ternary systems.
3) Before running the simulation, it is important to get all experimental densities. Therefore, it can be used to confirm a proposed force field of ionic liquid.

## REFERENCES


Adisasmito, S., Frank, R. J., & Sloan, E. D. (1991). Hydrates of carbon dioxide and methane mixtures. *Journal of Chemical & Engineering Data*, *36*(1), 68–71.

Aghaie, M., Rezaei, N., & Zendehboudi, S. (2018). A systematic review on $CO_2$ capture with ionic liquids: Current status and future prospects. *Renewable and Sustainable Energy Reviews, 96, 502-525.*

Ahmady, A., Hashim, M. A., & Aroua, M. K. (2011). Density, viscosity, physical solubility and diffusivity of $CO_2$ in aqueous MDEA+[Bmim][$BF_4$] solutions from 303 to 333K. *Chemical Engineering Journal*, *172*(2–3), 763–770.

Akhmetshina, A. I., Petukhov, A. N., Vorotyntsev, A. V., Nyuchev, A. V., & Vorotyntsev, I. V. (2017). Absorption Behavior of Acid Gases in Protic Ionic Liquid/Alkanolamine Binary Mixtures. *ACS Sustainable Chemistry and Engineering*, *5*(4), 3429–3437.

Allen, P., & Tildesley, D. J. (1989). Computer Simulation of Liquids. Oxford University Press, United States of America: Clarendon Press.

Amado Alviz, P. L., & Alvarez, A. J. (2017). Comparative life cycle assessment of the use of an ionic liquid ([Bmim]Br) versus a volatile organic solvent in the production of acetylsalicylic acid. *Journal of Cleaner Production*, *168*, 1614–1624.

Anantharaj, R., & Banerjee, T. (2011). Phase behaviour of 1-ethyl-3-methylimidazolium thiocyanate ionic liquid with catalytic deactivated compounds and water at several temperatures: Experiments and theoretical predictions. *International Journal of Chemical Engineering*, *2011*(2011), 1–13.

Aparicio, S., & Atilhan, M. (2012). Water effect on $CO_2$ absorption for hydroxylammonium based ionic liquids: A molecular dynamics study. *Chemical Physics*, *400*, 118–125.

Becke, A. (1993). Density functional thermochemistry III the role of exact exchange. *Journal of Chemical Physics*, *98*, 5648–5652.

Berendsen, H. J. C., Postma, J. P. M., Van Gunsteren, W. F., Dinola, A., & Haak, J. R. (1984). Molecular dynamics with coupling to an external bath. *Journal of Chemical Physics*, *81*(8), 3684–3690.

Bhargava, B. L., Yasaka, Y., & Klein, M. L. (2011). Computational studies of room temperature ionic liquid-water mixtures. *Chemical Communications*, *47*(22), 6228–6241.

Blauwhoff, P. M. M., Versteeg, G. F., & Van Swaaij, W. P. M. (1984). A study on the reaction between $CO_2$ and alkanolamines in aqueous solutions. *Chemical Engineering Science*, *39*(2), 207–225.

Bode, B., & Gordon, M. (1998). Macmolplt: A graphical user interface for GAMESS. *Journal of Molecular Graphics and Modelling*, *16*(3), 133–138.

Böttinger, W., Maiwald, M., & Hasse, H. (2008). Online NMR Spectroscopic study of species distribution in MDEA−$H_2O$−$CO_2$ and MDEA−PIP−$H_2O$−$CO_2$. *Industrial & Engineering Chemistry Research*, *47*(20), 7917–7926.

Bussi, G., Donadio, D., & Parrinello, M. (2007). Canonical sampling through velocity rescaling. *Journal of Chemical Physics*, *126*(1), 014101–014108.

Cadena, C., Anthony, J. L., Shah, J. K., Morrow, T. I., Brennecke, J. F., & Maginn, E. J. (2004). Why Is $CO_2$ So Soluble in Imidazolium-Based Ionic Liquids? *Journal of the American Chemical Society*, *126*(16), 5300–5308.

Canales, R. I., & Brennecke, J. F. (2016). Comparison of ionic liquids to conventional organic solvents for extraction of aromatics from aliphatics. *Journal of Chemical & Engineering Data*, *61*(5), 1685–1699.

Cardoso, P. F., Fernandez, J. S. L. C., Lepre, L. F., Ando, R. A., Costa Gomes, M. F., & Siqueira, L. J. A. (2018). Molecular dynamics simulations of polyethers and a quaternary ammonium ionic liquid as $CO_2$ absorbers. *Journal of Chemical Physics*, *148*(13), 134908-1–134908-9 .

Cesare Marincola, F., Piras, C., Russina, O., Gontrani, L., Saba, G., & Lai, A. (2012). NMR investigation of imidazolium-based ionic liquids and their aqueous mixtures. *Chemphyschem*, *13*(5), 1339–1346.

Chang, T. M., & Dang, L. X. (2008). Computational studies of structures and dynamics of 1,3-dimethylimidazolim salt liquids and their interfaces using polarizable potential models. *Journal of Physical Chemistry A*, *113*(10), 2127–2135.

Chang, T. M., Dang, L. X., Devanathan, R., & Dupuis, M. (2010). Structure and dynamics of N,N-Diethyl-N-methylammonium triflate ionic liquid, neat and with water, from molecular dynamics simulations. *Journal of Physical Chemistry A*, *114*(48), 12764–12774.

Chatel, G., & MacFarlane, D. R. (2014). Ionic liquids and ultrasound in combination: synergies and challenges. *Chemical Society Reviews*, *43*(23), 8132–8149.

Cramer, C. J. (2013). Essentials of computational chemistry : Theories and models. Chichester, United Kingdom: John Wiley and Sons Ltd.

Dai, Z., Noble, R. D., Gin, D. L., Zhang, X., & Deng, L. (2016). Combination of ionic liquids with membrane technology: A new approach for $CO_2$ separation. *Journal of Membrane Science*, *497*, 1–20.

Del Pópolo, M. G., & Voth, G. A. (2004). On the Structure and Dynamics of Ionic Liquids. *Journal of Physical Chemistry B*, *108*(5), 1744–1752.

DeLano, W. L. (2002). The PyMOL Molecular Graphics System, Version 2.0 Schrödinger, LLC. San Carlos, CA.

Derks, P. W. J., Huttenhuis, P. J. G., van Aken, C., Marsman, J.H., & Versteeg, G. F. (2011). Determination of the liquid-phase speciation in the MDEA - $H_2O$ - $CO_2$ system. *Energy Procedia*, *4*, 599–605.

Donaldson, T. L., & Nguyen, Y. N. (1980). Carbon dioxide reaction kinetics and transport in aqueous amine membranes. *Industrial & Engineering Chemistry Fundamentals*, *19*(3), 260–266.

Dong, K., Zhang, S., Wang, D., & Yao, X. (2006). Hydrogen bonds in imidazolium ionic liquids. *Journal of Physical Chemistry A*, *110*(31), 9775–9782.

Duan, Z., & Sun, R. (2003). An improved model calculating $CO_2$ solubility in pure water and aqueous NaCl solutions from 273 to 533 K and from 0 to 2000 bar. *Chemical Geology*, *193*(3–4), 257–271.

DuPart, M. S., Bacon, T. R., & Edwards, D. J. (1993). Understanding corrosion in alkanolamine gas treating plants. *Hydrocarbon Processing*, *72*, 89–94.

Dutcher, B., Fan, M., & Russell, A. G. (2015). Amine-based $CO_2$ capture technology development from the beginning of 2013—A review. *ACS Applied Materials & Interfaces*, *7*(4), 2137–2148.

Essmann, U., Perera, L., Berkowitz, M. L., Darden, T., Lee, H., & Pedersen, L. G. (1995). A smooth particle mesh Ewald method. *Journal of Chemical Physics*, *103*(19), 8577–8593.

Farmahini, A. H., Kvamme, B., & Kuznetsova, T. (2011). Molecular dynamics simulation studies of absorption in piperazine activated MDEA solution. *Physical Chemistry Chemical Physics*, *13*(28), 13070–13081.

Feng, Z., Cheng-Gang, F., You-Ting, W., Yuan-Tao, W., Ai-Min, L., & Zhi-Bing, Z. (2010). Absorption of $CO_2$ in the aqueous solutions of functionalized ionic liquids and MDEA. *Chemical Engineering Journal*, *160*(2), 691–697.

Fraser, K. J., Izgorodina, E. I., Forsyth, M., Scott, J. L., & MacFarlane, D. R. (2007). Liquids intermediate between "molecular" and "ionic" liquids: Liquid Ion Pairs? *Chemical Communications*, (37), 3817–3819.

Gillet, R., Fierro, A., Valenzuela, L. M., & Pérez-Correa, J. R. (2018). Using molecular dynamics simulations to predict the effect of temperature on aqueous solubility for aromatic compounds. *Fluid Phase Equilibria*, *472*, 85–93.

Gonzalez-Miquel, M., Massel, M., DeSilva, A., Palomar, J., Rodriguez, F., & Brennecke, J. F. (2014). Excess enthalpy of monoethanolamine + ionic liquid mixtures: How good are COSMO-RS predictions? *Journal of Physical Chemistry B*, *118*(39), 11512–11522.

Gorain, B., Choudhury, H., Pandey, M., Mohd Amin, M. C. I., Singh, B., Gupta, U., & Kesharwani, P. (2018). Chapter 10-Dendrimers as effective carriers for the treatment of brain tumor. In P. Kesharwani & U. Gupta (Eds.), Nanotechnology-based targeted drug delivery systems for brain tumors (pp. 267–305). San Diego, United States: Elsevier Science Publishing Company Incorporated.

Haron, N., Lee, V. S., Sairi, N. A., Zain, S. M., Alias, Y., & Aroua, M. K. (2017). Microstructures, interactions and dynamics properties studies of aqueous guanidinium triflate ionic liquid from molecular dynamics simulations. *Journal of Molecular Liquids*, *227*, 184–193.

Haron, N., Sairi, N. A., & Lee, V. S. (2015). Microstructures, interactions and dynamics properties studies of N-methyldiethanolamine + guanidinium triflate ionic liquid + water tertiary system at the standard temperature. *Molecular Simulation*, *42*(8), 655–666.

Harun, N., & Masiren, E. E. (2017). Molecular dynamic simulation of $CO_2$ absorption into mixed aqueous solutions MDEA/PZ. *Chemical Engineering Research Bulletin* ,*19*, 1–11.

Hegde, G. A., Bharadwaj, V. S., Kinsinger, C. L., Schutt, T. C., Pisierra, N. R., & Maupin, C. M. (2016). Impact of water dilution and cation tail length on ionic liquid characteristics: Interplay between polar and non-polar interactions. *Journal of Chemical Physics*, *145*(6), 064504-1–064504-13.

Hess, B. (2002). Determining the shear viscosity of model liquids from molecular dynamics simulations. *Journal of Chemical Physics*, *116*(1), 209–217.

Hess, B., Bekker, H., Berendsen, H. J. C., & Fraaije, J. G. E. M. (1997). LINCS: A Linear Constraint Solver for molecular simulations. *Journal of Computational Chemistry*, *18*(12), 1463–1472.

Huang, X., Margulis, C. J., Li, Y., & Berne, B. J. (2005). Why is the partial molar volume of $CO_2$ so small when dissolved in a room temperature ionic liquid? Structure and dynamics of $CO_2$ dissolved in $[Bmim^+][PF_6^-]$. *Journal of the American Chemical Society*, *127*(50), 17842–17851.

Huang, Y., Cui, G., Wang, H., Li, Z., & Wang, J. (2018). Tuning ionic liquids with imide-based anions for highly efficient $CO_2$ capture through enhanced cooperations. *Journal of $CO_2$ Utilization*, *28*, 299–305.

Huang, Y., Wan, Z., Yang, Z., Ji, Y., Li, L., Yang, D., &. Chen, X. (2017). Concentration-dependent hydrogen bond behavior of ethylammonium nitrate protic ionic liquid-water mixtures explored by molecular dynamics simulations. *Journal of Chemical and Engineering Data*, *62*(8), 2340–2349.

Humphrey, W., Dalke, A., & Schulten, K. (1996). VMD: Visual molecular dynamics. *Journal of Molecular Graphics*, *14*(1), 33–38.

Hurley, F. H. (1948). Electrodeposition of aluminum. Retrieved on April 20, 2016 from https://www.google.com/patents/US2446331.

Jensen, F. (2016). Introduction to Computational Chemistry (3rd edition). Chichester West Sussex, United Kingdom: John Wiley & Sons.

Jorgensen, W. L., Maxwell, D. S., & Tirado-Rives, J. (1996). Development and testing of the OPLS all-atom force field on conformational energetics and properties of organic liquids. *Journal of the American Chemical Society*, *118*(45), 11225–11236.

Ju, H., ElMoudir, W., Aboudheir, A., & Mahinpey, N. (2018). Development of a facile reclaiming process for degraded alkanolamine and glycol solvents used for $CO_2$ capture systems. *International Journal of Greenhouse Gas Control*, *74*, 174–181.

Kaneko, K., Saihara, K., Masuda, Y., Yoshimura, Y., & Shimizu, A. (2018). Dynamic properties of water molecules in ionic liquid/water mixture with various alkyl chain length. *Journal of Molecular Liquids*, *264*, 337–342.

Kar, S., Sen, R., Goeppert, A., & Prakash, G. K. S. (2018). Integrative $CO_2$ capture and hydrogenation to methanol with reusable catalyst and amine: toward a carbon neutral methanol economy. *Journal of the American Chemical Society*, *140*(5), 1580–1583.

Katiyar, R. S., & Jha, P. K. (2018). Molecular simulations in drug delivery: Opportunities and challenges. *Wiley Interdisciplinary Reviews: Computational Molecular Science*, *8*(4), 1-18.

Keblinski, P., Eggebrecht, J., Wolf, D., & Phillpot, S. R. (2000). Molecular dynamics study of screening in ionic fluids. *Journal of Chemical Physics*, *113*(1), 282–291.

Kelkar, M. S., & Maginn, E. J. (2007). Effect of temperature and water content on the shear viscosity of the ionic liquid 1-ethyl-3-methylimidazolium bis(trifluoromethanesulfonyl)imide as studied by atomistic simulations. *Journal of Physical Chemistry B*, *111*(18), 4867–4876.

Khan, I., Kurnia, K. A., Mutelet, F., Pinho, S. P., & Coutinho, J. A. P. (2014). Probing the interactions between ionic liquids and water: Experimental and quantum chemical approach. *Journal of Physical Chemistry B*, *118*(7), 1848–1860.

Kohno, Y., & Ohno, H. (2012). Ionic liquid/water mixtures: From hostility to conciliation. *Chemical Communications*, *48*(57), 7119–7130.

Kumar, S., Cho, J. H., & Moon, I. (2014). Ionic liquid-amine blends and $CO_2$ BOLs: Prospective solvents for natural gas sweetening and $CO_2$ capture technology—A review. *International Journal of Greenhouse Gas Control*, *20*, 87–116.

Kuo, I. F. W., Mundy, C. J., McGrath, M. J., Siepmann, J. I., VandeVondele, J., Sprik, M., & Parrinello, M. (2004). Liquid water from first principles: Investigation of different sampling approaches. *Journal of Physical Chemistry B*, *108*(34), 12990–12998.

Larriba, M., Navarro, P., Delgado-Mellado, N., Stanisci, V., García, J., & Rodríguez, F. (2016). Separation of aromatics from n-alkanes using tricyanomethanide-based ionic liquids: Liquid-liquid extraction, vapor-liquid separation, and thermophysical characterization. *Journal of Molecular Liquids*, *223*, 880–889.

Larriba, M., Navarro, P., Delgado-Mellado, N., Stanisci, V., García, J., & Rodríguez, F. (2017). Extraction of aromatic hydrocarbons from pyrolysis gasoline using tetrathiocyanatocobaltate-based ionic liquids: Experimental study and simulation. *Fuel Processing Technology*, *159*, 96–110.

Leach, A. R. (2001). Molecular modelling: principles and applications (2nd edition). Harlow, United Kingdom: Pearson Education Limited.

Lei, Z., Chen, B., Koo, Y. M., & MacFarlane, D. R. (2017). Introduction: Ionic liquids. *Chemical Reviews*, *117*(10), 6633–6635.

Lei, Z., Dai, C., & Chen, B. (2014). Gas solubility in ionic liquids. *Chemical Reviews*, *114*(2), 1289–1326.

Liu, H., Man, R., Zheng, B., Wang, Z., & Yi, P. (2014). Insight into capture of greenhouse gas ($CO_2$) based on guanidinium ionic liquids. *Chinese Journal of Chemical Physics*, *27*(2), 144–148.

Liu, Z., Huang, S., & Wang, W. (2004). A refined force field for molecular simulation of imidazolium-based ionic liquids. *Journal of Physical Chemistry B*, *108*(34), 12978–12989.

Lu, J., Liotta, C. L., & Eckert, C. A. (2003). Spectroscopically probing microscopic solvent properties of room-temperature ionic liquids with the addition of carbon dioxide. *Journal of Physical Chemistry A*, *107*(19), 3995–4000.

Lu, J., He, A., Li, S., Nie, L., Zhang, W., & Yao, S. (2015). Synthesis, purification and recycling of ionic liquid. *Mini-Reviews in Organic Chemistry*, *12*(5), 435–448.

MacKerell, A. D., Bashford, D., Bellott, Dunbrack, R. L., Evanseck, J. D., Field, M. J., & Karplus, M. (1998). All-atom empirical potential for molecular modeling and dynamics studies of proteins. *Journal of Physical Chemistry B*, *102*(18), 3586–3616.

Mai, N. L., & Koo, Y.M. (2016). Computer-aided design of ionic liquids for high cellulose dissolution. *ACS Sustainable Chemistry & Engineering*, *4*(2), 541–547.

Malek, N. I., & Ijardar, S. P. (2016). Binary mixtures of ([$C_4$mim][$NTf_2$] + molecular organic solvents): Thermophysical, acoustic and transport properties at various compositions and temperatures. *The Journal of Chemical Thermodynamics*, *93*, 75–85.

Martínez, J. M., & Martínez, L. (2003). Packing optimization for automated generation of complex system's initial configurations for molecular dynamics and docking. *Journal of Computational Chemistry*, *24*(7), 819–825.

Martinez, L., Andrade, R., Birgin, E. G., & Martínez, J. M. (2009). PACKMOL: A package for building initial configurations for molecular dynamics simulations. *Journal of Computational Chemistry*, *30*(13), 2157–2164.

Micaelo, N. M., Baptista, A. M., & Soares, C. M. (2006). Parametrization of 1-Butyl-3-methylimidazolium hexafluorophosphate/nitrate ionic liquid for the GROMOS force field. *Journal of Physical Chemistry B*, *110*(29), 14444–14451.

Miranda, A., Cova, T., Sousa, J., Vitorino, C., & Pais, A. (2018). Computational modeling in glioblastoma: from the prediction of blood–brain barrier permeability to the simulation of tumor behavior. *Future Medicinal Chemistry*, *10*(1), 121–131.

Modarres, H. P., Janmaleki, M., Novin, M., Saliba, J., El-Hajj, F., RezayatiCharan, M., & Sanati-Nezhad, A. (2018). In vitro models and systems for evaluating the dynamics of drug delivery to the healthy and diseased brain. *Journal of Controlled Release*, *273*, 108–130.

Mohamed, W. R., Metwally, S. S., Ibrahim, H. A., El-Sherief, E. A., Mekhamer, H. S., Moustafa, I. M. I., & Mabrouk, E. M. (2017). Impregnation of task-specific ionic liquid into a solid support for removal of neodymium and gadolinium ions from aqueous solution. *Journal of Molecular Liquids*, *236*, 9–17.

Moreno, M., Castiglione, F., Mele, A., Pasqui, C., & Raos, G. (2008). Interaction of water with the model ionic liquid [bmim][$BF_4$]: Molecular dynamics simulations and comparison with NMR data. *Journal of Physical Chemistry B*, *112*(26), 7826–7836.

Mou, Z., Li, P., Bu, Y., Wang, W., Shi, J., & Song, R. (2008). Investigations of coupling characters in ionic liquids formed between the 1-ethyl-3-methylimidazolium cation and the glycine anion. *Journal of Physical Chemistry B*, *112*(16), 5088–5097.

Moya, C., Gonzalez-Miquel, M., Rodriguez, F., Soto, A., Rodriguez, H., & Palomar, J. (2017). Non-ideal behavior of ionic liquid mixtures to enhance $CO_2$ capture. *Fluid Phase Equilibria*, *450*, 175–183.

Nascimento, M. da G., da Silva, J. M. R., da Silva, J. C., & Alves, M. M. (2015). The use of organic solvents/ionic liquids mixtures in reactions catalyzed by lipase from Burkholderia cepacia immobilized in different supports. *Journal of Molecular Catalysis B: Enzymatic*, *112*, 1–8.

Nematollahi, M. H., & Carvalho, P. J. (2018). Green Solvents for $CO_2$ Capture. *Current Opinion in Green and Sustainable Chemistry, 18*, 25-30.

Nookuea, W., Wang, F., Yang, J., Tan, Y., Li, H., Thorin, E.,Yan, J. (2017). Viscosity data of aqueous MDEA-[Bmim][$BF_4$] solutions within carbon capture operating conditions. *Energy Procedia*, *105*, 4581–4586.

Orozco, G. A., Lachet, V., & Mackie, A. D. (2014). A molecular simulation study of aqueous solutions of amines and alkanolamines: mixture properties and structural analysis. *Molecular Simulation*, *40*(1–3), 123–133.

Płotka-Wasylka, J., Rutkowska, M., Owczarek, K., Tobiszewski, M., & Namieśnik, J. (2017). Extraction with environmentally friendly solvents. *TrAC Trends in Analytical Chemistry*, *91*, 12–25.

Privalova, E. I., Karjalainen, E., Nurmi, M., Mäki-Arvela, P., Eränen, K., Tenhu, H., & Mikkola, J. P. (2013). Imidazolium-based poly(ionic liquid)s as new alternatives for $CO_2$ capture. *ChemSusChem*, *6*(8), 1500–1509.

Pullman, B., Berendsen, H. J. C., Postma, J. P. M., Gunsteren, W. F., & Hermans, J. (1981). Interaction models for water in relation to protein hydration. In B. Pullman (Eds.), Intermolecular forces (pp. 331–342). Dordrecht: Springer-Netherlands.

Qian, W., Xu, Y., Xie, B., Ge, Y., & Shu, H. (2017). Alkanolamine-based dual functional ionic liquids with multidentate cation coordination and pyrazolide anion for highly efficient $CO_2$ capture at relatively high temperature. *International Journal of Greenhouse Gas Control*, *56*, 194–201.

Qian, W., Texter, J., & Yan, F. (2017). Frontiers in poly(ionic liquid)s: Syntheses and applications. *Chemical Society Reviews*, *46*(4), 1124–1159.

Ramachandran, N., Aboudheir, A., Idem, R., & Tontiwachwuthikul, P. (2006). Kinetics of the absorption of $CO_2$ into mixed aqueous loaded solutions of monoethanolamine and methyldiethanolamine. *Industrial and Engineering Chemistry Research*, *45*(8), 2608–2616.

Rashidi, N. A., & Yusup, S. (2016). An overview of activated carbons utilization for the post-combustion carbon dioxide capture. *Journal of $CO_2$ Utilization*, *13*, 1–16.

Ratti, R. (2014). Ionic Liquids: Synthesis and Applications in Catalysis. *Advances in Chemistry*, *2014*, 1–16.

Reid, J. E. S. J., Gammons, R. J., Slattery, J. M., Walker, A. J., & Shimizu, S. (2017). Interactions in water ionic liquid mixtures: Comparing protic and aprotic systems. *Journal of Physical Chemistry B*, *121*(3), 599–609.

Rigual, V., Santos, T. M., Domínguez, J. C., Alonso, M. V., Oliet, M., & Rodriguez, F. (2017). Recovery and reuse of 1-allyl-3-methylimidazolium chloride in the fractionation of *pinus radiata* wood. *ACS Sustainable Chemistry & Engineering*, *5*(3), 2384–2392.

Rojas, M. F., Bernard, F. L., Aquino, A., Borges, J., Vecchia, F. D., Menezes, S., & Einloft, S. (2014). Poly(ionic liquid)s as efficient catalyst in transformation of $CO_2$ to cyclic carbonate. *Journal of Molecular Catalysis A: Chemical*, *392*, 83–88.

Rollet, A. L., Porion, P., Vaultier, M., Billard, I., Deschamps, M., Bessada, C., & Jouvensal, L. (2007). Anomalous diffusion of water in [Bmim][TfSi] room-temperature ionic liquid. *Journal of Physical Chemistry B*, *111*(41), 11888–11891.

Ruckart, K. N., O'Brien, R. A., Woodard, S. M., West, K. N., & Glover, T. G. (2015). Porous solids impregnated with task-specific ionic liquids as composite sorbents. *Journal of Physical Chemistry C*, *119*(35), 20681–20697.

Russell, V. A., Etter, M. C., & Ward, M. D. (1994). Layered materials by molecular design: Structural enforcement by hydrogen bonding in guanidinium alkane- and arenesulfonates. *Journal of the American Chemical Society*, *116*(5), 1941–1952.

Saha, D., & Mukherjee, A. (2018). Effect of water and ionic liquids on biomolecules. *Biophysical Reviews, 10*(3), 795–808.

Sairi, N. A., Ghani, N. A., Aroua, M. K., Yusoff, R., & Alias, Y. (2015). Low pressure solubilities of $CO_2$ in guanidinium trifluoromethanesulfonate–MDEA systems. *Fluid Phase Equilibria*, *385*, 79–91.

Sairi, N. A., Yusoff, R., Alias, Y., & Aroua, M. K. (2011). Solubilities of $CO_2$ in aqueous *N*-methyldiethanolamine and guanidinium trifluoromethanesulfonate ionic liquid systems at elevated pressures. *Fluid Phase Equilibria*, *300*(1-2), 89–94.

Samanta, A., & Bandyopadhyay, S. S. (2009). Absorption of carbon dioxide into aqueous solutions of piperazine activated 2-amino-2-methyl-1-propanol. *Chemical Engineering Science*, *64*(6), 1185–1194.

Sambasivarao, S. V, & Acevedo, O. (2009). Development of OPLS-AA force field parameters for 68 unique ionic liquids. *Journal of Chemical Theory and Computation*, *5*(4), 1038–1050.

Schmidt, M. W., Baldridge, K. K., Boatz, J. A., Elbert, S. T., Gordon, M. S., Jensen, J. H., Koseki, S., Matsunaga, N., Nguyen, K. A., Su, S., Windus, T. L., Dupuis, M. & Montgomery, J. A., Jr (1993). General atomic and molecular electronic structure system. *Journal of Computational Chemistry*, *14*(11), 1347–1363.

Seo, S., Quiroz-Guzman, M., DeSilva, M. A., Lee, T. B., Huang, Y., Goodrich, B. F., & Brennecke, J. F. (2014). Chemically tunable ionic liquids with aprotic heterocyclic anion (AHA) for $CO_2$ Capture. *Journal of Physical Chemistry B*, *118*(21), 5740–5751.

Sharma, A., & Ghorai, P. K. (2016). Effect of water on structure and dynamics of [BMIM][$PF_6$] ionic liquid: An all-atom molecular dynamics simulation investigation. *Journal of Chemical Physics*, *144*(11), 114505-1–114505-11.

Sheridan, Q. R., Schneider, W. F., & Maginn, E. J. (2018). Role of Molecular Modeling in the Development of $CO_2$-Reactive Ionic Liquids. *Chemical Reviews, 118*(10), 5242–5260.

Shi, H., Naami, A., Idem, R., & Tontiwachwuthikul, P. (2014). Catalytic and non catalytic solvent regeneration during absorption-based $CO_2$ capture with single and blended reactive amine solvents. *International Journal of Greenhouse Gas Control*, *26*, 39–50.

Shiflett, M. B., & Yokozeki, A. (2005). Solubilities and diffusivities of carbon dioxide in ionic liquids: [Bmim][$PF_6$ ] and [Bmim][$BF_4$ ]. *Industrial & Engineering Chemistry Research*, *44*(12), 4453–4464.

Songolzadeh, M., Soleimani, M., Takht Ravanchi, M., & Songolzadeh, R. (2014). Carbon dioxide separation from flue gases: A technological review emphasizing reduction in greenhouse gas emissions. *The Scientific World Journal*, *14*, 1–34.

Spohr, H. V, & Patey, G. N. (2010). The influence of water on the structural and transport properties of model ionic liquids. *The Journal of Chemical Physics*, *132*(23), 234510-1–234510-13.

Sun, H., Qiao, B., Zhang, D., & Liu, C. (2010). Structure of 1-Butylpyridinium tetrafluoroborate ionic liquid: quantum chemistry and molecular dynamic simulation studies. *Journal of Physical Chemistry A*, *114*(11), 3990–3996.

Sunda, A. P., & Venkatnathan, A. (2011). Molecular dynamics simulations of triflic acid and triflate ion/water mixtures: A proton conducting electrolytic component in fuel cells. *Journal of Computational Chemistry*, *32*(15), 3319–3328.

Tang, J., Tang, H., Sun, W., Plancher, H., Radosz, M., & Shen, Y. (2005). Poly(ionic liquid)s: a new material with enhanced and fast $CO_2$ absorption. *Chemical Communications*, *26*, 3325–3327.

Theo, W. L., Lim, J. S., Hashim, H., Mustaffa, A. A., & Ho, W. S. (2016). Review of pre-combustion capture and ionic liquid in carbon capture and storage. *Applied Energy*, *183*, 1633–1663.

Tian, S., Hou, Y., Wu, W., Ren, S., & Pang, K. (2012). Physical properties of 1-butyl-3-methylimidazolium tetrafluoroborate/ *N*-methyl-2-pyrrolidone mixtures and the solubility of $CO_2$ in the system at elevated pressures. *Journal of Chemical & Engineering Data*, *57*(3), 756–763.

Tomé, L. C., Mecerreyes, D., Freire, C. S. R., Rebelo, L. P. N., & Marrucho, I. M. (2013). Pyrrolidinium-based polymeric ionic liquid materials: New perspectives for $CO_2$ separation membranes. *Journal of Membrane Science*, *428*, 260–266.

Tomida, D., Kumagai, A., Qiao, K., & Yokoyama, C. (2007). Viscosity of 1-Butyl-3-methylimidazolium Hexafluorophosphate + $CO_2$ Mixture. *Journal of Chemical & Engineering Data*, *52*(5), 1638–1640.

Uehara, Y., Karami, D., & Mahinpey, N. (2018). Roles of cation and anion of amino acid anion-functionalized ionic liquids immobilized into a porous support for $CO_2$ capture. *Energy & Fuels*, *32*(4), 5345–5354.

van der Spoel, D., Lindahl, E., Hess, B., van Buuren, A. R. , Apol, E., Meulenhoff, P. J., Tieleman, D. P., Sijbers, A. L. T. M., Feenstra, K. A. , van Drunen, R., & Berendsen, H. J. C. (2010). Gromacs User Manual version 4.5.4. Retrieved on April 21, 2014 from http://www.gromacs.org/

Vekariya, R. L. (2017). A review of ionic liquids: Applications towards catalytic organic transformations. *Journal of Molecular Liquids*, *227*, 44–60.

Walden, P. (1914). Molecular weights and electrical conductivity of several fused salts. *Bulletin of the Imperial Academy of Sciences (Saint Petersburg)*, *1800*, 405–422.

Wiebe, R., & Gaddy, V. (1940). The solubility of carbon dioxide in water at various temperatures from 12 to 40° and at pressures to 500 atmospheres. Critical phenomena. *Journal of the American Chemical Society*, *62*(4), 815–817.

Wiebe, R., & Gaddy, V. L. (1939). The solubility in water of carbon dioxide at 50, 75 and 100°, at pressures to 700 atmospheres. *Journal of the American Chemical Society*, *61*(2), 315–318.

Wu, Y., & Zhang, T. (2009). Structural and electronic properties of amino acid based ionic liquids: A theoretical study. *Journal of Physical Chemistry A*, *113*(46), 12995–13003.

Xu, J., Wang, S., Yu, W., Xu, Q., Wang, W., & Yin, J. (2014). Molecular dynamics simulation for the binary mixtures of high pressure carbon dioxide and ionic liquids. *Chinese Journal of Chemical Engineering*, *22*(2), 153–163.

Yaghini, N., Pitawala, J., Matic, A., & Martinelli, A. (2015). Effect of water on the local structure and phase behavior of imidazolium-based protic ionic liquids. *Journal of Physical Chemistry B*, *119*(4), 1611–1622.

Yang, J., Yu, X., Yan, J., & Tu, S.T. (2014). $CO_2$ Capture using amine solution mixed with ionic liquid. *Industrial & Engineering Chemistry Research*, *53*(7), 2790–2799.

Zeng, S., Zhang, X., Bai, L., Zhang, X., Wang, H., Wang, J., Bao, D., Li, M., Liu, Z., & Zhang, S. (2017). Ionic-liquid-based $CO_2$ capture systems: Structure, interaction and process. *Chemical Reviews*, *117*(14), 9625–9673.

Zhang, W., Sun, C., Snape, C. E., Irons, R., Stebbing, S., Alderson, T., Fitzgerald, D., & Liu, H. (2017). Process simulations of post-combustion $CO_2$ capture for coal and natural gas-fired power plants using a polyethyleneimine/silica adsorbent. *International Journal of Greenhouse Gas Control*, *58*, 276–289.

Zhang, Yi, Wu, Z., Chen, S., Yu, P., & Luo, Y. (2013). $CO_2$ Capture by imidazolate-based ionic liquids: Effect of functionalized cation and dication. *Industrial & Engineering Chemistry Research*, *52*(18), 6069–6075.

Zhang, Y., Ji, X., Xie, Y., & Lu, X. (2016). Screening of conventional ionic liquids for carbon dioxide capture and separation. *Applied Energy, 162*, 1160–1170.

## LIST OF PUBLICATIONS

1. **Haron, N.**, Lee, V. S., Sairi, N. A., Zain, S. M., Alias, Y., & Aroua, M. K. (2017). Microstructures, interactions and dynamics properties studies of aqueous guanidinium triflate ionic liquid from molecular dynamics simulations. *Journal of Molecular Liquids*, *227*, 184–193.

2. **Haron, N.**, Sairi, N. A., & Lee, V. S. (2015). Microstructures, interactions and dynamics properties studies of N-methyldiethanolamine + guanidinium triflate ionic liquid + water tertiary system at the standard temperature. *Molecular Simulation*, *42*(8), 655–666.